



LUND
UNIVERSITY

**FRACTURE MECHANICS MODELS
FOR STRENGTH ANALYSIS OF TIMBER
BEAMS WITH A HOLE OR A NOTCH
- A Report of RILEM TC-133**

SIMON AICHER,
PER JOHAN GUSTAFSSON (Editor),
PEER HALLER and HANS PETERSSON

Structural
Mechanics

FRACTURE MECHANICS MODELS
FOR STRENGTH ANALYSIS OF TIMBER
BEAMS WITH A HOLE OR A NOTCH
- A Report of RILEM TC-133

SIMON AICHER,
PER JOHAN GUSTAFSSON (Editor),
PEER HALLER and HANS PETERSSON

Copyright © 2002 by Structural Mechanics, LTH, Sweden.
Printed by KFS I Lund AB, Lund, Sweden, January 2002.

For information, address:
Division of Structural Mechanics, LTH, Lund University, Box 118, SE-221 00 Lund, Sweden.
Homepage: <http://www.byggmek.lth.se>

Preface

The papers compiled in this report were written as a part of the work of the RILEM Technical Committee 133, "Fracture of Timber". The committee was active with meetings 1991-1995 and formed two subgroups, one on fracture property test methods and the second on fracture mechanics based strength calculation methods for beams with a hole, notch or crack. Most of the manuscripts of the papers compiled in this report were written during the active period of the TC and they present some of the work and findings of the second subgroup obtained during tests and discussions of various calculation methods. Most of the test calculations were carried out for a certain set of beams with a notch or a hole. The geometry of these beams is shown in the figure in the appendix. The initial idea to present the results in a continuous report was changed to publication of a compilation of separate papers. Active members of the second subgroup and authors of the papers in this report are:

Simon Aicher, FMPA, University of Stuttgart, Germany
Per Johan Gustafsson, Lund University, Sweden
Peer Haller, Technical University of Dresden, Germany
Hans Petersson, Chalmers University of Technology, Sweden

Active members of TC-133 also included:

Lars Boström, SP, Sweden
Martin Gierl, FMPA, Germany
Luc Job, EPFL, Switzerland
David Kretshman, USDA-FS-FPL, USA
Hugh Mansfield-Williams, Buckinghamshire College, UK
Barry Matthews, Buckinghamshire College, UK
Alpo Ranta-Maunus, VTT, Finland
Gerard Valentin, LRBB, France

We take this opportunity to thank our friends and colleagues in TC-133 for all good discussions and work on fracture mechanics of timber. This is a subject area believed to be of clear relevance before future developments of methods for timber structure strength design and still only in an initial phase of development and application.

Lund and Espoo, January 2002

Per Johan Gustafsson,
Convener of subgroup two

Alpo Ranta-Maunus,
Chairman of RILEM TC-133

Table of contents

Preface

Table of contents

Paper 1:

An Overview of Fracture Mechanics Concepts

Peer Haller and Per Johan Gustafsson, 1998, 16 pages

Paper 2:

Stress Intensity Factor Approach

Simon Aicher, 1996, 1+31 pages

Paper 3:

Energy Release Rate Analysis

Hans Petersson, 1995, 23 pages

Paper 4:

Energy Approach Used in a Draft Eurocode

Per Johan Gustafsson, 1993, 6 pages

Paper 5:

Mean Stress and Initial Crack Approaches

Per Johan Gustafsson, 1993, 15 pages

Appendix:

Geometry of Beams and Material Parameter Data

1993, 2 pages

FRACTURE MECHANICS MODELS FOR STRENGTH ANALYSIS OF
TIMBER BEAMS WITH A HOLE OR A NOTCH

Paper 1:

An Overview of Fracture Mechanics Concepts ¹⁾

by

Peer Haller

Abteilung Bauingenieurwesen, Technische Universität Dresden,
Mommensenstrasse 13, D-010 62 Dresden, Germany

and

Per Johan Gustafsson

Division of Structural Mechanics, Lund University,
Box 118, SE-221 00 Lund, Sweden

¹⁾1998, 16 pages

An Overview of Fracture Mechanics Concepts

by

Peer Haller and Per Johan Gustafsson

1. Introduction

The following overview of some concepts used in fracture mechanics has its emphasis on linear elastic fracture theory. The overview is intended to give a reader who is not very familiar with fracture mechanics some general background before studying the various methods and applications of fracture analysis of timber dealt with in subsequent chapters. A state-of-the-art report on the application of fracture mechanics to timber structures was presented by RILEM TC 110 in 1991 [Valentin, Boström, Gustafsson, Ranata-Maunus and Gowda, 1991].

Fracture mechanics is a branch of mechanics of materials. When a body made of a solid material is loaded it will ultimately respond by undergoing large deformations or fracture. Fracture is loss of contact between parts of the body. This separation results in the creation of new surfaces. Fracture is the topic of interest in fracture mechanics, and the concern is partly with microscopic mechanisms which govern the separation and partly with predictions from a macroscopic point of view. Of prime concern then is development of criteria and methods by which it is possible to predict the load-carrying capacity of a structural member based on knowledge about properties of the material.

The origin of fracture mechanics as a science can be ascribed to research conducted by A. A. Griffith about 80 years ago and presented in [Griffith, 1921] and [Griffith,1925]. The material first studied was glass, but soon applications to metals became of prime interest due to their importance for vehicles, ships and other load-carrying constructions. Fracture mechanics theory was extended to anisotropic, especially orthotropic materials, in the sixties [Sih, Paris and Irvin, 1965]. Also in the sixties, pioneering applications of linear elastic fracture mechanics, LEFM, to wood were made, e.g. [Atack et al., 1961]. Most of the early studies of wood were realised with small clear wood specimens, but soon similar studies were also undertaken for structural lumber. Although wood is a strongly orthotropic material, the evaluation of fracture mechanics test results has often been made as for an isotropic material.

The factors that govern fracture - load, material and defects - are sometimes illustrated as in Figure 1. The defect may be a sharp crack, a man-made stress concentrator or some natural discontinuity in the material. Consideration of the defect and the associated singularity or discontinuity in stress, strain or displacement

distinguishes fracture mechanics from strength analysis by classical continuum mechanics methods. By non-linear fracture mechanics methods, not only the performance and growth of existing defects can be analysed but also their origin. In conventional LEFM analysis it is assumed that there is a sharp crack in the structural element.

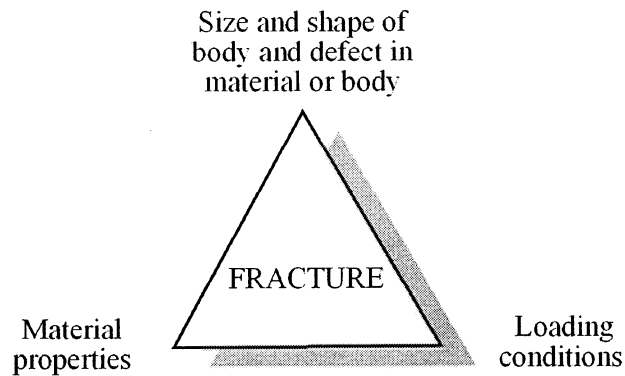


Figure 1. Factors governing fracture.

2. Modes of loading of a crack

Figure 2 shows the three basic types of relative displacements in the vicinity of a crack. Type of displacement is governed by the load acting on the structural element. The three types of relative displacements are commonly referred to as the modes of loading, or, if the crack is growing, as the modes of fracture or modes of cracking. Mode I is the opening mode, mode II the in-plane shear mode and mode III the perpendicular-to-plane shear mode. In general the loading is a combination of the three basic modes, giving a so-called mixed mode loading or mixed mode fracture. Since mixed mode I+II is the most common, mixed mode is sometimes used as a synonym for the I+II mixed mode.

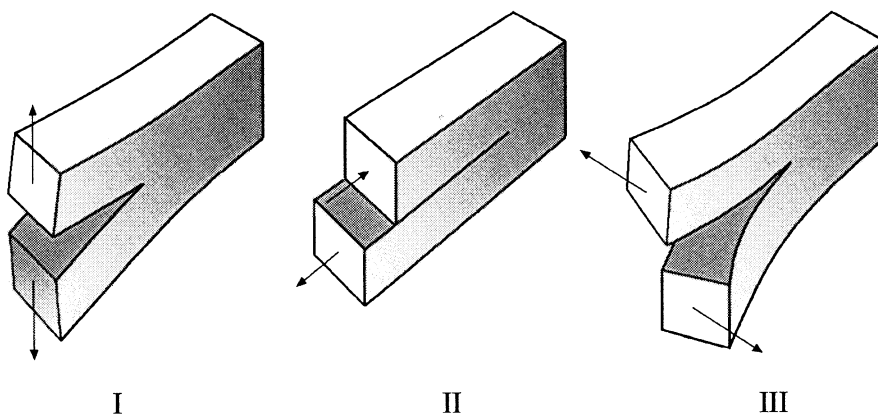


Figure 2. The three modes of loading and fracture.

3. Crack orientations

The orthotropic nature of wood gives 6 possible orientations of plane cracks located in the three principle planes of the material. The crack orientations are shown in Figure 3 and denoted RL, TL, LT, RT, LR and TR. R, T and L indicate radial, tangential and longitudinal direction of the wood, respectively. In the notation for crack orientation the first of the two indices indicates the direction of the normal to the crack plane, and the second indicates the straightforward direction of crack length extension. This second direction is accordingly the direction which is perpendicular to the first direction as well as to the front line of the crack. The crack orientations are not symmetrical, which means that inversion of the indices leads to a different orientation. Since there are three modes of loading for each crack orientation, 18 basic fracture situations can be identified. The fracture resistance for these 18 situations is in general different. As an example, due to the high tensile strength of the material in the L direction the resistance to mode I crack growth is high for orientations LR and LT.

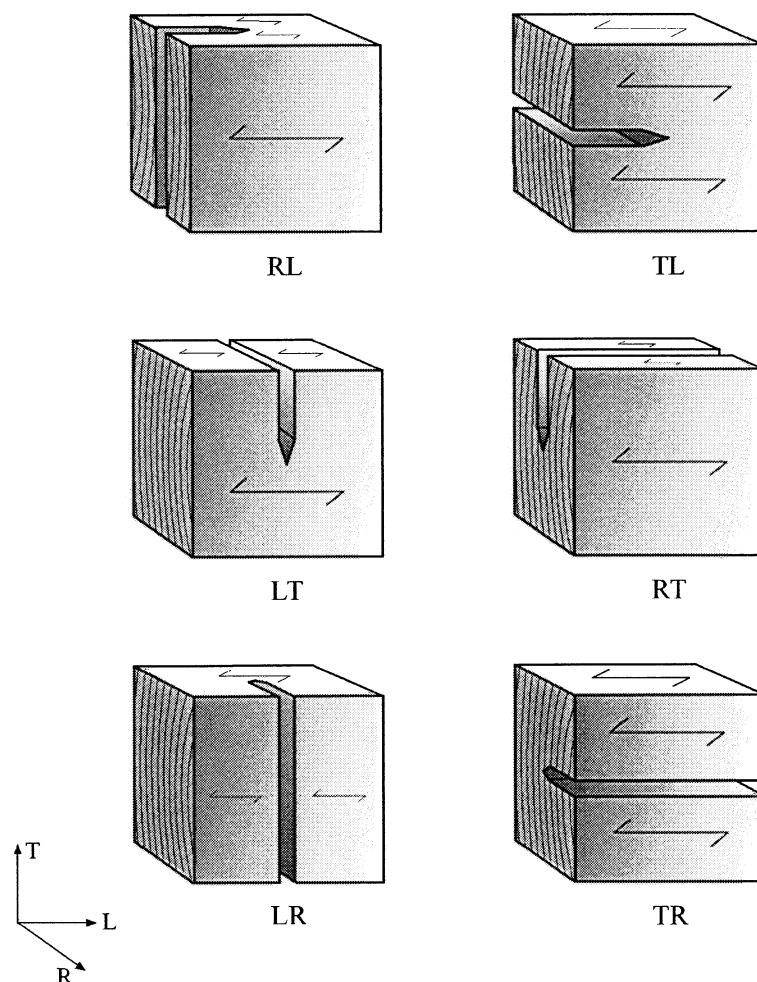


Figure 3. Basic crack orientations in an orthotropic material.

4. Linear elastic fracture mechanics, LEFM

In LEFM the material is assumed to be ideal linear elastic without any limiting stress or strain value. The material may be isotropic, orthotropic or anisotropic. Although the strains may be arbitrarily large without failure of the material, small strain and displacement theory is commonly adopted in stress analysis. The assumption of linear elastic performance implies singular or infinitely large stresses and strains at the tip of a sharp crack. Since stress and strain is singular other quantities must be used in fracture criteria. Two such quantities generally used and discussed in the following are energy release rate and stress intensity. To use these quantities it is required that there be a pre-existing sharp crack in the structural element to be analysed.

No real material has ideal linear elastic properties. Nevertheless, LEFM is in many cases very useful. The prime requirement for good applicability of LEFM is that the size of the fracture process region at the tip of the crack is small compared to the length of the crack and compared to the distance to boundaries and to points where load is applied. The fracture process region is the region where the material is being broken and performs in very heterogeneous and non-linear manner. The size of a fully developed fracture process region is governed by the properties of the material; for glass it is in the order of less than a mm, for wood in the order of one or a few cm and for concrete in the order of several dm or more.

If the size requirements of LEFM are fulfilled, the performance of the material in the fracture process region as well as its size for a given mode of loading and crack orientation are solely governed by the properties of the material, i.e. not affected by the geometry and size of the element. Fracture in this state is commonly referred to as being self-similar or autonomous.

5. Energy release rate

Crack propagation analysis by considering the energy release was proposed by Griffith and energy release rate is denoted G after him. In static or quasi-static LEFM the energy release is the decrease of the potential energy of the mechanical system under consideration during a virtual extension of the crack. The potential energy of the system is the elastic strain energy in the loaded structural element plus the potential energy of the loads acting on the element. The energy release rate is the decrease of the potential energy per increase in crack area

$$G = - \partial \Pi / \partial A \quad (1)$$

and has the dimension energy/area, e.g. J/m^2 . G is in general a positive number since the potential energy generally decreases during crack extension. G is often called the "crack driving force". For an elastic material with zero strain energy at zero external load, G is proportional to the square of the magnitude of the loads. The precise value of G for a given load is governed by the geometry of the element, the length of the crack, the boundary conditions and the elastic properties of the material. The numerical value of G can be determined in various ways, e.g. by finite element analysis or, for common cases, with the help of handbooks. In some cases analytical methods can also be used.

By making tests where the load acting on the test specimen is increased until the crack starts to grow, a critical value of G can be determined. This critical value is denoted G_c , the critical energy release rate. Unlike G , G_c is a material property parameter. G_c is sometimes called the crack resistance. When the crack driving force equals the crack resistance, i.e. when

$$G = G_c, \tag{2}$$

the crack is just about to start to grow. This crack growth may be stable or unstable. If

$$\partial(G-G_c)/\partial A > 0 \tag{3}$$

the growth becomes unstable, and it becomes stable if

$$\partial(G-G_c)/\partial A < 0. \tag{4}$$

In most cases the properties of the material are constant throughout the body, which implies constant G_c . If the external action is a load rather than an imposed displacement, in most cases G increases as the length of the crack increases. This common cases implies unstable crack growth once the crack has started to grow.

In cases of mixed mode loading, G is the total energy release rate. For isotropic and orthotropic materials, however, it is possible to separate the energy corresponding to the different modes, and then

$$G = G_I + G_{II} + G_{III}. \tag{5}$$

Depending on the properties of the material, the material parameter G_c may, or may not, have different values for the different modes of loading and may, or may not, have different values for the different crack orientations shown in Figure 3. In the case of mixed mode fracture, G_c may be expected to be more or less different than in single mode fracture.

6. Definition of stress intensity factors

The stresses in the vicinity of a crack tip approach infinity as the distance to the crack tip is decreased towards zero. In Figure 4 this is illustrated by the distribution of the normal stress σ_{yy} ahead of a crack loaded in mode I. In order to get a measure of the magnitude of the stress components although they approach a singular value, three stress intensity factors are defined, one for each mode of loading [Irvin, 1958]. The stress intensity factor that shows the magnitude of mode I loading of the crack is by definition

$$K_I = \lim (\sigma_{yy} (2\pi r)^{1/2}) \text{ for } r \rightarrow 0 \text{ and } \Theta = 0, \quad (6)$$

where the coordinates r and Θ are indicated in Figure 5. The corresponding stress intensity factors for mode II and III are defined by

$$K_{II} = \lim (\tau_{xy} (2\pi r)^{1/2}) \text{ for } r \rightarrow 0 \text{ and } \Theta = 0 \quad (7)$$

and

$$K_{III} = \lim (\tau_{yz} (2\pi r)^{1/2}) \text{ for } r \rightarrow 0 \text{ and } \Theta = 0, \quad (8)$$

respectively. The magnitude of the stresses in a linear elastic structural element, and accordingly the stress intensity factors, are proportional to the loads acting on the element. The dimension of K is (stress)(length)^{1/2} or (force)/(length)^{3/2}, e.g. N/m^{3/2}.

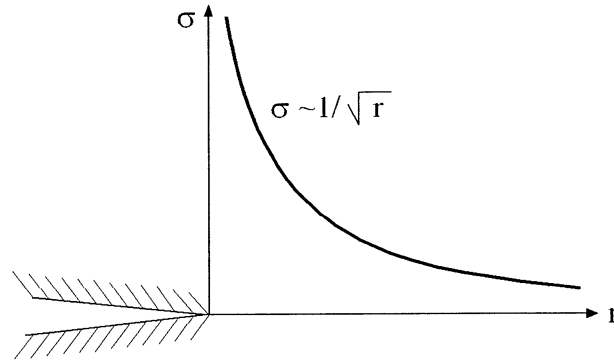


Figure 4. Stress distribution in front of a crack according linear elastic theory.

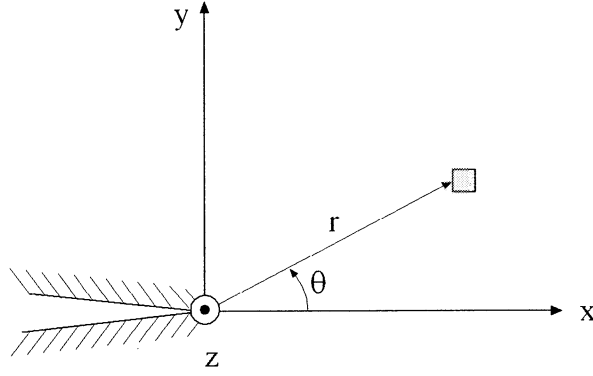


Figure 5. Coordinates x-y-z and r- Θ .

7. Stress and displacement in the vicinity of a crack tip

The stress distribution in the vicinity of a sharp crack in an isotropic linear elastic body has been derived by a power series assumption [Williams,1957]. The stress components for each mode of loading can be expressed as the sum of an infinite series of terms. Close to the crack tip however, i.e. for small r , the first term dominates. The other terms can accordingly be disregarded when analysing the state of stress in the very close vicinity of the crack tip. Along the line $\Theta = 0$, the magnitudes of the stress components are

$$[\sigma_{xx} , \sigma_{yy} , \sigma_{zz} , \tau_{xy} , \tau_{xz} , \tau_{yz}] = (2\pi r)^{-1/2} [K_I , K_I , \nu \xi K_I , K_{II} , 0 , K_{III}] + \dots \quad (9)$$

where the three dots represent the higher order terms which are negligible for small r . ν indicates the Poissons ratio of the material and ξ is a number which is 0 in the case of plane stress and 2 in the case of plane strain. The numerical values of the stress intensity factors are proportional to the external load acting on the structural element and governed by the geometry and support conditions of the structural element. For orthotropic materials, the ratios between the elasticity parameters do in general also affect the stress intensity factors. The factors may be calculated by various finite element methods or, in some cases , calculated analytically or are available in handbooks on mechanics of materials.

The stress in an arbitrary point (r,Θ) in the vicinity of the crack tip can be written as $(2\pi r)^{-1/2}$ times a function of Θ . In the case of mode I loading of a crack in an isotropic material, the in-plane stresses in the point (r,Θ) are

$$\sigma_{xx} = (2\pi r)^{-1/2} K_I \cos(\Theta/2) \{ 1 + \sin(\Theta/2) \sin(3\Theta/2) \} + \dots \quad (10)$$

$$\sigma_{yy} = (2\pi r)^{-1/2} K_I \cos(\Theta/2) \{ 1 - \sin(\Theta/2) \sin(3\Theta/2) \} + \dots \quad (11)$$

$$\tau_{xy} = (2\pi r)^{-1/2} K_I \cos(\Theta/2) \sin(\Theta/2) \cos(3\Theta/2) + \dots \quad (12)$$

The shear stresses τ_{xz} and τ_{yz} are zero, and the normal stress σ_{zz} is zero in the case of plane stress and $\nu(\sigma_{xx} + \sigma_{yy})$ in the case of plane strain.

Similar equations for modes II and III are given in textbooks on fracture mechanics. Also the corresponding equations for strain and displacement in the vicinity of the crack tip can be found in most textbooks on fracture mechanics.

For an orthotropic material with a crack orientated according to the axes of the material, the basic stresses σ_{yy} , τ_{xy} and τ_{yz} along the line $\Theta = 0$ are as for an isotropic material, i.e. according to equation (9). For $\Theta \neq 0$ there is an effect of Θ different than for an isotropic material but still separable from r [Leicester, 1971]. It is noteworthy that the stresses and displacements in the vicinity of the crack tip are determined by only three parameters, i.e. the three stress intensity factors. In the common case of pure mode I, the value of K_I is sufficient.

8. The J integral

The energy release rate and the stress intensity factors are two alternatives for defining how much a crack is loaded. Another alternative is the J integral. This integral is defined for elastic materials and the value of J equals G,

$$J = G \quad (13)$$

as indicated in [Rice, 1968]. The J integral, however, is calculated in a different manner than G. While G is calculated by a derivation, the J integral is obtained by integration of certain quantities along a line around the crack tip, from one crack surface to the other, as indicated in Figure 6. The integral is

$$J = \int_{\Gamma} (W dy - \sigma_{ij} n_j \frac{\partial u_i}{\partial x} ds) \quad (14)$$

where W is the elastic strain energy density, n_j the normal to the integration curve Γ , s is the arch length of this curve and u_i is the displacement vector.

The absolute value of J is not affected by the path of integration as long as the material is elastic and the path starts and stops at opposite crack surfaces. The stresses, strains and displacements needed for the integration can be calculated by the finite element method. The value of J at onset of crack propagation is denoted J_c , the critical value of the J integral. Just like G_c , J_c is a material property parameter and

may in general be expected to have different values for different modes of loading and, for an orthotropic material, different values for different orientations of the crack.

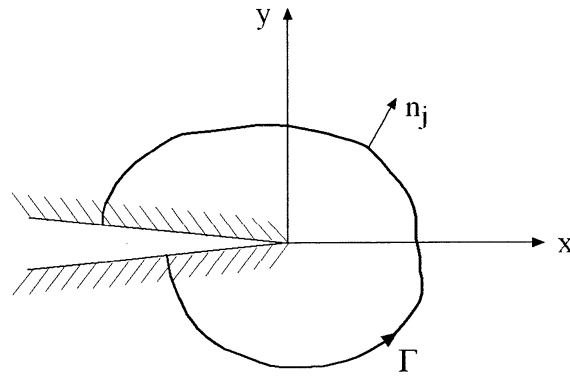


Figure 6. Integration path for the J-integral.

9. The crack open displacement, COD

The COD is the distance between the crack faces and is yet another alternative for quantification of the load acting on a crack. The COD is considered both in experimental observations of cracks and in theoretical stress analysis.

In experimental studies COD is applied primarily for ductile metals; for such materials an originally sharp crack tip becomes blunt before the crack starts to propagate. This means that a COD develops at the tip of the crack. This crack tip opening displacement, CTOD, may be used as the crack load parameter and for defining a critical value for onset of fracture.

In theoretical stress analysis the COD may be used as an alternative to the mode I stress intensity factor, K_I . The COD in the case of elastic materials is proportional to K_I and, for a short distance r behind the tip of crack, the relation for an isotropic material is

$$\text{COD} = K_I (32r/\pi)^{1/2} / E^* , \quad (15)$$

where $E^* = E$ at plane stress and $E^* = E/(1-\nu^2)$ at plane strain. E and ν denote modulus of elasticity and Poissons ratio, respectively.

10. Relation between G and K_I , K_{II} and K_{III} .

From the stresses in front of a crack tip and the crack opening during growth of a crack, both quantities given by the stress intensity factors, the corresponding energy release rate can be calculated. For an isotropic material

$$G = K_I^2/E^* + K_{II}^2/E^* + (1+\nu) K_{III}^2/E, \quad (16)$$

where E^* is as in equation (15). The corresponding plane stress relation for a crack with an orientation yx in an orthotropic material, i.e. according to Figure 5 with the normal to the crack plane in the y -direction of the material and with the straight ahead direction of the crack in the x -direction, is

$$G = K_I^2/E_I^* + K_{II}^2/E_{II}^* + K_{III}^2/E_{III}^* \quad (17)$$

where

$$E_I^* = (2E_x E_y)^{1/2} [(E_x/E_y)^{1/2} - \nu_{xy} + E_x/(2G_{xy})]^{-1/2}, \quad (18)$$

$$E_{II}^* = (2E_x^2)^{1/2} [(E_x/E_y)^{1/2} - \nu_{xy} + E_x/(2G_{xy})]^{-1/2} \quad (19)$$

and

$$E_{III}^* = (4G_{xz} G_{yz})^{1/2}. \quad (20)$$

E_x , E_y , G_{xy} , G_{yz} and G_{xz} are the elastic normal and shear stiffnesses of the material, and ν_{xy} is the strain ratio $-\varepsilon_y/\varepsilon_x$ for uniaxial stress in the x -direction.

11. Mixed mode crack growth criteria

Mixed mode is when a crack is loaded in two or three of the three modes at the same time. Combinations of mode I and II are encountered most frequently, and the following is focused on that I+II combination. For that combination a general crack growth criteria is

$$f(K_I, K_{II}, \text{material parameters}) = 0 \quad (21)$$

The function f may be determined by tests or by some assumption which then has to be verified by tests. Examples of assumptions are:

- fracture is governed by the maximum of the tangential stress $\sigma_{\Theta\Theta}$ for arbitrary Θ and constant r ;

- fracture is governed by the maximum of the strain energy density for arbitrary Θ and constant r ;
- fracture is governed by the maximum of the energy release rate for arbitrary direction, Θ , of the crack growth;
- some more or less arbitrary empirical function with parameters that are determined by fitting to test results.

An often used empirical function is

$$f = (K_I/K_{IC})^m + (K_{II}/K_{IIC})^n - 1.0, \quad (22)$$

where the exponents m and n are determined by fitting to tests results. For wood it is often assumed that $m=1$ and $n=2$ as proposed by [Wu,1967] and [Mall et al., 1983].

12. Crack growth direction rules

For mode I loading of a crack in an isotropic material it is a general rule, with only few exceptions, that the crack will grow in its initial direction. For a crack loaded in other basic or mixed modes and for anisotropic materials, the direction of the crack growth is not equally evident. Consequently, various rules have been proposed for the prediction of crack growth direction. Many of these rules are quite analogous to the criteria for the prediction of start of crack growth, as discussed in section 1.10 above.

Wood is a strongly orthotropic material with much higher strength and stiffness in the L direction than in the R and T directions. It is therefore a common approximate assumption that a crack with orientation TL, RL, LR or LT will grow in the L direction regardless of the mode of loading. The crack growth from cracks with orientation LR and LT is then symmetrical for modes I and III in the sense that two opposite crack growth directions are equally probable.

A crack with orientation TR or RT and loaded in mode I or mode III may be assumed to grow in its initial direction, or possibly in the perpendicular direction. If loaded in mode II, the TR and RT cracks might grow in the R or T direction, or somewhere in between.

13. Non-linear fracture mechanics, the R curve and the σ -w curve

Non-linear fracture mechanics, NLFM, deviates from the LEFM in one or both of two respects: in the NLFM the non-linear stress-strain performance of the material outside

the tip of the crack may be considered, and/or the non-zero size, the limited stress capacity and the non-linear stress-deformation performance of the material in the fracture process region may be considered.

For a material like mild steel with a very significant plastic strain hardening capacity, it is often important to consider non-linearity of the performance of the material around the fracture region. The LEFM assumption of zero size of the fracture region may, however, still be reasonable for this kind of material. For other materials, e.g. concrete, the pre-peak stress stress-strain performance is about linear, but the size of the fracture region is significant and of importance for the fracture performance and global strength of the actual structural element.

The second kind of non-linear performance can be considered in fracture analysis by various approaches. One such approach is the R curve. Another more direct method is by characterisation of fracture properties of the material by a stress versus deformation relation. Such a stress-deformation relation for the case of mode I fracture is commonly referred to as the σ -w curve of the material.

From the computational point of view the R curve concept is within the framework of LEFM. The R curve is assumed to be characteristic for the material and shows how the resistance to crack growth increases as the fracture zone develops. The curve may show K_{Ic} (or G_c) versus the length of the crack growth. In the very beginning of crack growth, the fracture zone has just started to develop, and the resistance to crack growth is then small. As the fracture advances, the size of the fracture zone and the value of K_{Ic} reach constant values that correspond to the size and fracture resistance of a fully developed fracture zone. Since the crack driving force, G , commonly increases as the length of the crack increases, global failure of the structural member may occur before the fracture zone is fully developed. The possibility to consider the risk for such premature structural failure is the main advantage of the R curve concept over the straightforward conventional LEFM. The concept is dealt with in i.a. [Eftis et al., 1975] and [Schwalbe, 1980].

Fracture property characterisation by a σ -w curve is useful before non-linear finite element fracture analysis. A σ -w curve shows the stress-deformation properties of the material in the fracture process region much as a stress-strain curve shows the properties of the material outside the fracture region. By finite element analysis where the fracture properties of the material are given by a σ -w curve, it is possible to calculate how the fracture region initiates, develops and moves as the external load or imposed deflection is increased. This kind of modelling opens up new possibilities, such as the analysis of structural elements without any initial crack and makes predictions more modulated. Application of NLFM to wood is essentially still in the stage of basic research, but some applications can be found in i.a. [Gustafsson,1985] and [Boström,1992].

14. Energy release, fracture energy, surface energy and fracture work

The concepts critical energy release rate, G_c , fracture energy, G_f , surface energy, γ , and fracture work are related but different. The critical energy release rate has been discussed already in the above, and is the value of G when a crack starts to propagate. The fracture energy G_f is the energy required to open a unit area fracture section, i.e. separate a piece of material into two parts. The surface energy γ is energy per fractured surface area, which for ideal plane fracture surfaces is twice the area of the fracture section. By surface energy is commonly meant the energy related to the higher density of molecules at the surface of a material rather than in the interior the material. Minimization of the surface energy is what makes a drop of water round by minimizing the surface area for a given volume. Fracture work is the total work done, e.g. by a testing machine, when a specimen or structural element is broken into two parts.

G_c is commonly evaluated by LEFM from the experimentally obtained failure load of some test specimen with an initial crack. G_f is often obtained from fracture work of a notched three-point bend specimen or a tensile specimen with or without a notch. The surface energy, γ , is seldom used in engineering analysis of solid materials. For most materials 2γ is much less than G_c and G_f due to energy consuming processes in the fracture process region other than net increase of fracture surface area.

Since G_c is evaluated from fracture load at the assumption of zero size of the fracture zone, low values of G_c are obtained if the size of the test specimen is not big enough. In the evaluation of G_f from fracture work it is often assumed that possible plastic dissipation outside the fracture region is negligible. This means that too high values may be obtained, in particular if the volume of the specimen is large. For an ideal elastic material, $G_c = G_f = 2\gamma =$ fracture work per area of the fracture section.

15. Numerical methods in LEFM

In most cases some numerical method is needed for the calculation of K , G or J . In particular the finite element method is extensively used, but the boundary element method is also used. Today many commercial finite element packages include an option for automatic calculation of K , G or J of a crack.

Although stress and strain approach infinity at the tip of a crack, the finite elements used in LEFM analysis may be of any ordinary type. As in conventional stress analysis, one may generally expect improved accuracy of the numerical results if the number of finite elements is increased or if elements with more nodes are used. A somewhat improved accuracy can be achieved for a given number of elements if

special crack tip elements are used. In such elements the displacement shape function is such that the square root singularity in stress and strain can be reproduced. The modelling work becomes somewhat more complex if special elements are used at the crack tip.

Disregarding the choice of elements, there are many more or less different methods for the calculation of K , G or J by means of finite element analysis. They can be divided into three main groups:

- Substitution methods
- Energy rate methods
- Line integration (J integral) methods.

In substitution methods, some quantity such as stress, strain, displacement (e.g. crack opening displacement) or strain energy density is calculated numerically for some point or points in the vicinity of the tip of the crack. The numerical value of that quantity is then substituted into the corresponding analytical expression, e.g. equation (10), for stress and strain etc in the vicinity of a crack tip. That expression can then be solved for K . If the load is a pure mode I load, one substitution is sufficient for the calculation of K_I . For cases of mixed mode, the quantity has to be calculated and substituted for two or three points to obtain K_I and K_{II} , or K_I , K_{II} and K_{III} , respectively. Improved accuracy can in general be achieved if mean values are calculated by making substitution calculations for several points in the vicinity of the crack tip. Knowing the stress intensity factors, G and J can be calculated by equations (18)-(21) and (13).

In energy rate methods the change of some energy quantity during an increase of the crack length is considered. In finite element analysis, increased crack length can be achieved in different ways: by opening of the node at the tip of the crack, by changing the geometry of the elements in the vicinity of the crack or by assigning zero stiffness to the element ahead of the crack tip. The change of energy during the crack length increase can be calculated in different ways:

- From the difference in work by the external load when acting on the element before and after the crack length increase. This is equivalent to calculation of global stiffness before and after the crack length increase.
- From the forces, e.g. the nodal forces, acting across the crack length to be opened and the crack opening displacement after the crack length has been opened. From these forces and displacements the so-called crack closing energy can be calculated. This energy equals the energy release when the crack is opened. Separation into the different crack loading modes can be made according to the direction of the forces.
- From the change of stiffness of the elements in the vicinity of the crack tip, provided the crack length increase is achieved by changing elements, e.g. by changing the geometry of elements at the crack tip.

In contrast to the substitution methods, the energy rate methods require in general two finite element calculations, one to determine the state before crack length increase and one to determine the state after the increase. On the other hand, it is in most cases found that the energy rate methods give better accuracy than the substitution methods. The energy rate methods can give fairly accurate results even if the element mesh is rather coarse. The energy release rate values obtained can be transformed into stress intensity value by equations (18)-(21).

The line integration (J integral) method represents numerical integration of components of stress and displacement according to equation (14) along a line that encloses the crack tip. In theory the path of integration should not affect the result, but due to the numerical approximations involved one may expect somewhat different results for different paths. Due to different strategies for choosing the path and due to different methods for the numerical integration, the line integration method may be considered as a group of methods. It seems that the line integration methods are not as frequently used as the substitution and energy rate methods.

16. References

Atack, May, Morris and Sproule (1961), "The energy of tensile and cleavage fracture of black spruce", *Tappi* 44-8, pp 555-567.

Boström, L. (1992), "Method for Determination of the Softening Behaviour of Wood and the Applicability of a Nonlinear Fracture Mechanics Model", Thesis TVBM-1012, Div. of Building Materials, Lund University, Sweden.

Eftis, J., Jones, D.L. and Liebowitz, H. (1975), "On Fracture Toughness in the Nonlinear Range" and "On Fracture Toughness Evaluation for Semi Brittle Materials", *Engineering Fracture Mechanics*, vol 7, pp 491-503 and pp 101-135.

Gustafsson, P.J. (1985), "Fracture Mechanics Studies of Non-Yielding Materials like Concrete", Thesis TVBM-1007, Div. of Building Materials, Lund University, Sweden.

Griffith, A.A. (1921), "The Phenomena of Rupture and Flow in Solids", *Phil. Trans. Royal Soc. London*, A221:163-198.

Griffith, A.A. (1925), "The Theory of Rupture", *Proc. 1st Int. Cong. Appl.Mech.*, Delft, pp. 55-63.

Irvin, G.R. (1958), "Fracture", in "Encyclopedia of Physics", ed. S. Flygge, vol. 6, Springer, Berlin, pp 551-590.

Leicester, R.H. (1971), "Some Aspects of Stress Fields at Sharp Notches in Orthotropic Materials", Paper 57, Div. of Forest Products Techn., CSIRO, Australia.

Mall, S., Murphy, J.F. and Shottafer, J.E. (1983), "Criterion for Mixed Mode Fracture in Wood", ASCE, J. of Engineering Mech., 109-3, pp 680-690.

Rice, J.R (1968), "A Path Independent Integral and the Approximate Analysis of Strain Concentration by Notches and Cracks", Journal of Applied Mechanics, 35:379-386.

Schwalbe, K.H (1980), "Bruchmechanik metallischer Werkstoffe", Carl Hanser Vlg Munchen und Wien.

Sih, G.C., Paris, P.C. and Irwon, G.R. (1965), "On Cracks in Rectilinearly Anisotropic Bodies", Int. J. of Fracture, vol 1, no 3, pp 189-203.

Valentin, Boström, Gustafsson, Ranata-Maunus and Gowda (1991), "Application of fracture mechanics to timber structures - RILEM state-of-the-art report", Research Note 1262, VTT, Espoo, Finland.

Williams, M.L. (1957), Journal of Applied Mechanics 24:109-114.

Wu , E.M. (1967), "Application of Fracture Mechanics to Anisotropic Plates", ASME, J. of Applied Mech. Series E, 34-4, pp 967-974.

FRACTURE MECHANICS MODELS FOR STRENGTH ANALYSIS OF
TIMBER BEAMS WITH A HOLE OR A NOTCH

Paper 2:

Stress Intensity Factor Approach ¹⁾

by

Simon Aicher

Department of Wood and Timber Engineering, FMPA – Otto-Graf-Institute
Pfaffenwaldring 4, D-70569 Stuttgart, Germany

¹⁾1996, 1+31 pages

CONTENTS

1	<i>Introduction</i>	1
1.1	<i>General remarks on stress intensity factors and K-concept</i>	1
1.2	<i>Hypothetic crack approach</i>	2
1.3	<i>Basic types of structure responses</i>	3
2	<i>Review of finite element approaches for stress intensity factor determination in mixed mode problems of discrete cracks in orthotropic materials</i>	4
3	<i>Details of applied method</i>	5
3.1	<i>Determination of stress intensity factors</i>	5
3.2	<i>Determination of critical load</i>	8
4	<i>Investigated structures, modelling</i>	10
4.1	<i>Structures, material properties</i>	10
4.2	<i>On-set of hypothetic crack</i>	11
4.3	<i>Some modeling details</i>	11
5	<i>Results</i>	13
5.1	<i>Geometries with round and square holes</i>	13
5.2	<i>Geometries with rectangular and tapered end-notches</i>	18
6	<i>Comparison of results with other fracture mechanics approaches</i>	18
6.1	<i>Comparison to mean stress resp. initial crack method</i>	18
6.2	<i>Comparison to beam compliance method</i>	28
7	<i>Design proposal for beams with holes</i>	29
8	<i>Literature</i>	30

STRESS INTENSITY FACTOR APPROACH

by

Simon Aicher, FMPA – Otto-Graf-Institute, Stuttgart

1 Introduction

1.1 General remarks on stress intensity factors and K -concept

The stress and displacement fields in any linear elastic continuum containing a sharp crack can be written as sums of eigenfunctions with stresses resp. displacements varying with a polar coordinate r resp. angle φ with origin at the crack tip. Approaching the crack tip ($r \rightarrow 0$) the first term of the respective sums becomes dominating within a certain area surrounding the crack tip ($r \leq R$) termed nearfield and rather completely (see below) describes the stress resp. displacement field. Stresses in the nearfield are singular of type $1/\sqrt{r}$ and displacements show a non singular \sqrt{r} dependency.

The stresses resp. displacements in the singularity dominated zone ($r \leq R$) are completely described by the $1/\sqrt{r}$ singularity delivering infinite stresses for $r \rightarrow 0$ and a proportionality factor termed stress intensity factor K which determines the magnitude of the singular stress field. The variations of stresses and displacements in angle ϑ are prescribed by dimensionless functions φ_{ij} , g_{ij} , which in case of isotropic materials solely depend on ϑ and in case of orthotropic materials are further related to constitutive equations. According to the three types of loading a crack can experience (mode I = opening, mode II = in-plane shear, mode III = out-plane shear) the respective singular stress fields, which can be linearly superpositioned, are described by three different stress intensity factors K_I , K_{II} , K_{III} resp. functions f_{ij}^k , g_{ij}^k ($k = I, II, III$).

The stress intensity factors, depending on the geometry and loading of the continuum including the crack, thus completely define the stresses and displacements in the nearfield what also holds vice versa. The latter is most important for complex structures where closed form solutions for K -factors are hardly to derive but stresses and displacements can be conveniently computed by numerical, especially finite element methods.

Important is, that the K -dominated nearfield also contains an interior validity boundary $r = r_{nl}$ close to the crack tip resp. front. Within the range $r < r_{nl} \ll R$ the linear elasticity based nearfield no more describes the material behaviour appropriately. The reason therefore is that stresses and strains in reality can not increase to infinity but are subject to nonlinear processes such as plastification or softening. Further the nonlinear area $r < r_{nl}$ includes an interior region termed (fracture) process zone $r < r_{nl}$ where the actual debonding phenomena on the micro scale occurs. In case that the K -factor dominated nearfield $r_{nl} < r < R$ is large compared to the enclosed inelastic region (r_p , $r_{nl} \ll R$), it can be assumed that the nearfield indirectly governs the material behaviour in the inelastic region and especially in the fracture determining process zone. This actually is the hypothesis underlying the so-called K -concept: The state of the fracture is sufficiently defined by the stress intensity factor thus enabling a simple fracture criterion whereby fracture occurs when K reaches a critical value termed fracture toughness K_c . In overlaid crack loading modes (mixed mode condition) fracture is determined by interacting K -factors and their critical values.

1.2 Hypothetic crack approach

Fracture mechanics and K -concept can be employed straight forward in a deterministic manner to structures with distinct single or multiple macro cracks of defined

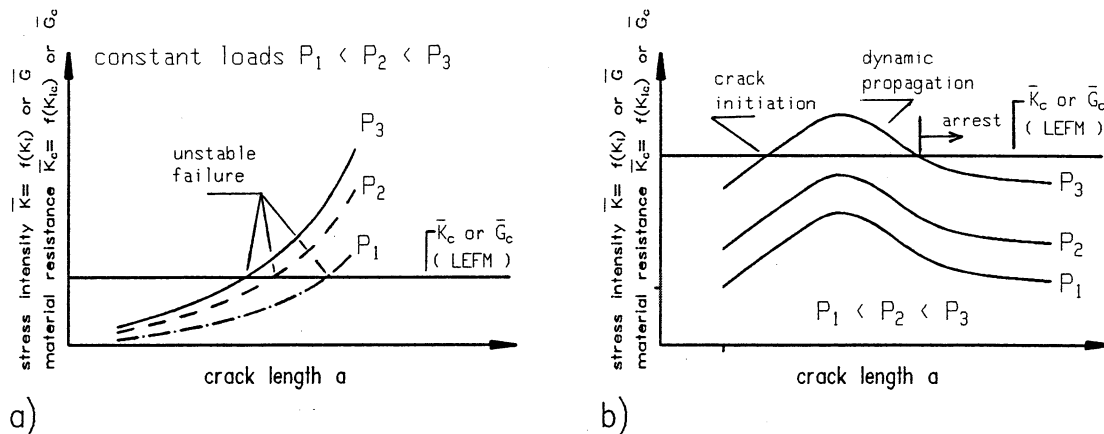
dimensions. However, in most real structures no macro singularities exist in the perfect state, so for instance in case of beams with round holes or with rectangular openings resp. notches which in general are performed with rounded corners. The singularities here are confined to the imperfect state of the structures when stochastically distributed defects (flaws) on the micro level due to local stress concentration have grown, agglomerated and eventually localized into macro cracks. In case of wood, flaw growth resp. agglomeration and macro crack formation can be mutually caused from stresses resulting due to gravity loads and from climate caused eigenstresses. The sizes and to a lesser extent the locations of the macro cracks, to be investigated by fracture mechanics, are unknown what founds the probabilistic nature of the problem.

A suitable way to examine and design such structures is the hypothetical crack approach where the load carrying capacity is traced depending on one or several extending hypothetical macro cracks. Then, considerations based on plausibility and/or probability have to be applied to crack length and load in order to find a reliable design load. Obviously these considerations depend largely on the function of the generalized stress intensity factor \mathbf{K} (or strain energy release rate \mathbf{G}) vs. crack length. The expressions »generalized \mathbf{K} or \mathbf{G} values« mean that the mixed mode quantities K_i , G_i ($i = \text{I, II, III}$) are summarized in one idealized term \mathbf{K} , \mathbf{G} , which is compared to the equally idealized material resistances \mathbf{K}_c , \mathbf{G}_c . Quantitatively this summarizing is performed by means of an appropriate mixed mode interaction criterion.

1.3 Basic types of structure responses

Structures can show completely different functions of \mathbf{K} (or \mathbf{G}) and of corresponding ultimate loads with increasing crack lengths (dead load conditions). Fig. 1a gives a typical example of a simple structure with steadily increasing \mathbf{K} -values and hence generally steeply decreasing ultimate loads. In more complex structures \mathbf{K} functions are encountered which first increase with crack length and after having reached a maximum, \mathbf{K} remains constant or decreases (Fig. 1b). In the latter case the critical load has a stable minimum and crack arrest can occur after initiation and unstable propagation of a crack.

Crack arrest may also occur when the material shows a (non)linear increase in crack resistance with crack elongation. This case shall not be considered here, as all problems due to relative structure sizes and wood brittleness will be considered in a conservative approximation to behave acc. to linear elastic fracture mechanics (LEFM).



Figs. 1a, b Structures with different courses of generalized stress intensity factor vs. crack length
a) structure with unstable failure due to monotonic increasing stress intensity
b) structure with crack arrest after dynamic propagation due to decreasing stress intensity

2 Review of finite element approaches for stress intensity factor determination in mixed mode problems of discrete cracks in orthotropic materials

Several approaches can be applied in case of mixed mode loading conditions for determination resp. separation of the interacting single mode stress intensities K_i resp. of the linear elastically equivalent strain energy release rates or J-integrals G_i , J_i ($i = I, II, III$). At least five major methods (i)–(vi) can be differentiated, whereby methods (i), (ii) are based on the basic definitions of K-factors defining the power of the stress resp. strain field in the crack tip nearfield. Methods (IIIi)–(vi) are principally energy based methods which due to assumptions of linear fracture mechanics, can be employed equally for determination of K-values. Following, only mixed mode I and II in 2D structures with inplane loading in the x-y plane is regarded:

- (i) method based on the explicit singular displacement resp. stress field in the crack tip vicinity. Hereby K_i values are determined from FE computed displacements u , v or stresses σ_x , σ_y , τ_{xy} at the crack faces resp. at the ligament through comparison with closed form expressions for stresses resp. displacements in the nearfield [1] containing K_i as sole unknown quantities.
- (ii) similar to method (i), however the analytical singular displacement fields are implemented in a specific singular fracture mechanics crack tip element [2].

- (IIIi) method based on crack closure integral [3]. The two crack closure integrals G_I , G_{II} ($\rightarrow K_I, K_{II}$) are derived from FE-computed nodal forces F_x, F_y and displacements u, v at the ligament resp. at the crack faces [4], [5], [6], [7].
- (IVi) a rough separation of G_i ($\rightarrow K_i$) values may be performed by assuming the G_I/G_{II} ratio equal to the ratio of opening to shearing forces at the crack tip or to the ratio of opening to shearing forces or stresses within a certain distance on the crack ligament. Total strain energy release rate $G = G_I + G_{II}$ hereby may be computed from various methods, a few of them stated here.
- (Vi) method based on J integral [8]. The splitting of J into components J_I, J_{II} ($\rightarrow K_I, K_{II}$) on a symmetric integration path with coinciding start and end is performed via use of symmetric and anti-symmetric parts of the stress resp. displacement components along the integration path around the crack [9], [10] (see also [11], [12]).

All approaches have advantages and disadvantages with respect to FE discretization effort and further data processing. The finest meshing is needed in (i), the most coarse in (Vi) where however automatic meshing is inconvenient with respect to the symmetric integration path. Method (ii) is bound to non standard FEM software; method (IIIi) needs the least effort for post-processing. Essential is, that all approaches apart from (Vi) are confined to purely linear elastic material behaviour. In this study, method (i) and hereby the more accurate displacement based approach was chosen.

3 Details of applied method

3.1 Determination of stress intensity factors

The calculation approach (i), as said, is based on finite element computed displacements $\bar{\delta}_i$ in the immediate crack tip vicinity resp. extrapolations of these vs. the crack tip ($\lim_{r \rightarrow 0} [\bar{\delta}_i(r)]$). The limit values are then equated with closed form displacement expressions [1] including stress intensities K_I, K_{II} as sole unknown quantities. Once the stress intensities are determined for plane stress or plain strain condition the elastically equivalent energy release rates G_I, G_{II} resp. J-integrals may be computed (or vice versa) as

$$G_I = K_I^2 / E_I^* , \quad G_{II} = K_{II}^2 / E_{II}^* , \quad (1a, b)$$

where $E_{I,II}^*$ are substitute E-moduli depending on orthotropic material constants. In case of plane stress one obtains

$$E_I^* = 1 / \left[g \sqrt{\frac{s_{11} s_{22}}{2}} \right] , \quad E_{II}^* = 1 / \left[g \frac{s_{11}}{\sqrt{2}} \right] , \quad (2a, b)$$

$$g = \left[\sqrt{\frac{s_{22}}{s_{11}}} + \frac{2 s_{12} + s_{66}}{2 s_{11}} \right]^{1/2} . \quad (2c)$$

with quantities s_{ij} as compliances of the generalized Hooke's law

$$\epsilon_i = s_{ij} \sigma_j \quad (i, j = 1, 2, \dots, 6). \quad (3)$$

In case of plane stress in the $1 = x, 2 = y$ plane ($\epsilon_1 = \epsilon_x, \epsilon_2 = \epsilon_y, \epsilon_6 = \gamma_{xy}$) and principal orthotropic material axes coinciding with the coordinate axes, four independent compliance values s_{ij} ($i, j = 1, 2, 6$) remain i. e.: $s_{11}, s_{22}, s_{12} = s_{21}, s_{66}$. The compliances are related to the engineering constants by (note that definitions of Poisson ratios ν_{xy}, ν_{yx} differ compared to [13])

$$s_{11} = 1/E_x , \quad s_{22} = 1/E_y , \quad s_{66} = G_{xy} , \quad s_{12} = -\nu_{xy}/E_y , \quad s_{21} = -\nu_{yx}/E_x . \quad (4a-e)$$

In case of plain strain the compliances s_{ij} in eqs. (2) have to be replaced by analogous values b_{ij} which are related to compliances acc. to

$$b_{ij} = s_{ij} - s_{12} s_{j3} / s_{33} \quad (i, j = 1, 2, 6). \quad (5)$$

The closed form expressions for the near field displacements u, v in the $1 = x, 2 = y$ directions of an orthotropic continuum where the principal material axes coincide with the coordinate axes are [1]:

$$u = \sqrt{\frac{2r}{\pi}} \left[K_I \operatorname{Re}(a_{11}) + K_{II} \operatorname{Re}(a_{12}) \right] , \quad (6a, b)$$

$$v = \sqrt{\frac{2r}{\pi}} \left[K_I \operatorname{Re}(a_{21}) + K_{II} \operatorname{Re}(a_{22}) \right]$$

where

$$a_{11} = \frac{1}{\mu_1 - \mu_2} [\mu_1 p_2 c_1 - \mu_2 p_1 c_2] , \quad (7a)$$

$$a_{12} = \frac{1}{\mu_1 - \mu_2} [p_2 c_1 - p_1 c_2] , \quad (7b)$$

$$a_{21} = \frac{1}{\mu_1 - \mu_2} [\mu_1 q_2 c_1 - \mu_2 q_1 c_2] , \quad (7c)$$

$$a_{22} = \frac{1}{\mu_1 - \mu_2} [q_2 c_1 - q_1 c_2] , \quad (7d)$$

$$c_1 = \sqrt{\cos \vartheta + \mu_2 \sin \vartheta} , \quad c_2 = \sqrt{\cos \vartheta + \mu_1 \sin \vartheta} , \quad (8a, b)$$

$$p_j = s_{11} \mu_j^2 + s_{12} , \quad q_j = (s_{12} \mu_j^2 + s_{22}) / \mu_j \quad (j = 1, 2) . \quad (8c, d)$$

Quantities μ_j are the roots of the algebraic auxiliary equation

$$s_{11} \mu^4 + (2s_{12} + s_{66}) \mu^2 + s_{22} = 0 \quad (9)$$

which are always complex – here purely imaginary [13] – occur in conjugate pairs and may be explicitly given as (in case of plain strain, quantities s_{ij} have to be replaced by b_{ij})

$$\mu_{1,2} = \sqrt{\frac{-(2s_{12} + s_{66}) \pm \sqrt{(2s_{12} + s_{66})^2 - 4s_{11}s_{22}}}{2s_{11}}} , \quad (10a, b)$$

$$\bar{\mu}_{1,2} = -\mu_{1,2} . \quad (10c, d)$$

It is evident from definition of mode I and II when displacements u, v are regarded at the crack faces ($\vartheta = 180^\circ$) eqs. (6a, b) decouple: $\text{Re}(a_{11}) = \text{Re}(a_{22}) \equiv 0$. So for $\vartheta = 180^\circ$ one receives for the total opening and sliding displacements (see Fig. 2)

$$\Delta u(r) = 2 u(r) = \sqrt{r} K_{II} \operatorname{Re}(a_{12}) 2 \sqrt{\frac{2}{\pi}}, \quad (11a)$$

$$\Delta v(r) = 2 v(r) = \sqrt{r} K_I \operatorname{Re}(a_{21}) 2 \sqrt{\frac{2}{\pi}} \quad (11b)$$

and then

$$K_I = c_I \lim_{r \rightarrow 0} \frac{\Delta v(r)}{\sqrt{r}}, \quad K_{II} = c_{II} \lim_{r \rightarrow 0} \frac{\Delta u(r)}{\sqrt{r}} \quad (12a, b)$$

where

$$c_I^{-1} = \operatorname{Re}(a_{21}) 2 \sqrt{\frac{2}{\pi}}, \quad c_{II}^{-1} = \operatorname{Re}(a_{12}) 2 \sqrt{\frac{2}{\pi}}.$$

The limit values $\lim_{r \rightarrow 0} \Delta v/\sqrt{r}$ resp. $\lim_{r \rightarrow 0} \Delta u/\sqrt{r}$ are determined from finite element computed displacements $\Delta \bar{v}$, $\Delta \bar{u}$ as approximations of exact solutions Δv , Δu . Figure 2 shows the FE displacement results in a generalized manner. For evaluation of the limit values, the $\Delta \bar{v}(r)$, $\Delta \bar{u}(r)$ functions in the easiest case may be regarded linear [14], but generally any non linear fit and limit procedure may be used. The linear approximation simply forwards

$$\frac{\Delta \bar{v}(r)}{\sqrt{r}} = a_I r + b_I \quad \rightarrow \quad \lim_{r \rightarrow 0} \frac{\Delta \bar{v}(r)}{\sqrt{r}} = b_I, \quad (13a)$$

$$\frac{\Delta \bar{u}(r)}{\sqrt{r}} = a_{II} r + b_{II} \quad \rightarrow \quad \lim_{r \rightarrow 0} \frac{\Delta \bar{u}(r)}{\sqrt{r}} = b_{II}. \quad (13b)$$

Inserting eqs. (13a, b) in eqs. (12a, b) gives

$$K_I = c_I b_I, \quad K_{II} = c_{II} b_{II}. \quad (14a, b)$$

3.2 Determination of critical load

Having determined K_I , K_{II} for a deliberate load P resp. load arrangement $P = f(P_1, P_2, \dots, P_n)$ the load multiplier for critical load, $n = P_{cr}/P$, can be determined

from an appropriate mixed mode fracture criterion. Without further discussion the interaction criterion acc. to [15]

$$\left(\frac{K_I}{K_{Ic}}\right) + \left(\frac{K_{II}}{K_{IIc}}\right)^2 = 1. \quad (15)$$

shall be assumed; the load multiplier then is

$$n = \frac{-s + \sqrt{s^2 + 4r}}{2r}, \quad r = \left(\frac{K_{II}}{K_{IIc}}\right)^2, \quad s = \frac{K_I}{K_{Ic}}. \quad (16a, b, c)$$

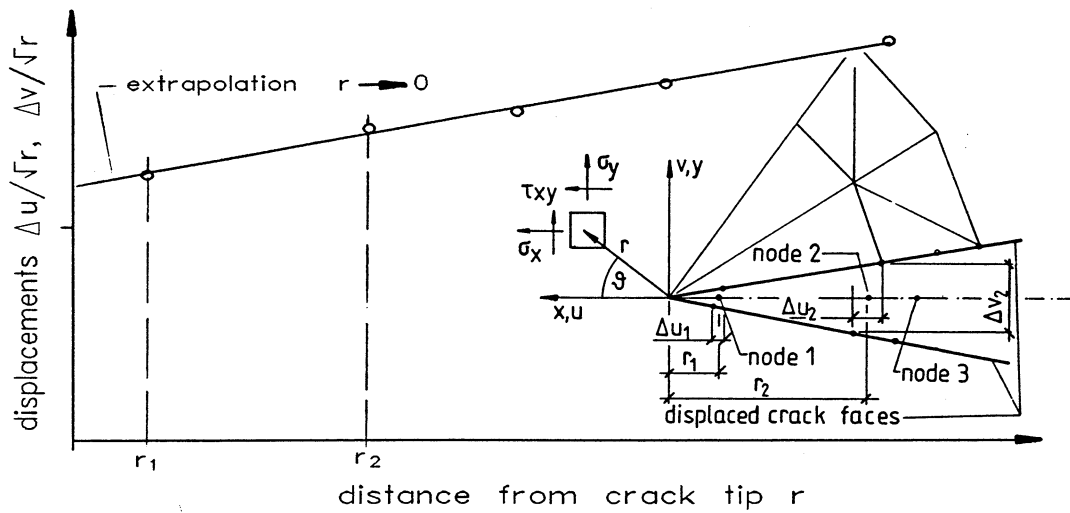


Fig. 2 Definition of displacement resp. stress field in crack tip vicinity and illustration of extrapolation of finite element computed crack face displacements for derivation of mixed mode stress intensities K_I , K_{II}

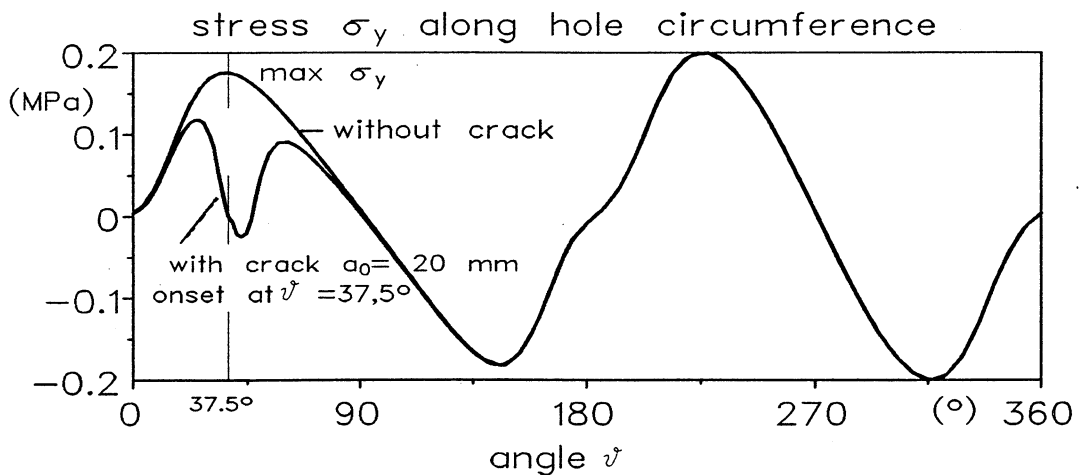


Fig. 3 Stress σ_y perpendicular to beam axis along the contour of a round hole in a straight beam; the stress course is given for a hole without crack and for the case of a crack ($a_0 = 20$ mm) at location $\vartheta = \pi/4$

4 Investigated structures, modelling

4.1 Structures, material properties

Table 1 summarizes the shapes and dimensions of the investigated structures (a–h), all being one-span beams with a concentrated vertical force in mid-span. The computations comprised

- end-notched beams either with a rectangular or a tapered end-notch; structures a resp. b
- beams with round holes of different diameters $\varnothing = h/8$ and $\varnothing = h/3$; structures d resp. e
- beams with square holes of edge lengths $h/3$ either with sharp or rounded corners; structures g resp. h

The notch height of the end-notched beams was throughout $h/4$ and located resp. starting , the latter in case of the tapered notch, at a distance of $h/3$ from the support. The holes were always placed at mid-depth, the distance of the hole centroid from the support in case of the round holes measured $1,5 h$ and $3 h$ in case of the square holes.

All different geometries were evaluated for two significantly different sizes denoted by 1 resp. 2; so, for instance in case of the beam with a rectangular end-notch, structures a1 and a2 were investigated. Size 1 represents a small size with $h = 95$ mm, $b = 45$ mm and size 2 is a large one with $h = 600$ mm and $b = 120$ mm.

The material properties (elasticity constants, fracture toughnesses and shear strength) of the timber beams in the 2D plane stress computations were assumed as following (grain direction coinciding with beam axis is denoted by subscript $x = 1$):

$$E_x = 12000 \text{ MPa} , \quad E_y = 400 \text{ MPa} , \quad G_{xy} = 750 \text{ MPa} ,$$

$$\nu_{xy} = \nu_{yx} E_y/E_x = 0,015 , \quad f_v = 9 \text{ MPa} ,$$

$$K_{Ic} = 16,05 \text{ N}/\sqrt{\text{mm}^3} = 0,5075 \text{ MPa}\sqrt{\text{m}} ,$$

$$K_{IIc} = 70,27 \text{ N}/\sqrt{\text{mm}^3} = 2,2219 \text{ MPa}\sqrt{\text{m}} .$$

The employed elasticity values conform to strength class C30 acc. to European draft standard prEN 338.

4.2 *On-set of hypothetical crack*

In case of structures with *one* explicit geometric discontinuity (structures a, b) the crack on-set was located at this point. In case of square holes with sharp corners (structures g) with *four* singularity locations and two of these located in stress fields with tension perpendicular to the grain, the crack on-set was located at the support oriented corner at the tension edge of the beam. In fact, the stress concentrations resp. stress intensity factors at the diagonally opposite upper corner are somewhat higher and the first crack in tests predominantly occurs at that corner. The differences in stress intensity factors at both corners are revealed in [7].

In case of round holes without explicit strain singularities along the hole contour, similarly to holes with sharp corner, there are two diagonally opposite locations with high stresses perpendicular to the grain. The extreme values in both stress fields very roughly occur at $\vartheta = 45 \pm 10^\circ$ resp. 135 ± 10 , whereby the maximum as in case of sharp corners is at the upper right position. The crack on-set at these locations and first predominantly at upper right position is experimentally substantiated. In this study the crack on-set in circular holes resp. in rectangular holes with rounded corners as in case of square holes with sharp corners was modelled at $\vartheta = \pi/4$.

With respect to crack growth it was assumed that the crack propagates parallel to grain direction, i. e. parallel to beam axis.

4.3 *Some modeling details*

Figures (4a, b) to (9a, b) show for all investigated structures a contour plot of the complete deformed and undeformed structure and close-ups of the finite element meshing (deformed structure) including the complete notch or hole resp. the immediate crack tip vicinity. Due to loading and geometry symmetry only half of the entire structures were discretized. All structures were automatically meshed specifying maximum element sizes for the remote areas and the crack tip area.

Throughout a six node triangular element was used and for the first element row around the crack tip the element option of a distorted mid-side node in quarter position, in order to introduce a strain singularity, was taken. Nearly all crack tip areas were modelled with 16 elements in circumference and the edge lengths of elements connected to the crack tip were mostly 1/8 of the crack length a . For one structure (b2) the influence of element sizes in the crack tip area was investigated

Geometry	structure	h	b	distance of notch (start) to support	notch depth	distance of hole centroid to support	hole diameter d	square hole edge length	corner radius r
		[mm]	[mm]	[mm]	[mm]	[mm]	[mm]	[mm]	[mm]
	a1	95	45	31,7	23,8	-	-	-	-
	a2	600	120	200	150	-	-	-	-
	b1	95	45	31,7	23,8	-	-	-	-
	b2	600	120	200	150	-	-	-	-
	d1	95	45	-	-	142,5	11,9	-	-
	d2	600	120	-	-	900	75	-	-
	e1	95	45	-	-	142,5	31,7	-	-
	e2	600	120	-	-	900	200	-	-
	g1	95	45	-	-	285	44,8	31,7	-
	g2	600	120	-	-	1800	282,4	200	-
	h1	95	45	-	-	285	44,8	31,7	4,75
	h2	600	120	-	-	1800	282,4	200	30

Table 1 Compilation of investigated geometries resp. structures

with respect to displacement extrapolation resp. K-evaluation. In this specific case an edge length of the crack tip elements of $a/4$ gave only a 3 % difference to the results obtained with $a/8$. Further, the results of the displacement extrapolations seemed to be quite insensitive whether the first two or three nodes were used for the linear displacement extrapolations (13a, b).

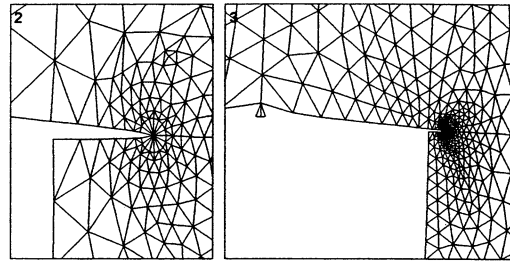
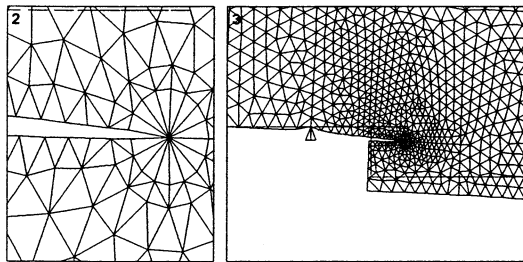
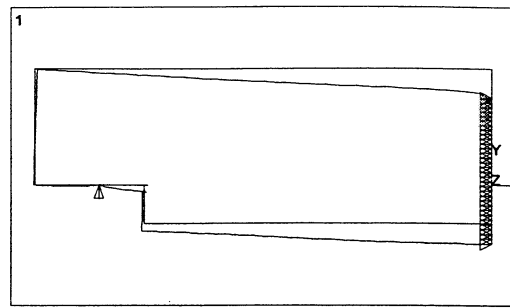
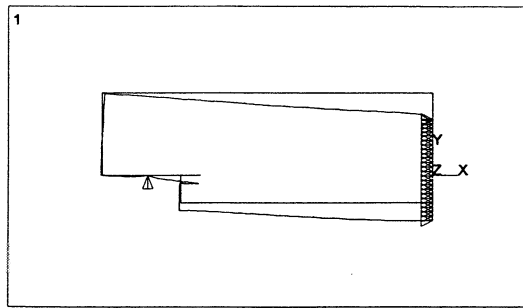
5 Results

The major computational results, i. e. stress intensities K_I , K_{II} and absolute resp. normalized shear force capacities V_f , \bar{V}_f are compiled in tables 2 to 7. Normalized shear force capacity $\bar{V}_f = V_f/V_0$ is defined as the ratio of absolute shear force capacity V_f divided by respective "formal" shear force capacity $V_0 = b \cdot h (2/3) f_v$, thus illustrating the impact of the hole or notch ($f_v = 9$ MPa). For comparison with other computational approaches the results according to initial crack and mean stress method (paper 5) are given, too. Figs. 10 to 15 give graphical illustrations of obtained K_I , K_{II} functions resp. of related normalized shear force capacities vs. hypothetical crack lengths.

5.1 Geometries with round and square holes

For all investigated structures with round holes and square holes with rounded corners stress intensity K_I increases with crack length a up to a maximum and then decreases with further crack elongation. The maximum is reached at rather small crack lengths of about 5 mm in case of small structures (size 1) and is located at about 20 mm in case of large structures (size 2). In case of the square hole with sharp corners, K_I is a decreasing function of crack length throughout, what is also true for K_{II} of all structures discussed in this chapter.

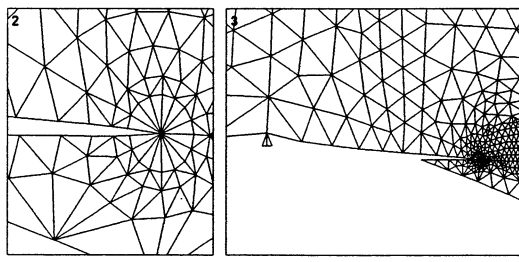
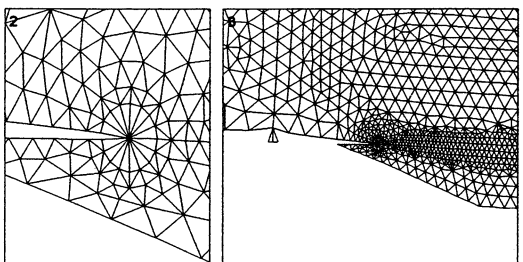
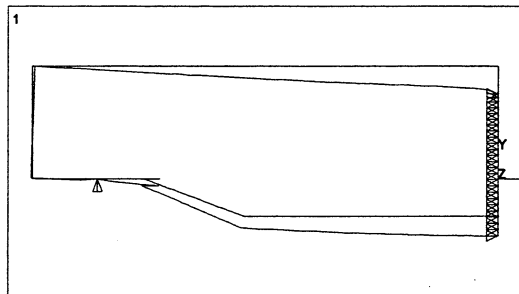
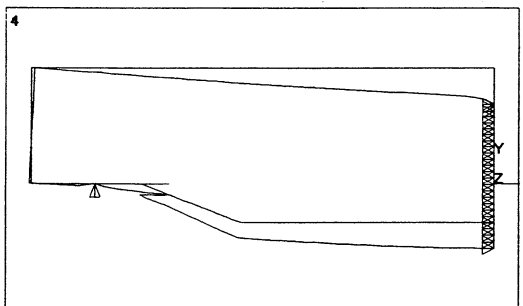
The load capacities obtained from interaction criterion (15) represent coarsely the inverse of the sketched different K_I , K_{II} courses – where K_{II} contribution is strongly relativated by the assumed fourfold higher magnitude of fracture toughness in mode II and the quadratic consideration of the ratio K_{II}/K_{IIc} . In general, except structures g1, g2, the load bearing capacities first drop with increasing crack length; after having reached a minimum the load bearing capacities remain rather constant or even show a slight increase in some cases. Structures g1, g2 with stress singularities show a continuous capacity increase vs. crack length up to very large crack lengths of about 60 resp. 250 mm in case of small and large beams. This behaviour actually reveals that the singularity situation in the area of the sharp edged corner is smoothed with the developing crack.



crack length= 20 mm, H=95

crack length 20 mm, H=600

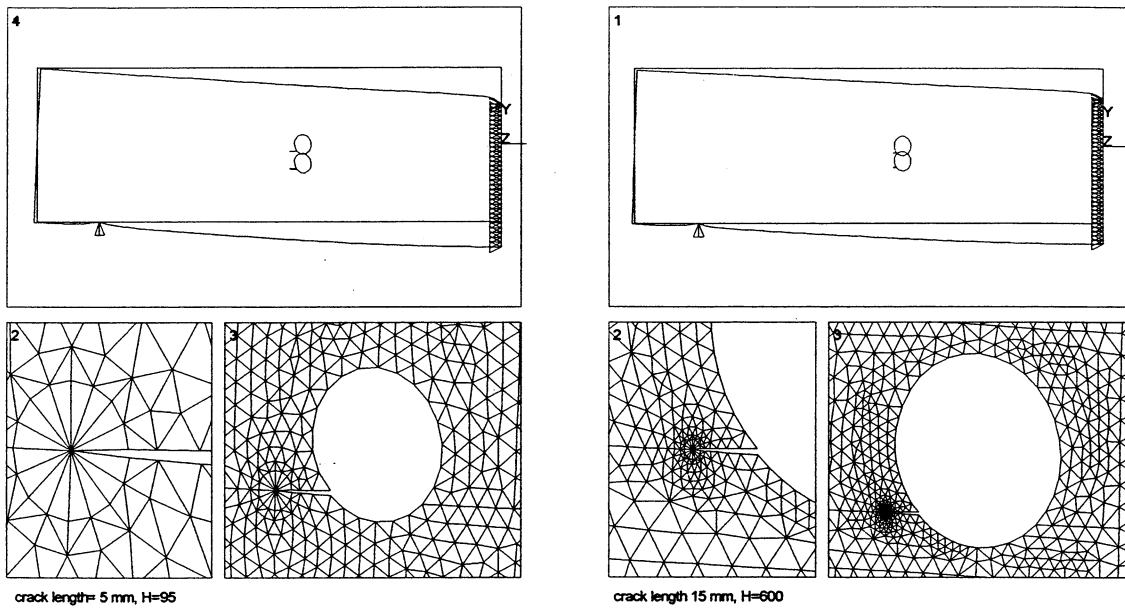
Figs. 4a, b Rectangularly end-notched beam; contour plot of undeformed and deformed structure and finite element meshing of crack tip resp. notch
 a) small beam (structure a1) with relatively large crack
 b) large beam (structure a2) with relatively small crack



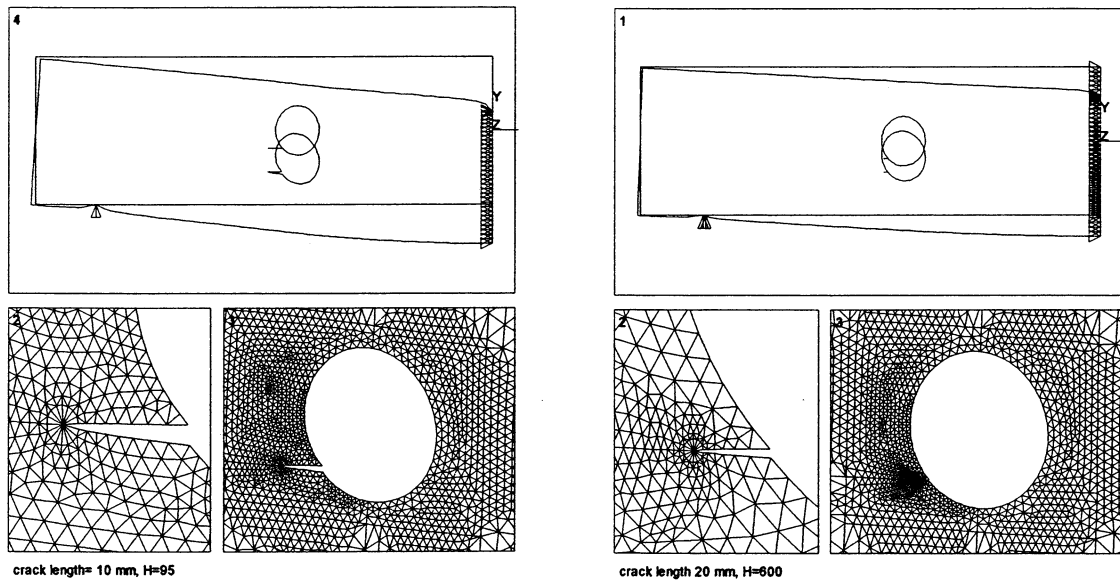
crack length 20 mm, H=95

crack length 75 mm, H=600

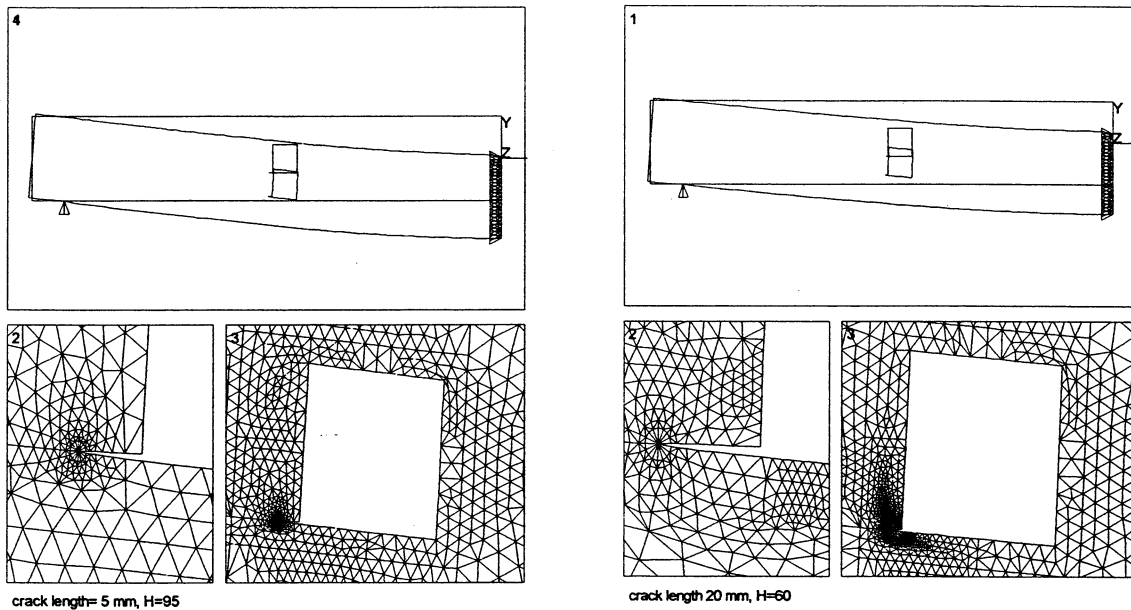
Figs. 5a, b Tapered end-notched beam; contour plot of undeformed and deformed structure and finite element meshing of crack tip resp. notch
 a) small beam (structure b1) with relatively large crack
 b) large beam (structure b2) with relatively large crack



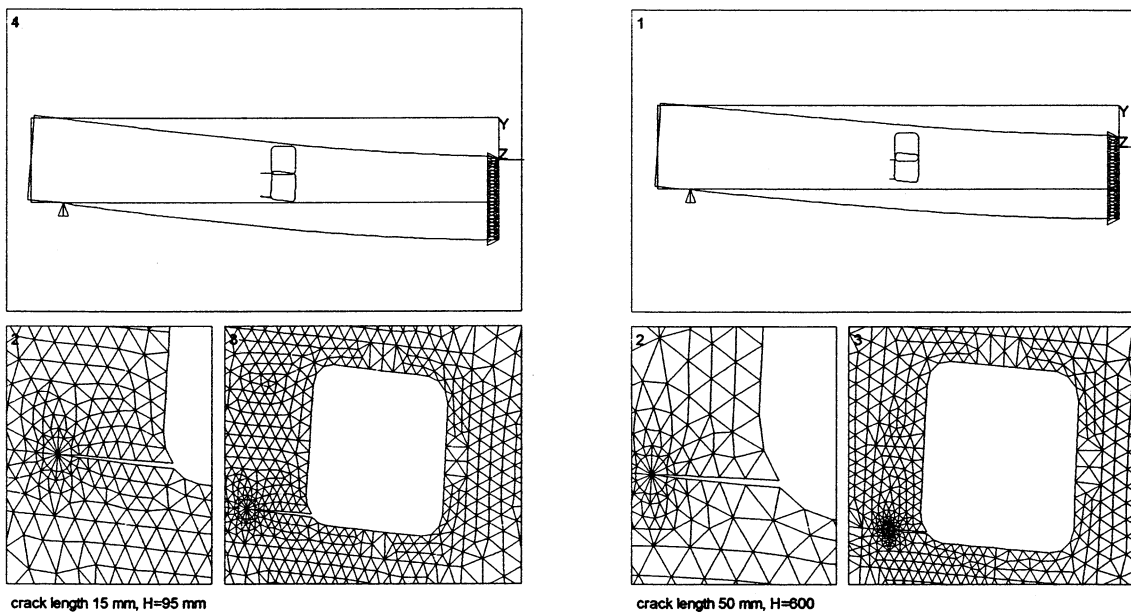
Figs. 6a, b Beam with round hole of relatively small diameter; contour plot of undeformed and deformed structure and finite element meshing of crack tip resp. crack area
 a) small beam (structure d1) with relatively medium sized crack
 b) large beam (structure d2) with relatively small crack



Figs. 7a, b Beam with round hole of relatively large diameter; contour plot of undeformed and deformed structure and finite element meshing of crack tip resp. crack area
 a) small beam (structure e1) with relatively medium sized crack
 b) large beam (structure e2) with relatively small crack



Figs. 8a, b Beam with square hole and sharp corners; contour plot of undeformed and deformed structure and finite element meshing of crack tip resp. crack area
 a) small beam (structure g1) with relatively small crack
 b) large beam (structure g2) with relatively small crack



Figs. 9a, b Beam with square hole and rounded corners; contour plot of undeformed and deformed structure and finite element meshing of crack tip resp. crack area
 a) small beam (structure h1) with relatively medium sized crack
 b) large beam (structure h2) with relatively medium sized crack

The crack lengths associated with the minimum capacities $\min V_f$ differ with respect to structural sizes and slightly with respect to relative hole geometry. In a rough approximation, in case of the small structures with round holes resp. rounded corners (d1, e1, h1) minimum load capacity V_f resp. \bar{V}_f is related to a crack length a of 5–10 mm and in case of the geometrically similar large structures (d2, e2, h2) $\min V_f$ is bound to crack lengths in the range of 20–25 mm. In case of structures g1, g2 (square holes with sharp corners) irrespective of size, minimum load capacity is related to vanishing crack length.

For the large structures the dependency of V_f vs. a was investigated up to crack lengths of 1–1,5 times of the size of the hole itself i. e. $a \approx 130\text{--}200$ mm (structure g2: $a = 500$ mm). In case of the small structures the investigated crack lengths were in the range of about 2–5 times of the hole sizes of 32 resp. 12 mm. The increase of load capacity from $\min V_f$ onward roughly holds true for crack lengths which are smaller or of comparable size of the hole. In case, the crack exceeds the hole dimension (diameter) of very small holes $\varnothing \approx 10$ mm (structure d1) the load capacity drops rapidly; in this case the crack itself represents the major defect.

Apart from the unrealistically small hole (d1) a hypothetical crack length of about 25 mm delivers a conservative estimation of the load bearing capacity within the range of investigated structures with holes. A comparison of the load capacities of the beams with square holes, made of either sharp or rounded corners, reveals as might be supposed, that rounded corners result in higher load capacities only for very tiny cracks of a few millimeters. From crack lengths of about 5 (small structures g1, h1) resp. 25 mm (large structures g2, h2) onward, no more noticeable difference between rectangular holes with sharp or rounded corners exists, at least in case of investigated corner curvatures.

With respect to different relative sizes of holes, apparently relatively smaller ones result in higher load capacities. The influence of relative hole sizes on load capacity seems to be in the same order of magnitude for small and large sizes. So, quite similar for beams with small (d1, e1) resp. large (d2, e2) sizes a hole diameter of $h/8$ is associated to roughly 60 % higher load capacity compared to holes with a diameter of $h/3$.

With respect to observed influence of absolute dimensions, no difference exists between beams with holes and subsequently discussed beams with end-notches. Comparing load capacities of geometrically similar beams – structures a_i to h_i ($i = 1, 2$) – throughout capacity ratios of

$$V_2/V_1 \approx (b_2/b_1) \sqrt{h_2/h_1} \quad (17)$$

i. e. the general size effect law of linear elastic fracture mechanics (proportionality of load capacity to square root of characteristic dimension (here: h)) emanate as clearly as anticipated. Observe that similar geometry also includes relative crack length to some extent. In absolute

numbers in case of the investigated structures shear force capacities of both sizes 1, 2 – after normalization to equal width – differ by a ratio of about $\sqrt{600/95} = 2,51$ whereas in case of validity of strength of materials approach the load capacity ratio would be $600/95 = 6,32$.

5.2 Geometries with rectangular and tapered end-notches

In case of the rectangularly end-notched beams (structures a1, a2) K_I is roughly constant vs. crack length (a minor increase is encountered for the small structure a1 from crack length $a \approx 20$ mm onwards). Stress intensity K_{II} , alike as for all structures with holes, shows a steady increase with augmenting crack lengths. According to interaction criterion (15) ultimate load for both sizes remains roughly constant with increasing crack length in case of structure a1 a slightly decreasing ultimate load is obtained for crack length $a > 20$ mm. Any deliberately chosen hypothetic crack length in the range of about 10 mm (small size 1) resp. 25–50 mm (large size 2) as in case of the beams with holes – delivers an unconservative estimation of the load bearing capacity as the crack propagates dynamically at given dead load condition. The comparison of the load capacities of the large and small endnotched structures a1, a2 reveals a strong size effect, slightly less than the rigorous \sqrt{h} LEFM effect ($(V_{f,2} b_1 / (V_{f,1} b_2)) \approx 3,2$; $\sqrt{h_2/h_1} = 2,5$).

The tapered end-notched beams b1, b2 show similarly for the small and large size closely matching increases of stress intensities K_I and K_{II} along the whole investigated crack length range. Accordingly ultimate loads decrease degressively until the structures – due to crack lengths equaling taper lengths of $3/4 h$ – approach the response character of rectangular end-notched beams with a notch length of about $1.1 h$ (notch depth: $h/4$).

6 Comparison of results with other fracture mechanics approaches

6.1 Comparison to mean stress resp. initial crack method

The results obtained by mean stress resp. initial crack methods (paper 5) take into account the mixed mode situation. The load bearing capacities are given for one distinct, method dependent hypothetic crack length, which in case of initial crack method varies from 9,1 to 12,9 mm, i. e. can be roughly taken as 10 mm. For mean stress method crack lengths vary from 18 to 22 mm, i. e. an average value of 20 mm can be assumed. Initial crack method throughout with one exception (structure d1), forwards lower to equal shear force capacities than mean stress approach. When comparing the K-concept based load capacities to results obtained by initial crack method consequently roughly equal crack lengths of about 10 mm have to be regarded. Tables 2 to 7 reveal a very good agreement in case of geometries a, b

Geometry resp. struc- ture acc. to Table 1	Hypothetic crack length a mm	Stress intensities		Shear force capacity V_f kN	Normalized shear force capacity ¹⁾ \bar{V}_f -	Absolute and normalized shear force capacity computed by other fracture mechanics approaches			
		K_I $N/\sqrt{\text{mm}^3}$	K_{II} $N/\sqrt{\text{mm}^3}$			»init. crack«		»mean stress«	
						V_f kN	\bar{V}_f -	V_f kN	\bar{V}_f -
a ₁	1	4,15	4,16	8,29	0,32	-	-	-	-
	2	4,14	4,39	8,26	0,32	-	-	-	-
	5	4,08	4,87	8,26	0,32	-	-	-	-
	7	4,05	5,13	8,27	0,32	-	-	-	-
	9,5	-	-	-	-	8,6	0,34	-	-
	10	4,03	5,49	8,24	0,32	-	-	-	-
	15	4,03	5,97	8,11	0,32	-	-	-	-
	19	-	-	-	-	-	-	10,3	0,40
	20	4,08	6,36	7,94	0,31	-	-	-	-
	50	4,83	8,31	6,58	0,26	-	-	-	5
a ₂	5	1,64	1,63	56,04	0,13	-	-	-	-
	9,4	-	-	-	-	56,5	0,13	-	-
	10	1,65	1,72	55,30	0,13	-	-	-	-
	15	1,65	1,78	55,04	0,13	-	-	-	-
	19	-	-	-	-	-	-	55,2	0,13
	20	1,65	1,84	55,11	0,13	-	-	-	-
	50	1,58	2,07	56,16	0,13	-	-	-	-
	75	1,58	2,24	55,54	0,13	-	-	-	-
	100	1,59	2,38	54,84	0,13	-	-	-	-

Table 2: Computational results for stress intensities and absolute resp. normalized shear force capacities depending on hypothetic crack length of rectangular end-notched beam with two different small resp. large sizes (structures a₁, a₂ in table 1). For comparison results acc. to initial crack and mean stress approach (paper 5) are enclosed.

¹⁾ Normalized shear force capacity \bar{V}_f is shear force capacity V_f divided by formal shear force capacity $b \cdot h \cdot (2/3) \cdot f_v$ of gross cross section

Geometry resp. struc- ture acc. to Table 1	Hypothetic crack length a mm	Stress intensities		Shear force capacity V_f kN	Normalized shear force capacity ¹⁾ \bar{V}_f -	Absolute and normalized shear force capacity computed by other fracture mechanics approaches			
		K_I $N/\sqrt{\text{mm}^3}$	K_{II} $N/\sqrt{\text{mm}^3}$			»init. crack«		»mean stress«	
						V_f kN	\bar{V}_f -	V_f kN	\bar{V}_f -
b_1	0,5	1,46	2,39	22,00	0,86	-	-	-	-
	1	1,74	2,78	18,53	0,72	-	-	-	-
	2	2,07	3,24	15,64	0,61	-	-	-	-
	5	2,66	3,99	12,28	0,48	-	-	-	-
	7	2,93	4,31	11,20	0,44	-	-	-	-
	9,5	-	-	-	-	10,6	0,41	-	-
	10	3,20	4,63	10,28	0,40	-	-	-	-
	15	3,66	5,19	9,00	0,35	-	-	-	-
	20	3,95	5,59	8,35	0,33	-	-	-	-
	21	-	-	-	-	-	-	13,9	0,54
	50	4,94	7,83	6,54	0,25	-	-	-	-
b_2	2	0,53	0,87	161,39	0,32	-	-	-	-
	5	0,65	1,06	131,93	0,31	-	-	-	-
	9,7	-	-	-	-	114,3	0,26	-	-
	10	0,78	1,23	110,79	0,26	-	-	-	-
	15	0,86	1,34	100,48	0,23	-	-	-	-
	20	0,96	1,47	90,72	0,21	-	-	-	-
	21	-	-	-	-	-	-	140,2	0,32
	50	1,19	1,74	73,51	0,17	-	-	-	-
	75	1,34	1,93	65,32	0,15	-	-	-	-
	100	1,46	2,08	60,08	0,14	-	-	-	-

Table 3: Computational results for stress intensities and absolute resp. normalized shear force capacities depending on hypothetic crack length of tapered end-notched beams with two different small resp. large sizes (structures b_1 , b_2 in table 1). For comparison results acc. to initial crack and mean stress approach (paper 5) are enclosed.

¹⁾ see Table 2

Geometry resp. struc- ture acc. to Table 1	Hypothetic crack length a mm	Stress intensities		Shear force capacity V_f kN	Normalized shear force capacity ¹⁾ \bar{V}_f -	Absolute and normalized shear force capacity computed by other fracture mechanics approaches			
		K_I $N/\sqrt{mm^3}$	K_{II} $N/\sqrt{mm^3}$			»init. crack«		»mean stress«	
						V_f kN	\bar{V}_f -	V_f kN	\bar{V}_f -
d_1	0,5	1,19	0,72	29,86	1,16	-	-	-	-
	1	1,51	0,97	23,40	0,91	-	-	-	-
	2	1,94	1,43	18,08	0,71	-	-	-	-
	5	1,82	2,15	18,59	0,72	-	-	-	-
	7	1,54	2,60	20,68	0,81	-	-	-	-
	10	0,95	3,26	26,64	1,04	-	-	-	-
	12	0,92	3,69	25,40	0,99	-	-	-	-
	12,9	-	-	-	-	27,70	1,08	-	-
	15	1,07	4,70	20,83	0,81	-	-	-	-
	20	1,31	5,25	17,89	0,70	-	-	-	-
	22	-	-	-	-	-	-	22,60	0,88
	50	1,28	9,22	12,69	0,50	-	-	-	-
d_2	2	0,43	0,25	219,89	0,51	-	-	-	-
	5	0,62	0,39	152,21	0,35	-	-	-	-
	9,2	-	-	-	-	135,6	0,31	-	-
	10	0,74	0,52	126,88	0,29	-	-	-	-
	15	0,78	0,62	119,72	0,28	-	-	-	-
	19	-	-	-	-	-	-	152,3	0,35
	25	0,76	0,78	119,99	0,28	-	-	-	-
	50	0,59	1,14	139,52	0,32	-	-	-	-
	75	0,40	1,52	160,70	0,37	-	-	-	-
	100	0,33	1,86	155,78	0,36	-	-	-	-
	130	0,24	2,23	150,07	0,35	-	-	-	-

Table 4: Computational results for stress intensities and absolute resp. normalized shear force capacities depending on hypothetic crack length for beams of two different small resp. large sizes (structures d_1 , d_2 in table 1) with small round holes (diameter $h/8$). For comparison results acc. to initial crack and mean stress approach (paper 5) are enclosed.

¹⁾ see Table 2

Geometry resp. structure acc. to Table 1	Hypothetic crack length a mm	Stress intensities		Shear force capacity V_f kN	Normalized shear force capacity ¹⁾ \bar{V}_f -	Absolute and normalized shear force capacity computed by other fracture mechanics approaches			
		K_I $N/\sqrt{\text{mm}^3}$	K_{II} $N/\sqrt{\text{mm}^3}$			»init. crack«		»mean stress«	
						V_f kN	\bar{V}_f -	V_f kN	\bar{V}_f -
e ₁	1	2,01	1,19	17,62	0,69	-	-	-	-
	2	2,63	1,66	13,46	0,52	-	-	-	-
	5	3,08	2,57	11,32	0,44	-	-	-	-
	7	3,45	3,17	10,05	0,39	-	-	-	-
	9,2	-	-	-	-	8,20	0,32	-	-
	10	3,42	3,57	10,02	0,39	-	-	-	-
	12	3,05	3,92	10,95	0,43	-	-	-	-
	15	3,16	4,43	10,46	0,41	-	-	-	-
	19	-	-	-	-	-	-	10,30	0,40
	20	2,82	4,41	11,49	0,45	-	-	-	-
	50	1,51	9,78	11,61	0,45	-	-	-	-
e ₂	2	0,47	0,27	200,03	0,46	-	-	-	-
	5	0,74	0,42	128,08	0,30	-	-	-	-
	7	0,84	0,51	112,17	0,26	-	-	-	-
	9,2	-	-	-	-	75,60	0,18	-	-
	10	0,96	0,60	97,88	0,23	-	-	-	-
	12	1,06	0,67	89,01	0,21	-	-	-	-
	15	1,10	0,72	85,54	0,20	-	-	-	-
	19	-	-	-	-	-	-	90,30	0,21
	20	1,21	0,83	77,59	0,18	-	-	-	-
	35	1,35	1,07	69,31	0,16	-	-	-	-
	50	1,35	1,25	68,25	0,16	-	-	-	-
	75	1,31	1,54	69,08	0,16	-	-	-	-
	100	1,22	1,80	71,76	0,17	-	-	-	-
	130	1,11	2,15	74,46	0,17	-	-	-	-
200	0,82	2,81	82,38	0,19	-	-	-	-	

Table 5: Computational results for stress intensities and absolute resp. normalized shear force capacities depending on hypothetic crack length for large round hole with two different small resp. large sizes (structures e₁, e₂ in table 1). For comparison results acc. to initial crack and mean stress approach (paper 5) are enclosed.

¹⁾ see Table 2

Geometry resp. struc- ture acc. to Table 1	Hypothetic crack length a mm	Stress intensities		Shear force capacity V_f kN	Normalized shear force capacity ¹⁾ \bar{V}_f -	Absolute and normalized shear force capacity computed by other fracture mechanics approaches			
		K_I $N/\sqrt{\text{mm}^3}$	K_{II} $N/\sqrt{\text{mm}^3}$			»init. crack«		»mean stress«	
						V_f kN	\bar{V}_f -	V_f kN	\bar{V}_f -
g_1	1	4,89	5,39	6,96	0,27	-	-	-	-
	2	4,72	5,67	7,15	0,28	-	-	-	-
	5	4,46	6,45	7,37	0,29	-	-	-	-
	7	4,34	6,70	7,48	0,29	-	-	-	-
	9,1	-	-	-	-	6,0	0,23	-	-
	10	4,19	7,11	7,61	0,30	-	-	-	-
	15	3,81	7,65	8,05	0,31	-	-	-	-
	18	-	-	-	-	-	-	7,2	0,28
	20	3,56	8,30	8,25	0,32	-	-	-	-
	30	3,04	9,44	8,68	0,34	-	-	-	-
	50	2,10	11,62	9,24	0,36	-	-	-	-
	60	1,75	11,27	10,04	0,39	-	-	-	-
g_2	5	1,91	2,12	47,65	0,11	-	-	-	-
	9,1	-	-	-	-	45,5	0,11	-	-
	10	1,87	2,23	47,20	0,11	-	-	-	-
	18	-	-	-	-	-	-	48,3	0,11
	20	1,83	2,41	48,65	0,11	-	-	-	-
	50	1,68	2,67	51,18	0,12	-	-	-	-
	75	1,58	2,87	53,03	0,12	-	-	-	-
	100	1,47	3,03	55,11	0,13	-	-	-	-
	150	1,33	3,44	56,85	0,13	-	-	-	-
	200	1,14	3,72	60,50	0,14	-	-	-	-
	300	0,88	4,52	61,65	0,14	-	-	-	-
	400	0,66	5,22	61,40	0,14	-	-	-	-
500	0,51	5,84	59,63	0,14	-	-	-	-	

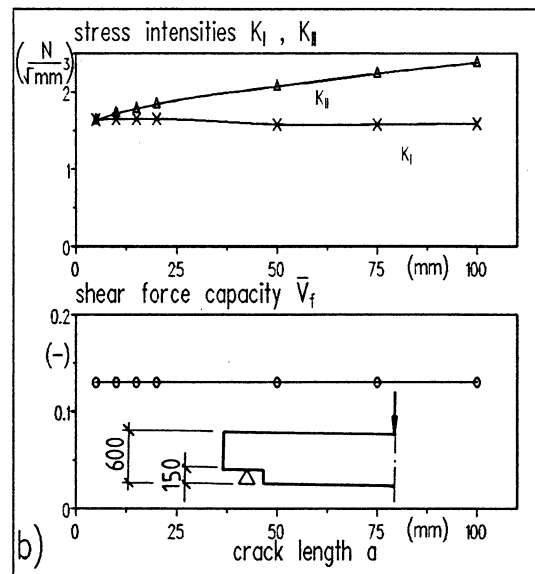
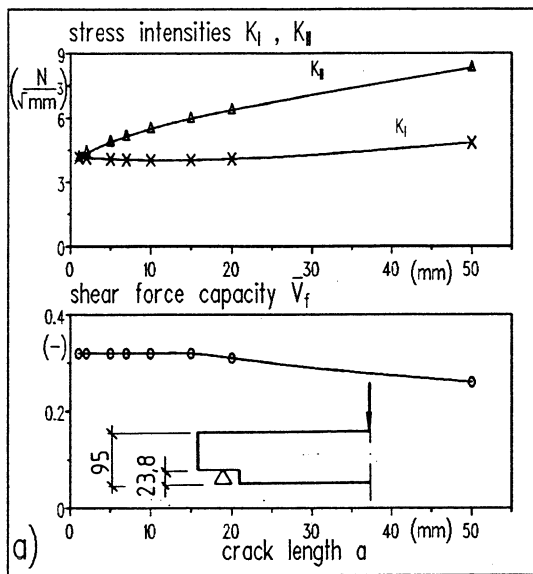
Table 6: Computational results for stress intensities and absolute resp. normalized shear force capacities depending on hypothetic crack length for large square hole with sharp corners (edge length $h/3 = 31,7$ mm) in beam with two different small resp. large sizes (structures g_1 , g_2 in table 1). For comparison results acc. to initial crack and mean stress approach (Paper 5) are enclosed.

¹⁾ see Table 2

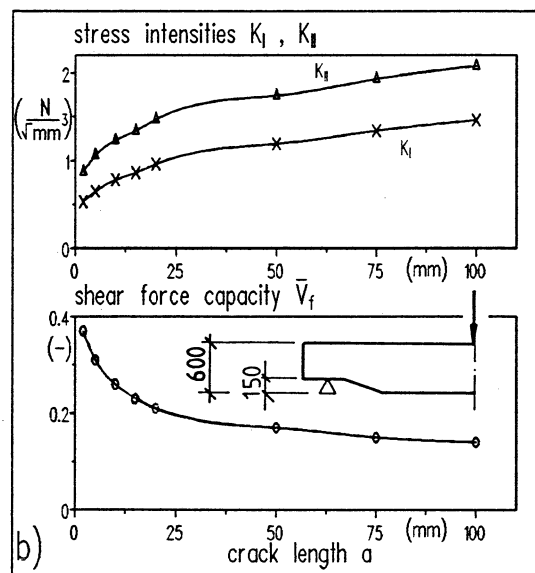
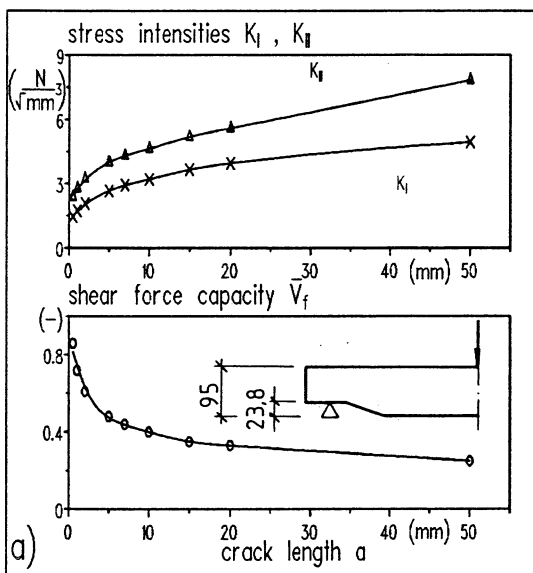
Geometry resp. structure acc. to Table 1	Hypothetic crack length a mm	Stress intensities		Shear force capacity V_f kN	Normalized shear force capacity ¹⁾ \bar{V}_f -	Absolute and normalized shear force capacity computed by other fracture mechanics approaches			
		K_I $N/\sqrt{\text{mm}^3}$	K_{II} $N/\sqrt{\text{mm}^3}$			»init. crack«		»mean stress«	
						V_f kN	\bar{V}_f -	V_f kN	\bar{V}_f -
h_1	1	3,20	2,26	11,02	0,43	-	-	-	-
	2	3,89	3,14	8,98	0,35	-	-	-	-
	5	4,15	4,66	8,19	0,32	-	-	-	-
	7	4,05	5,26	8,24	0,32	-	-	-	-
	9,1	-	-	-	-	6,2	0,24	-	-
	10	3,95	5,99	8,25	0,32	-	-	-	-
	15	3,63	6,79	8,59	0,33	-	-	-	-
	18	-	-	-	-	-	-	7,6	0,31
	20	3,32	7,53	8,92	0,35	-	-	-	-
	50	1,91	11,09	9,85	0,38	-	-	-	-
h_2	5	1,15	0,79	82,10	0,19	-	-	-	-
	9,1	-	-	-	-	52,6	0,12	-	-
	10	1,45	1,12	64,40	0,15	-	-	-	-
	18	-	-	-	-	-	-	61,8	0,14
	20	1,59	1,55	57,70	0,13	-	-	-	-
	30	1,63	1,82	55,53	0,13	-	-	-	-
	50	1,65	2,26	53,50	0,12	-	-	-	-
	75	1,57	2,57	54,62	0,13	-	-	-	-
	100	1,45	2,84	56,61	0,13	-	-	-	-
	200	1,10	3,69	61,88	0,14	-	-	-	-

Table 7: Computational results for stress intensities and absolute resp. normalized shear force capacities depending on hypothetic crack length for large square hole with rounded corners (edge length $h/3 = 31,7$ mm) in beam with two different small resp. large sizes (structures h_1 , h_2 in table 1). For comparison results acc. to initial crack and mean stress approach (paper 5) are enclosed.

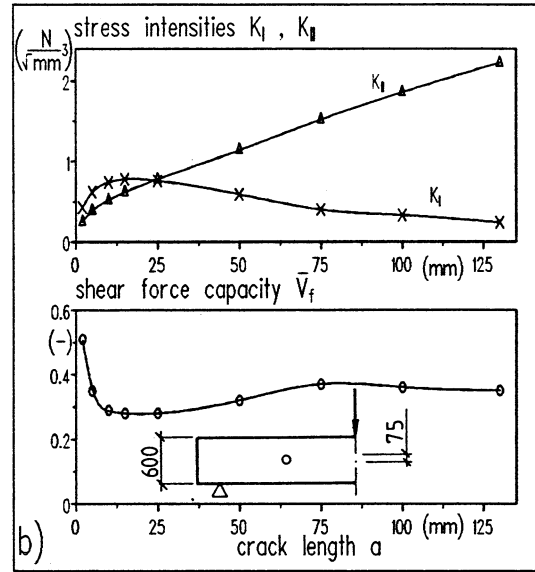
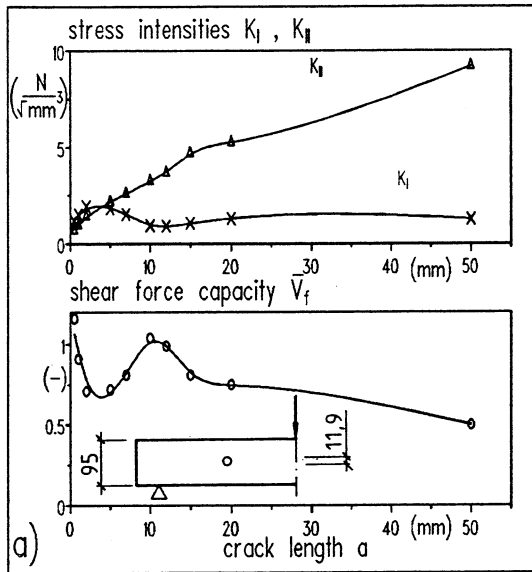
¹⁾ see Table 2



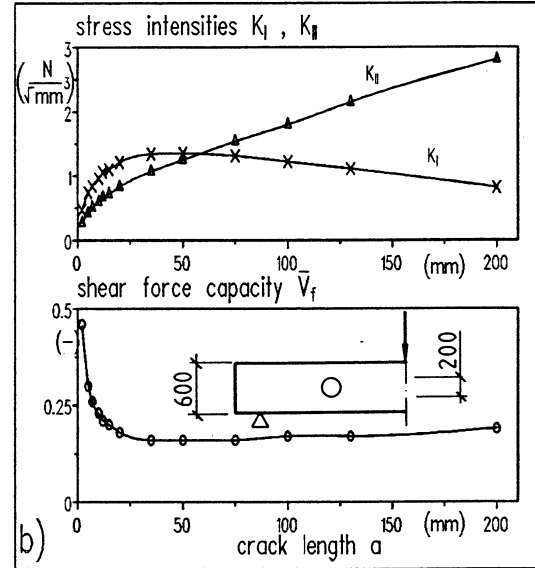
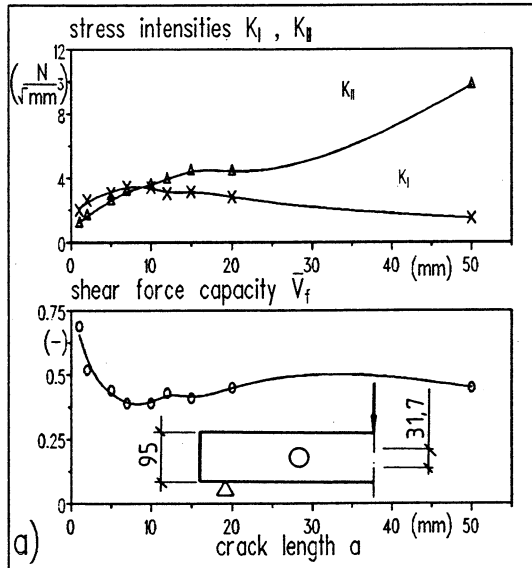
Figs. 10a, b Stress intensities K_I, K_{II} and normalized shear force capacity \bar{V}_f vs. hypothetical crack length a of rectangularly end-notched beam
 a) small structure (a1) b) large structure (a2)



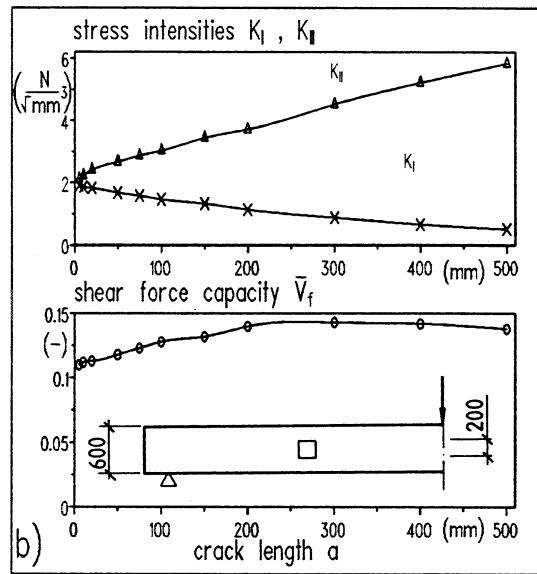
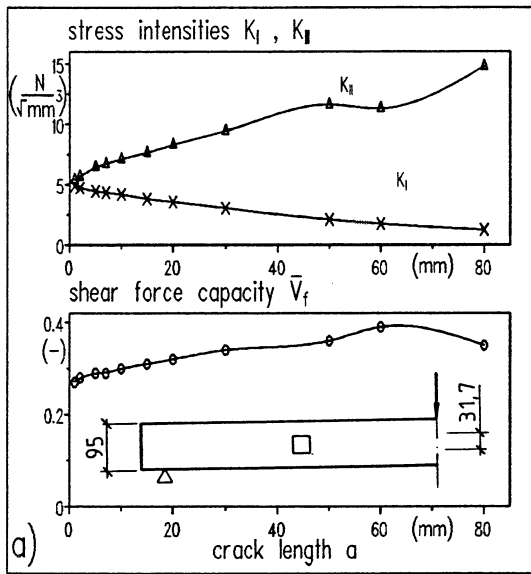
Figs. 11a, b Stress intensities K_I, K_{II} and normalized shear force capacity \bar{V}_f vs. hypothetical crack length a of tapered end-notched beam
 a) small structure (b1) b) large structure (b2)



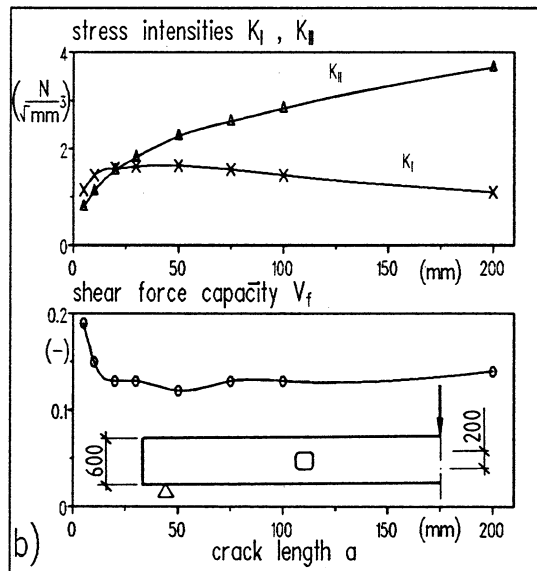
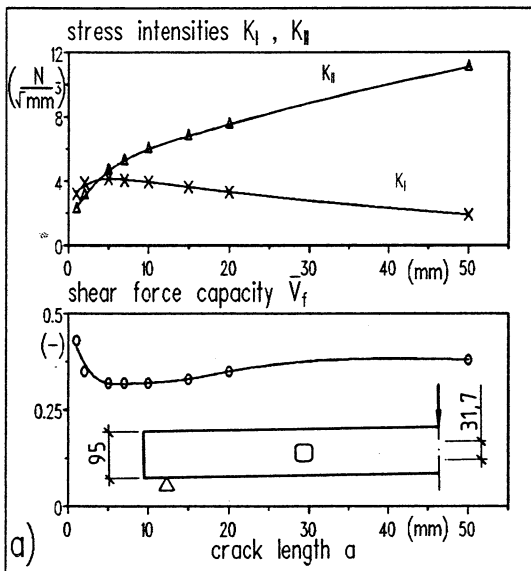
Figs. 12a, b Stress intensities K_I , K_{II} and normalized shear force capacity \bar{V}_f vs. hypothetical crack length a of beam with relatively small round hole
 a) small structure (d1) b) large structure (d2)



Figs. 13a, b Stress intensities K_I , K_{II} and normalized shear force capacity \bar{V}_f vs. hypothetical crack length a of beam with relatively large round hole
 a) small structure (e1) b) large structure (e2)



Figs. 14a, b Stress intensities K_I , K_{II} and normalized shear force capacity \bar{V}_f vs. hypothetic crack length a of beam with relatively large square hole with sharp corners
 a) small structure (g1) b) large structure (g2)



Figs. 15a, b Stress intensities K_I , K_{II} and normalized shear force capacity \bar{V}_f vs. hypothetic crack length a of beam with relatively large square hole with rounded corners
 a) small structure (h1) b) large structure (h2)

and d, whereby values acc. to K-concept are throughout slightly (2 to 7 %) lower. Results of mean stress method in case of structures a1 and b1 are far on the unsafe side.

The comparison of results for structures e, g, h, i. e. structures with relatively large holes ($\varnothing = h/3$), reveals in all cases (apart from structure g2 where identic results are obtained) load capacities which are between 25 to 33 % higher for K-concept approach compared to initial crack method when equal crack lengths of about 10 mm are assumed. When, however in case of the larger size 2 – being of building practice relevancy – the comparison to initial crack method (there: $a \approx \text{const} = 10 \text{ mm}$) is based on a crack length of 20 mm, again a very good agreement of both approaches within a few percent deviation is obtained.

With respect to the tapered end-notched beams (structures b1, b2), despite the good agreement of results between K-concept and initial crack method at "initial" crack length of about 10 mm it should be beared in mind, that increased crack lengths ($a \geq 10 \text{ mm}$) – unlike all other investigated structures – result in further significantly decreasing load capacities. The latter example reveals that a design based on a single crack length ($a \approx 10 \text{ to } 20 \text{ mm}$) is insufficient with certain structures.

6.2 Comparison to beam compliance method

Comparison between results of K-concept and beam compliance method due to the nature of the latter method based on engineering beam theory in case of investigated geometries is only possible for the rectangularly end-notched beam, i. e. structures a1, a2. Beam compliance solutions for tapered end-notched beams (structures b1, b2) include a semi-empiric factor. The analytical solution for shear force capacity of an end-notched beam given by Gustafsson (paper 2) in case of $E_x/G_{xy} \approx 16$ is

$$V_f = b \sqrt{h} \alpha \frac{1/3,1 \sqrt{G_{Ic} E_x}}{\sqrt{\alpha (1-\alpha)} + 0,79 \beta \sqrt{1/\alpha - \alpha^2}} \quad (18)$$

thus delivering for the small and large rectangularly end-notched structures ($G_{Ic} = 0,3 \text{ N/mm}$, $\alpha = 0,75$, $\beta = 0,33$):

$$V_f = 9,59 \text{ kN} \quad \rightarrow \quad \bar{V}_f = 9,59 / 25,65 = 0,37 \quad , \quad (\text{structure a1})$$

$$V_f = 64,26 \text{ kN} \quad \rightarrow \quad \bar{V}_f = 64,26 / 432,00 = 0,15 \quad . \quad (\text{structure a2})$$

Taking into account that the compliance based method only considers the mode I action the given results show a very good agreement with the displacement based K-concept results derived here.

As outlined K-concept delivers for both structures a1, a2 rather constant load capacities \bar{V}_f of 0,34 resp. 0,13 for all investigated crack lengths (restricted to the range of the notch length ($h/3$)). Important is that K-concept capacities remain constant for crack length a approaching zero. Actually the limit value $\lim a \rightarrow 0$ is regarded in the compliance method. The capacities according to the latter method are for both structures roughly 15 % higher compared to K-concept.

In order to apply the principle of eq. (18) for rectangularly end-notched beams also to tapered end-notched beams the equation was extended by an empirically determined multiplier [16]

$$k_i = 1 + 1,1 \cdot i^{1,5}/\sqrt{h} \quad (19)$$

where i is the inverse slope of the taper. Equations (19) and (18) deliver for k_i multipliers resp. for load capacities V_f , \bar{V}_f in case of the investigated tapered end-notched beams ($i = 3$):

$$k_i = 1,586 \rightarrow V_f = 15,21 \text{ kN} \rightarrow \bar{V}_f = 0,59 \text{ ,} \quad (\text{structure b1})$$

$$k_i = 1,233 \rightarrow V_f = 79,23 \text{ kN} \rightarrow \bar{V}_f = 0,18 \text{ .} \quad (\text{structure b1})$$

Compared to K-concept results the compliance based capacities for both structures are far too high when crack lengths $a \rightarrow 0$ are considered. When the comparison of both methods is based on hypothetical crack lengths of $a \approx 10\text{--}20$ mm the agreement of both approaches is reasonable in case of the large structure b2 whereas in case of the small structure b1 the capacity overestimation by semi-empiric compliance method is still 50 to 80 %.

7 Design proposal for beams with holes

It seems appropriate to choose the interaction criterion (15) as a basis of the following simple and transparent design proposal

$$\frac{K_{I,d}}{K_{Ic,d}} + \left(\frac{K_{II,d}}{K_{IIc,d}} \right)^2 \leq 1 \text{ ,} \quad K_{Ic,d} = \frac{K_{Ic,k} \cdot k_{\text{mod}}}{\gamma_M} \text{ ,} \quad K_{IIc,d} = \frac{K_{IIc,k} \cdot k_{\text{mod}}}{\gamma_M} \text{ ,} \quad (20a\text{--}c)$$

where $K_{Ic,k}$, $K_{IIc,k}$ are the characteristic values of fracture toughnesses of respective strength classes. The stress intensities $K_{I,d}$, $K_{II,d}$ at design load should be provided by means of solely geometry and load case dependant values, normalized with respect to dimensions and load, i. e. $k_{I,d} = K_{I,d} b \sqrt{h}/F$.

With respect to the material side, derivation of characteristic K-values as one part of the work could probably be resolved quite reasonable with existing material data; a proposal is given in [7]. However, very little knowledge is available at the moment to settle appropriate k_{mod} values accounting for duration of load and climate. A mere adoption of the modification factors given in EC5 seems too rough due to the different physical nature of fracture toughnesses compared to elastic strength values.

With respect to coherent design it is suggested to alter the formal appearance of the EC 5 design formula for end-notched beams, as today's appearance may lead the engineer to a wrong idea of the true fracture mechanics failure nature of the problem. Recognizing that $\sqrt{G_{Ic} E_x}$ in eq. (18) has the dimension of a fracture toughness value, a definitely more transparent form of the design formula would be

$$\tau_d = \frac{3 V}{2 b h \alpha} \leq k K_{Ic,d}, \quad k = [3s \sqrt{h} \sqrt{\alpha(1-\alpha)} + 0,8 \beta \sqrt{1/\alpha - \alpha^2}]^{-1}. \quad (21a, b)$$

The value $s = s_1 \cdot s_2$ in eq. (21b) represents a proportionality factor to be fixed, where component s_1 accounts for the ratio $K_{Ic,k}/\sqrt{G_{Ic,k} E_x}$ and s_2 is an empiric correction factor for adjusting the formula to test results (in EC 5: $s_2 = 1,5$). Note, that solely substitutions were introduced in the basic eq. (18); but now it is immediately obvious to the design engineer that he deals with a brittle fracture problem, the material resistance is transparent and the formula would be in line with afore proposed design equations for holes.

8 Literature

- [1] SIH, G. C., PARIS, P. C., IRWIN, G. R. (1965): On cracks in rectilinearly anisotropic bodies. Int. Journ. of Fracture Mech. 1, pp. 189–203
- [2] FOSCHI, R. O., BARRETT, J. D. (1976): Stress intensity factors in anisotropic plates using singular isoparametric elements. Int. Journ. for Numerical Methods in Eng., Vol. 10, pp. 1281–1287
- [3] IRWIN, G. R. (1957): Analysis of stresses and strains near the end of a crack traversing a plate. Journ. of Applied Mechanics. Vol. 24, pp. 361–364
- [4] RYBICKI, E. F., KANNINEN, M. F. (1977): A finite element calculation of stress intensity factors by a modified crack closure integral. Engineering Fracture mechanics, Vol. 9, pp. 931–938

- [5] SHIVAKUMAR, K. N. et al. (1988): A virtual crack closure technique for calculating stress intensity factors for cracked three dimensional bodies. *Int. Journ. of Fracture*, Vol. 36, pp. R43–R50
- [6] PIZIO, S. (1991): Die Anwendung der Bruchmechanik zur Bemessung von Holzbauteilen, untersucht am durchbrochenen und am ausgeklinkten Träger. Thesis Nr. 9433, University of Zürich
- [7] AICHER, S., SCHMIDT, J., BRUNOLD, S. (1995): Design of timber beams with holes by means of fracture mechanics. Proceedings meeting 28, International Council for Building Research Studies and Documentation, Working Commission W18, paper 28-19-4, Copenhagen
- [8] RICE, J. R. (1968): A path independent integral and the approximate analysis of strain concentration by notches and cracks. *Journ. of applied Mechanics*, Vol. 35, pp. 379–386
- [9] OSHIKAWA, H., KITAGAWA, H., OKAMURA, H. (1979): J integral of a mixed mode crack and its application. in: *Mechanical Behaviour of materials*, Vol. 3, ICM, Cambridge
- [10] LOGEMANN, M. (1991): Abschätzung der Tragfähigkeit von Holzbauteilen mit Ausklinkungen und Durchbrüchen. Thesis, University of Hannover
- [11] YAU, J. F. (1979): Mixed mode fracture analysis using a conversation integral. Thesis, University of Illinois
- [12] BUI, H. D. (1983): Associated path independent J-Integrals for separating mixed modes; in: *J. Mech. Phys. Solids*, Vol. 31, H. 6, pp. 439–448
- [13] LEKHNITSKII, S. G. (1963): *Theory of elasticity of an anisotropic elastic body*. Holden-Day, Inc.
- [14] SOLECKI, J. S. (1989): ANSYS®, *Fracture Mechanics. Revision 4.4 Tutorial DN-T019*, Houston
- [15] WU, E. M. (1967): Application of fracture mechanics to anisotropic plates. *ASME Journal of Applied Mechanics*, Series E, 34, pp. 967–974
- [16] RIBERHOLT, H., ENQUIST, B., GUSTAFSSON, P. J., JENSEN, R. B. (1991): Timber beams notched at the support. Technical University of Denmark, Department of Structural Engineering, Serie R, No. 280, Lyngby

FRACTURE MECHANICS MODELS FOR STRENGTH ANALYSIS OF
TIMBER BEAMS WITH A HOLE OR A NOTCH

Paper 3:

Energy Release Rate Analysis ¹⁾

by

Hans Petersson

Division of Structural Mechanics, Lund University,
Box 118, SE-221 00 Lund, Sweden

¹⁾1995, 23 pages

ENERGY RELEASE RATE ANALYSIS

by

Hans Petersson, LTH, Lund

Abstract

First some basic theory is presented which is then applied on beams with cracks propagating in the longitudinal direction. Some formulae for determining the crack load are given both for finite element analysis and for hand calculations. A procedure for the numerical analysis is outlined. Results from a number of analysed beams with notches and holes are shown and remarks are given on the results from a design point of view.

1 Introduction

Different models may be used in design for fracture analysis of wooden structures. One of the most promising models is based on an energy approach and will be treated and applied in the following subsections. It is often called the energy release rate approach, the compliance method or the virtual crack extension method.

In this study only linear elastic approximations are used for the material behaviour and dynamic and nonlinear geometrical effects are not considered.

The wooden beam structures with notches and holes analysed are summarised in Figure 1 and more accurately described in Appendix 1. Results from the analysis are given after the theoretical treatment of the energy approach for crack analysis.

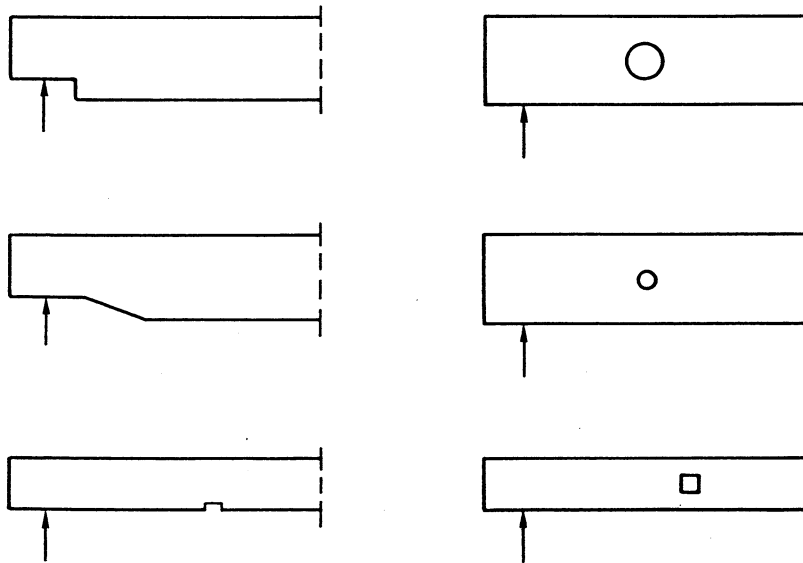


Figure 1 Studied types of beam structures

2 Basic theory

Study a body of linear elastic material loaded in such a way that the strains can be considered as small (except for the cracking process zone). We may write the equilibrium equations as

$$\frac{\partial \sigma_{ij}}{\partial x_j} + b_i = 0 \quad (1)$$

in the volume V , where $\sigma_{ij} = \sigma_{ji}$ denotes a stress component, b_i a body force component and x_j refers to a Cartesian coordinate system. Conventional summation rule is applied. On the boundary surface S the tractions are defined by

$$p_i = n_j \sigma_{ij} \quad (2)$$

where n_j is a direction cosine for the outward normal to the surface S . The stresses are related to the strains ϵ ,

$$\sigma_{ij} = D_{ijkl} \epsilon_{kl} \quad (3)$$

where D is a symmetric tensor. Due to small deformations the strains are

$$\epsilon_{ij} = \frac{1}{2} \left(\frac{\partial u_i}{\partial x_j} + \frac{\partial u_j}{\partial x_i} \right) \quad (4)$$

where u_i denotes a displacement component. Due to the tensor symmetry we may write

$$\epsilon_{ij} \sigma_{ij} = \frac{\partial u_i}{\partial x_j} D_{ijkl} \frac{\partial u_k}{\partial x_l} \quad (5)$$

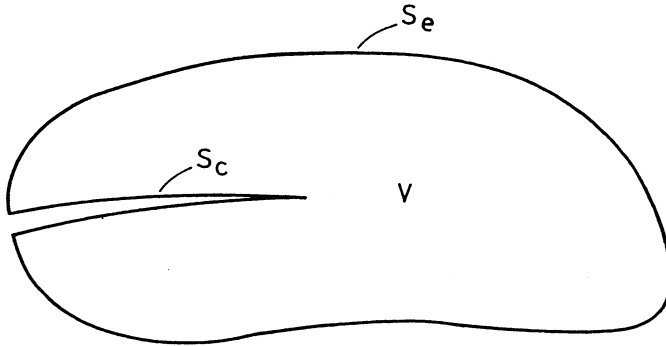


Figure 2 Studied body with a crack. Total boundary surface $S = S_e + S_c$.

For a body with a crack, see Figure 2, a weak formulation of the equilibrium equations may be established, starting from Eq. (1). Weighting functions v_i ($i = 1, 2, 3$) are introduced [1]

$$\int_V v_i \frac{\partial \sigma_{ij}}{\partial x_j} dV + \int_V v_i b_i dV = 0 \quad (6)$$

By integration by parts and utilizing Eq. (2) we get

$$\int_V \frac{\partial v_i}{\partial x_j} \sigma_{ij} dV = \int_V v_i b_i dV + \int_S v_i p_i dS \quad (7)$$

or

$$\int_V \frac{\partial v_i}{\partial x_j} D_{ijkl} \frac{\partial u_k}{\partial x_l} dV = \int_V v_i b_i dV + \int_S v_i p_i dS \quad (8)$$

Let us now assume a disturbance between two studied states, ① and ②. For state ① we choose the weighting functions as

$$v_i = v_i^{①} = u_i^{②} \quad (9)$$

and for state ②

$$v_i = v_i^{②} = u_i^{①} \quad (10)$$

This yields that

$$\int_V \frac{\partial u_i^{②}}{\partial x_j} D_{ijkl} \frac{\partial u_k^{①}}{\partial x_l} dV = \int_V \frac{\partial u_i^{①}}{\partial x_j} D_{ijkl} \frac{\partial u_k^{②}}{\partial x_l} dV \quad (11)$$

and according to Eq. (7) and Eq. (8) that

$$\int_V u_i^{②} b_i^{①} dV + \int_S u_i^{②} p_i^{①} dS = \int_V u_i^{①} b_i^{②} dV + \int_S u_i^{①} p_i^{②} dS \quad (12)$$

Alternatively,

$$\int_V (u_i^{②} b_i^{①} - u_i^{①} b_i^{②}) dV + \int_S (u_i^{②} p_i^{①} - u_i^{①} p_i^{②}) dS = 0 \quad (13)$$

We may now study a case where b_i and p_i are constant between states ① and ② except for p_i over the cracking area S_c . By use of the notation

$$\delta u_i = u_i^{②} - u_i^{①} \quad (14)$$

$$\delta b_i = b_i^{②} - b_i^{①} \quad (15)$$

$$\delta p_i = p_i^{②} - p_i^{①} \quad (16)$$

equation (13) can then be rewritten as

$$\int_V b_i \delta u_i dV + \int_{S_c} p_i \delta u_i dS = \int_{S_c} (u_i \delta p_i - \delta u_i p_i) dS \quad (17)$$

The crack region is assumed to be so thin that the tractions p_i approximately are equal on two adjacent points on the surface S_c (symbolically $S_c = 2A_c$). This makes it meaningful to introduce the relative displacements w_i (crack opening and slips) with respect to the surface A_c instead of the displacements u_i on S_c . By this Eq. (17) can be written as

$$\int_V b_i \delta u_i dV + \int_{S_c} p_i \delta u_i dS = \int_{A_c} (w_i \delta p_i - \delta w_i p_i) dA \quad (18)$$

Let us then study a case where the influence of a disturbance to the system can be expressed by a single crack coordinate a and where $dA = b_c \cdot da$ with constant width b_c . Let us further assume that the crack propagation occurs in a self-similar way corresponding to

$$\delta w_i = \frac{dw_i}{da} \delta a \quad (19)$$

$$\delta p_i = \frac{dp_i}{da} \delta a \quad (20)$$

By these assumptions we may write Eq. (18) as

$$\int_V b_i \frac{du_i}{da} dV + \int_{S_c} p_i \frac{du_i}{da} dS = b_c \int_{A_c} (w_i \frac{dp_i}{da} - \frac{dw_i}{da} p_i) da \quad (21)$$

In order to simplify we assume that the relations between p_i and w_i ($i = 1, 2, 3$) are unique (for the current ratios between p_1, p_2 and p_3 or w_1, w_2 and w_3), see Figure 3. This means that we can write $p_i = p_i(w_i)$ or $w_i = w_i(p_i)$. This yields

$$\int_{a_c} (w_i \frac{dp_i}{da} - \frac{dw_i}{da} p_i) da = \int_0^{p_{i0}} w_i dp_i - \int_{w_{i0}}^0 p_i dw_i = 2G_c \quad (22)$$

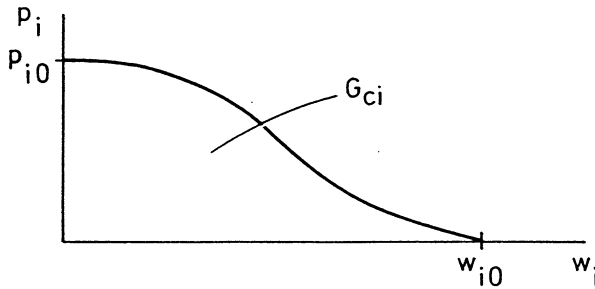


Figure 3 Relation between cohesive stress p_i and relative displacement w_i

where

$$G_c = \sum_{i=1}^3 G_{ci} = \int_0^{p_{i0}} w_i dp_i = \int_0^{w_{i0}} p_i dw_i \quad (23)$$

Substitution of Eq. (22) into (21) results into

$$\int_V b_i \frac{du_i}{da} dV + \int_{S_e} p_i \frac{du_i}{da} dS = 2b_c G_c \quad (24)$$

In case of concentrated forces $\{P\}$ only we may introduce for the cracking load level

$$\{P_c\}^T = [P_{c1} \ P_{c2} \ \dots \ P_{cn}] \quad (25)$$

with the associated displacements $\{u_c\}$,

$$\{u_c\}^T = [u_{c1} \ u_{c2} \ \dots \ u_{cn}] \quad (26)$$

Eq. (24) can then be rewritten on the form

$$\{P_c\}^T \left\{ \frac{du_c}{da} \right\} = 2b_c G_c \quad (27)$$

This basic matrix equation, Eq. (27), can conveniently also be used in finite element analysis.

3 Applied theory

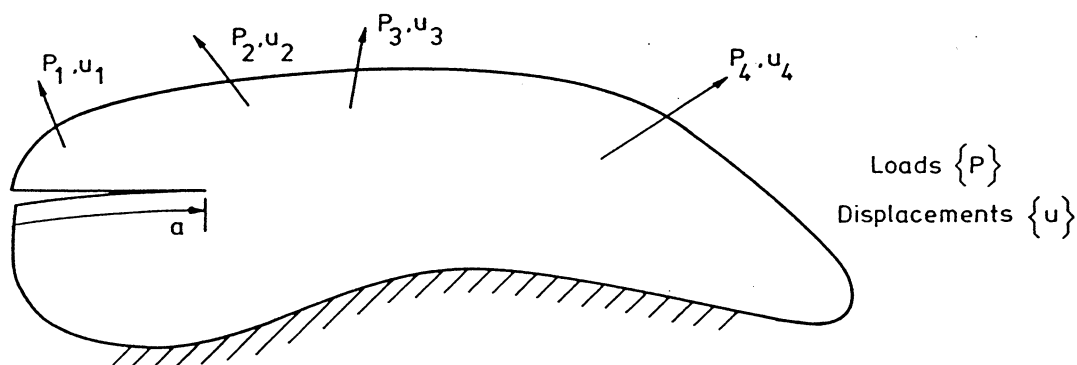


Figure 4 Two-dimensional body with a crack

Study the two-dimensional structure in Figure 4 with a set of constant reference loads $\{P\}$. Assume that the material is linear elastic and denote the associated displacements with $\{u\}$, where

$$\{P\} = \begin{bmatrix} P_1 \\ P_2 \\ \vdots \\ P_n \end{bmatrix} \quad \{u\} = \begin{bmatrix} u_1 \\ u_2 \\ \vdots \\ u_n \end{bmatrix} \quad (28)$$

Denote the crack length with a and the fracture energy per unit length with $b_c G_c$ where G_c is a material parameter. Then assume that the loads are increased proportionally, i.e. the actual loads are $\alpha\{P\}$ where α is gradually increased up to the value α_c , corresponding to stable or unstable crack growth. As the structure is linear elastic the corresponding displacements are $\alpha\{u\}$.

Let us now assume that the reference load $\{P\}$ and the load multiplication factor α are kept constant with respect to a variation of the crack length a . This gives us for the critical value of $\alpha = \alpha_c$ that

$$\{P_c\} = \alpha_c \{P\} \quad (29)$$

$$\{u_c\} = \alpha_c \{u\} \quad (30)$$

According to Eq. (27), we can then write

$$\alpha_c^2 \{P\}^T \left\{ \frac{du}{da} \right\} = 2 b_c G_c \quad (31)$$

or

$$\alpha_c = \sqrt{\frac{2b_c G_c}{\{P\}^T \left\{ \frac{du}{da} \right\}}} \quad (32)$$

This expression is straightforward to apply in finite element analysis.

In order to obtain a pure force formulation the flexibility relation is introduced,

$$\{u\} = [f]\{P\} \quad (33)$$

where the flexibility matrix $[f]$ is square and symmetric. Observing that the external loading is not assumed to be changed during the crack propagation, we get

$$\left\{ \frac{du}{da} \right\} = \left[\frac{df}{da} \right] \{P\} \quad (34)$$

and

$$\alpha_c = \sqrt{\frac{2b_c G_c}{\{P\}^T \left[\frac{\partial f}{\partial a} \right] \{P\}}} \quad (35)$$

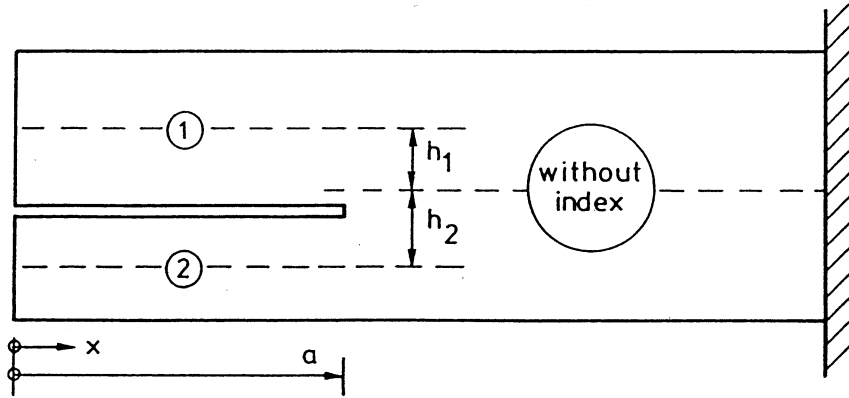


Figure 5 Cantilever beam with a crack

From a hand calculation point of view it is of special interest to study cases the matrix $[f]$ is diagonal and where each component of $[f]$ can be expressed simply as a function of the crack length a .

If $[f]$ is diagonal with the diagonal elements, $f_1, f_2 \dots f_n$ we get

$$\alpha_c = \sqrt{\frac{2b_c G_c}{\sum_{i=1}^n \frac{\partial f_i}{\partial a} (P_i)^2}} \quad (36)$$

Let us next study some simple beam structures with an opening crack, say a simply supported beam or the cantilever beam as shown in Figure 5.

It is assumed that we have some reference loading and a load multiplication factor α that is common to all loads. The sectional forces will be functions of the current crack length a and the notations used are shown in Figure 6.

In order to simplify the following derivations it is assumed that the cross sections remain undeformed. Including energy contributions according to beam theory only, we may approximately write

$$\alpha_c = \sqrt{\frac{2b_c G_c}{\frac{\beta V_1^2}{GA_1} + \frac{\beta V_2^2}{GA_2} - \frac{\beta V^2}{GA} + \frac{M_1^2}{EI_1} + \frac{M_2^2}{EI_2} - \frac{M^2}{EI} + \frac{N_1^2}{EA_1} + \frac{N_2^2}{EA_2} - \frac{N^2}{EA}} \quad (37)$$

This expression is astonishing exact, except for a cross-coupling effect between shear forces and relative rotations over the crack region. Eq. (37) may be generalized taken

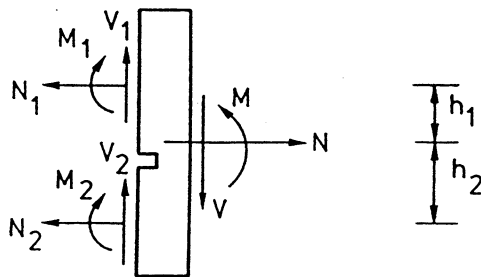


Figure 6 Sectional forces close to the crack tip for $\alpha = 1$ (h_1 and h_2 denote distances between gravity axes).

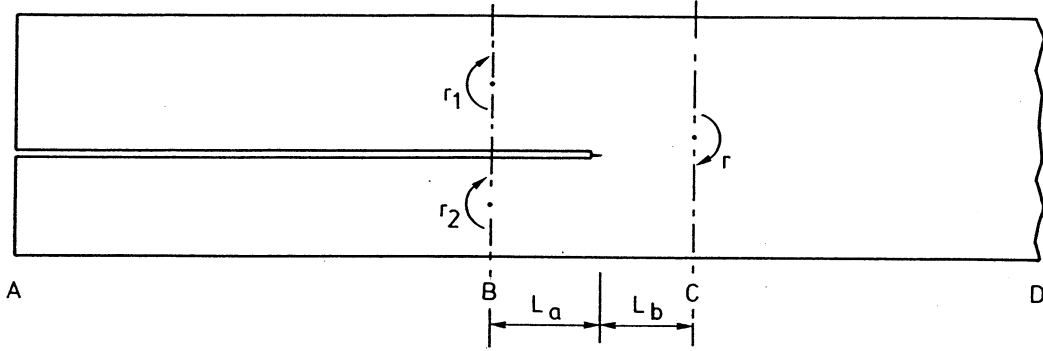


Figure 7 Rotations of cracked beam. Regions AB and CD are loaded and beam theory gives a good approximation. Crack tip region BC has no external loads

into account additional deformations of the beam in the region close to the crack tip. For wood especially the deformation related to the elasticity modulus perpendicular to the grain might be of importance to consider.

For a case where beam theory gives a good approximation outside the crack region, see Figure 7, it can be shown that the additional influence of the shear forces (not considered in Eq. (37)) results into

$$\alpha_c = \sqrt{\frac{2b_c G_c}{\frac{\beta V_1^2}{GA_1} + \frac{\beta V_2^2}{GA_2} - \frac{\beta V^2}{GA} + \frac{M_1^2}{EI_1} + \frac{M_2^2}{EI_2} - \frac{M^2}{EI} + \frac{N_1^2}{EA_1} + \frac{N_2^2}{EA_2} - \frac{N^2}{EA} + 2(V_1 \Delta r_1 + V_2 \Delta r_2)}} \quad (38)$$

In the extra energy terms $V_1 \Delta r_1 + V_2 \Delta r_2$ in Eq. (10), the relative rotation contributions Δr_i can be defined as

$$\Delta r_i = (r_i - r)_{exact} - (r_i - r)_{beam \ theory} \quad \text{for } i = 1, 2 \quad (39)$$

where for beam theory shear deformations will not give any contribution to the rotations in Eq. (39).

This gives us

$$2 \sum_{i=1}^2 V_i (r_i - r)_{beam \ theory} = \frac{L_a}{EI_1} (L_a V_1^2 - 2M_1 V_1) + \frac{L_a}{EI_2} (L_a V_2^2 - 2M_2 V_2) - \frac{L_b}{EI} (L_b V^2 + 2MV) \quad (40)$$

while the exact relative rotations might be found by a finite element analysis.

To give an idea of the influence of the relative rotations on Eq. (38) the symmetric case in Figure 8 is studied for $V_1 = -V_2$ and $M_1 = -M_2$ in a pure opening crack mode. Using assumptions for beams on elastic foundations we may get

$$\Delta r_1 = -\Delta r_2 = \frac{2\beta^2}{k} (V_1 + 2\beta M_1) \quad (41)$$

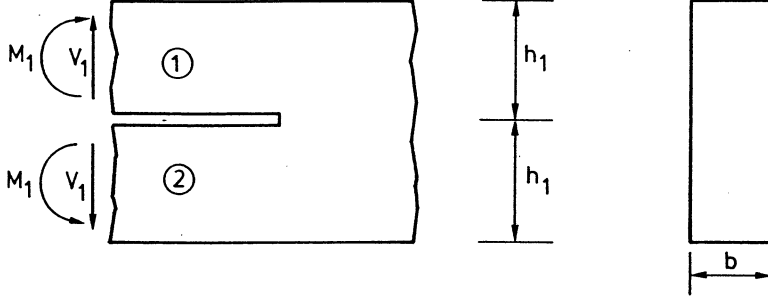


Figure 8 Symmetric case of crack propagation

where the equivalent spring stiffness k corresponding to beam part ① is set to

$$k = \frac{E_{\perp} b}{0.5h_1} \quad (42)$$

and

$$\beta = \frac{1}{h_1} \sqrt[4]{6 \frac{E_{\perp}}{E}} \quad (43)$$

In Eqs. (42) and (43) E_{\perp} denotes the elasticity modulus in the transverse direction and E refers as previously to the longitudinal direction. Substitution of Eqs. (42) and (43) into Eq. (41) yields

$$\Delta r_1 = \frac{1}{A_1} \sqrt{\frac{6}{E_{\perp} E}} (V_1 + 2\beta M_1) \quad (44)$$

with $A_1 = bh_1$, and further according to Eq. (38)

$$\alpha_c = \sqrt{\frac{2b_c G_c}{\frac{2V_1^2}{GA_1} + \frac{2M_1^2}{EI_1} + \frac{4\sqrt{6}}{\sqrt{E_{\perp} E} A_1} (V_1^2 + 2\beta V_1 M_1)}} \quad (45)$$

We may observe that if the transverse modulus E_{\perp} is sufficiently large then Eq. (45) will give the same results as Eq. (37).

4 Numerical analysis

For the numerical analysis based on the finite element method, mainly Eq. (32) will be applied. The current load factor α_c at cracking is thus calculated from

$$\alpha_c = \sqrt{\frac{2b_c G_c}{\{P\}^T \left\{ \frac{du}{da} \right\}}} \quad (46)$$

where $\{P\}$ are the given reference loads. The crack length a is gradually increased and for each value $a = a_i$ the corresponding displacements $\{u\}_i$ are calculated (for $i = 0, 1, 2, \dots$). We introduce the notation

$$\Delta a_i = a_{i+1} - a_i \quad (47)$$

and obtain by a simple approximation

$$\alpha_{ci} = \sqrt{\frac{2b_c \Delta a_i G_c}{\{P\}^T (\{u\}_{i+1} - \{u\}_i)}} \quad \text{for } a \approx \frac{a_{i+1} + a_i}{2} \quad (48)$$

In the finite element analysis presented in the following low order elements were used in order to determine $\{u_i\}$. Only two-dimensional computations have been performed and where possible rectangular four-node elements were used. Plane stress state was assumed.

One difficulty in the analysis is that G_c is depending on the mode of cracking. An idea of which value to choose for G_c is to estimate some average value of the ratio $\bar{\sigma}_\perp / \bar{\tau}$ between the normal and shear stresses (with respect to the crack plane in the cracking process zone), see Figure 9. In a finite element analysis an evaluation of the nodal forces from the individual elements close to the crack tip can give a reasonable estimate of the mixed mode state. An illustration is given by Figure 10, where the summations for elements (i), (j) and (k) and elements (l), (m) and (n) gives identical results

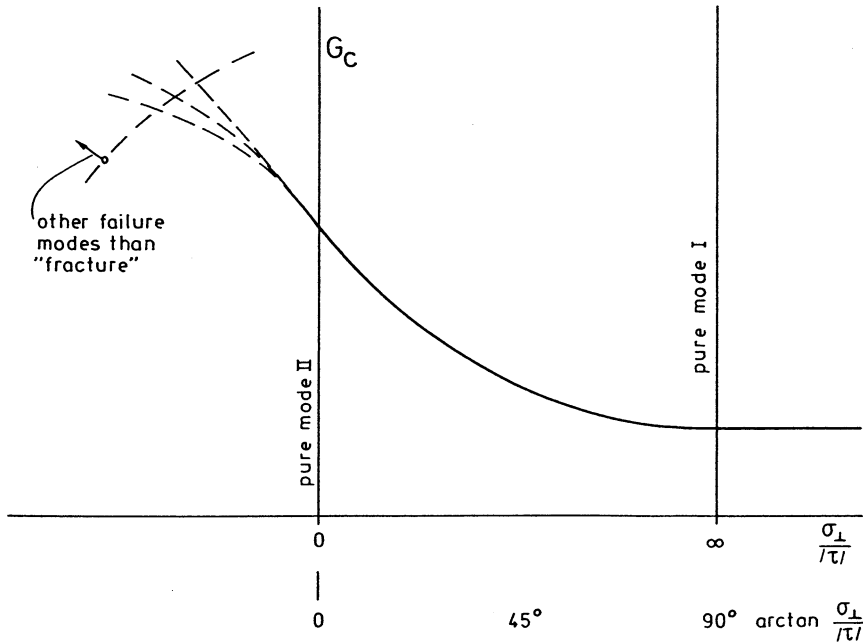


Figure 9 Fracture criterion for mixed mode

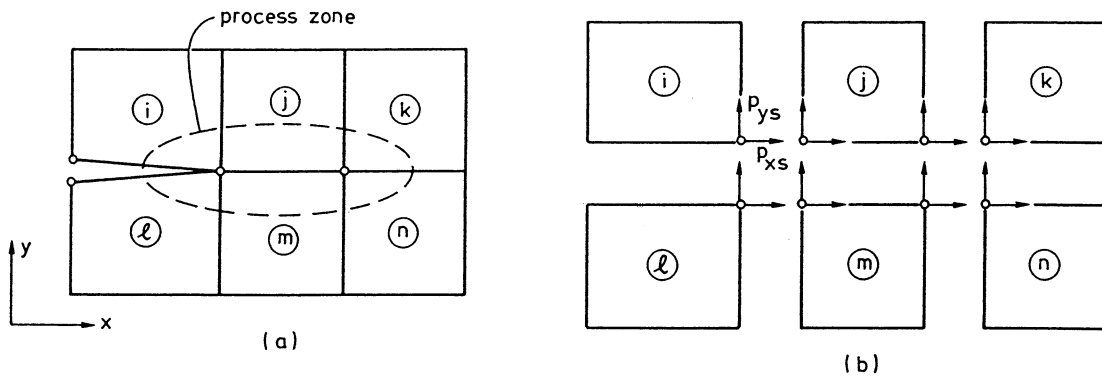


Figure 10 Nodal element forces close to cracking process zone.

- (a) assembly of elements
- (b) individual elements

except for the sign. By this approach we may write

$$\frac{\sigma_{\perp}}{\tau} \approx \frac{\sum_s P_{ys}}{\sum_s P_{xs}} \quad (49)$$

after a summation over for example elements \textcircled{l} , \textcircled{m} and \textcircled{n} .

In order to find a reasonable relation between G_c and $\bar{\sigma}_{\perp}/\bar{\tau}$ we may start from a case illustrated in Figure 11, where we approximate

$$\frac{\bar{\sigma}}{\bar{\tau}} \approx \frac{K_I}{K_{II}} \quad (50)$$

and where the stress intensity factors K_I and K_{II} can be related to elasticity and fracture parameters [2]. We have

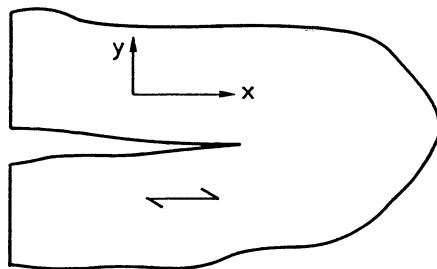


Figure 11 Crack propagation in grain direction

$$K_I = \sqrt{E_I G_I} \quad (51)$$

$$K_{II} = \sqrt{E_{II} G_{II}} \quad (52)$$

and, referring to Figure 11,

$$\frac{E_I}{E_{II}} = \sqrt{\frac{E_y}{E_x}} = \sqrt{\frac{E_{\perp}}{E_{\parallel}}} \quad (53)$$

where E_{\perp} and E_{\parallel} are the elasticity modulus perpendicular to and parallel with the grain direction. The fracture energy G_c in mixed mode

$$G_c = G_I + G_{II} \quad (54)$$

is assumed to be related to the fracture energy in pure mode I (G_{cI}) and pure mode II (G_{cII}) by

$$\frac{K_I}{K_{Ic}} + \frac{(K_{II})^2}{(K_{IIc})^2} = 1 \quad (55)$$

or alternatively according to Eqs. (51) and (52)

$$\frac{\sqrt{G_I}}{\sqrt{G_{Ic}}} + \frac{G_{II}}{G_{IIc}} = 1 \quad (56)$$

After some manipulations of Eqs. (50) to (56) we get

$$G_c = \frac{1}{a} \left[1 + \frac{b^2}{2a} \left(1 - \sqrt{1 + \frac{4a}{b^2}} \right) \right] \quad (57)$$

where

$$a = \frac{1 - \kappa^2}{G_{IIc}} \quad (58)$$

$$b^2 = \frac{\kappa}{G_{Ic}} \quad (59)$$

and

$$\kappa^2 = \frac{1}{1 + \sqrt{\frac{E_{\perp}}{E_{\parallel}} \left(\frac{\tau}{\sigma} \right)^2}} \quad (60)$$

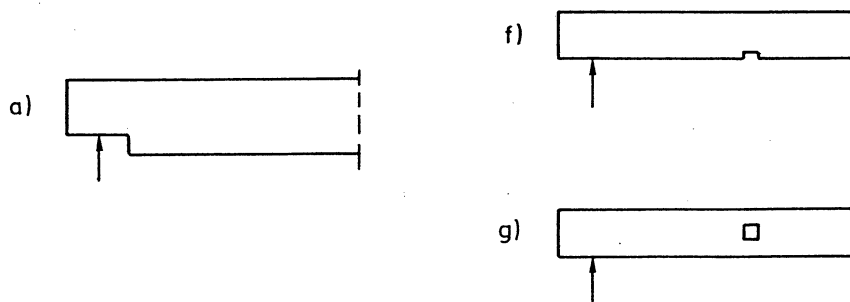


Figure 12 Examples of analysed beam geometries

5 Results

The material data used in the analysis are given in Appendix 1 except for the relation between $G_c = G_c(\bar{\sigma}_\perp/|\bar{\tau}|)$. A conservative assumption is to set $G_c = G_{Ic}$, which is a reasonable approximation as long as mode II not is too dominating. Results will be given for this approximation as well as for the mixed mode influence according to Eq. (60).

Three different geometries are analysed first, see Figure 12 and Appendix 1. The results from these finite element calculations are based on meshes with about 50 to 100 elements in the longitudinal direction and about 20 elements in the depth direction. The hand calculations are based on Eq. (37).

Some of the results obtained are given in Table 1. As expected Eq. (37) based on beam theory yields too high values for case *a* due to the assumption of $E_\perp = \infty$ while the approximation is reasonably good for the case *f*.

The problem of choosing a proper initial crack length when determining the load-bearing capacity is illustrated in Figure 13. It is shown how the load V_f varies as a function of the crack length. For case *a* the values for V_f in Table 1 are based on a linear extrapolation to $a = 0$ while the minimum value of V_f is chosen for case *g*, corresponding to $a \approx 0.08h$. It is obvious that the choice of a proper initial crack length needs a sound engineering judgement in practical design.

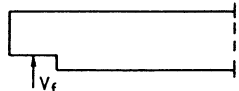
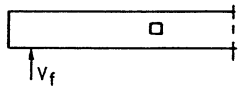
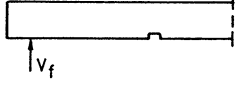
Geometry	h (mm)	V_f (kN) FEM	V_f (kN) Eq. (37)
a) 	95	8.3	13.0
	600	56.2	87.0
g) 	95	4.3	4.9
	600	28.6	32.9
f) 	95	6.8	-
	600	45.8	-

Table 1. Some obtained results for $G_c = G_{Ic}$

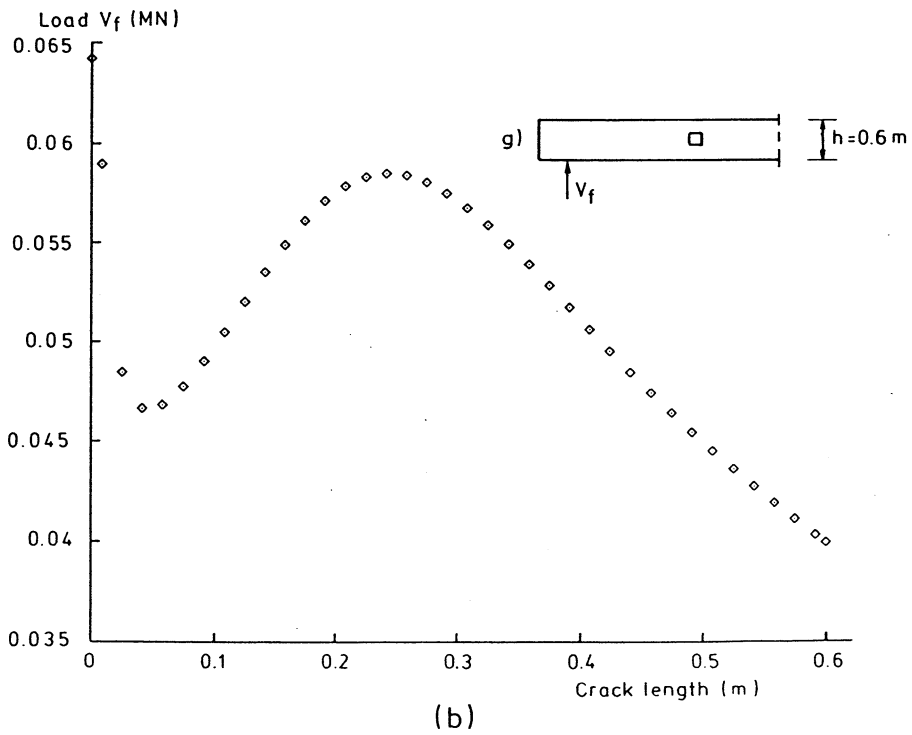
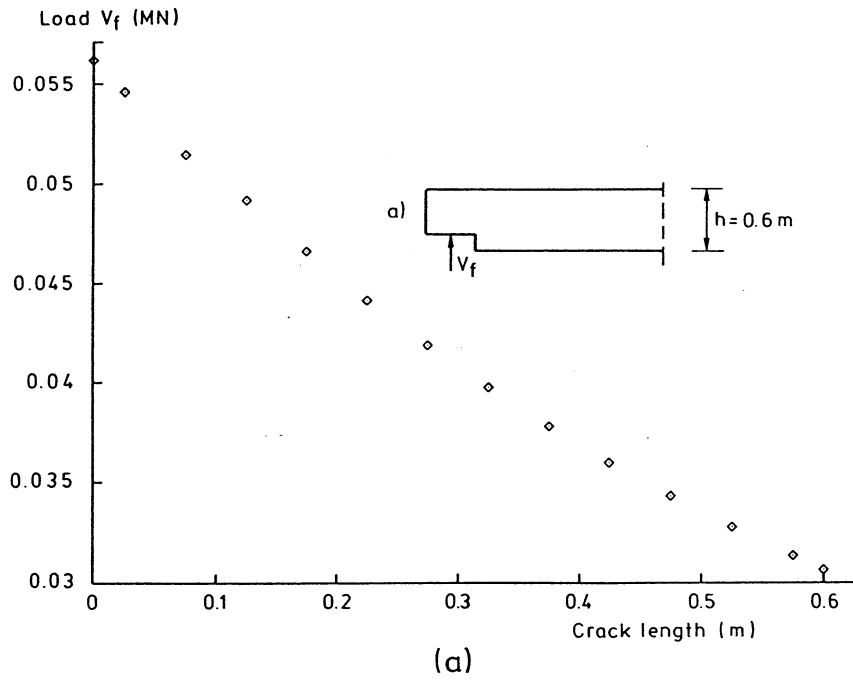


Figure 13 Load versus crack length for $G_c = G_{Ic}$. Coarse mesh with 20 elements in the depth direction.

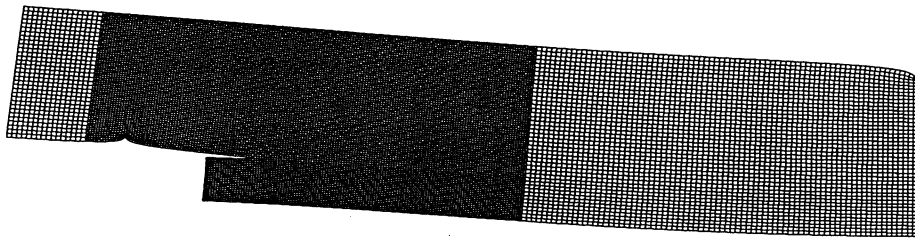
- (a) Case a
- (b) Case g

In order to get better understanding of the relation between loadbearing capacity and initial crack length all examples in Appendix 1 have been calculated using a fine finite element subdivision. In beam parts with the finest mesh the number of elements are 95 in the depth direction. Calculations have been performed for different values of the fracture energy. G_c is set to G_{Ic} , G_{c6mm} , G_{c12mm} ..., respectively, where for example G_{c6mm} means that the ratio $\bar{\sigma}/\bar{\tau}$ in Eq. (49) is based on a summation over a length of 6 mm.

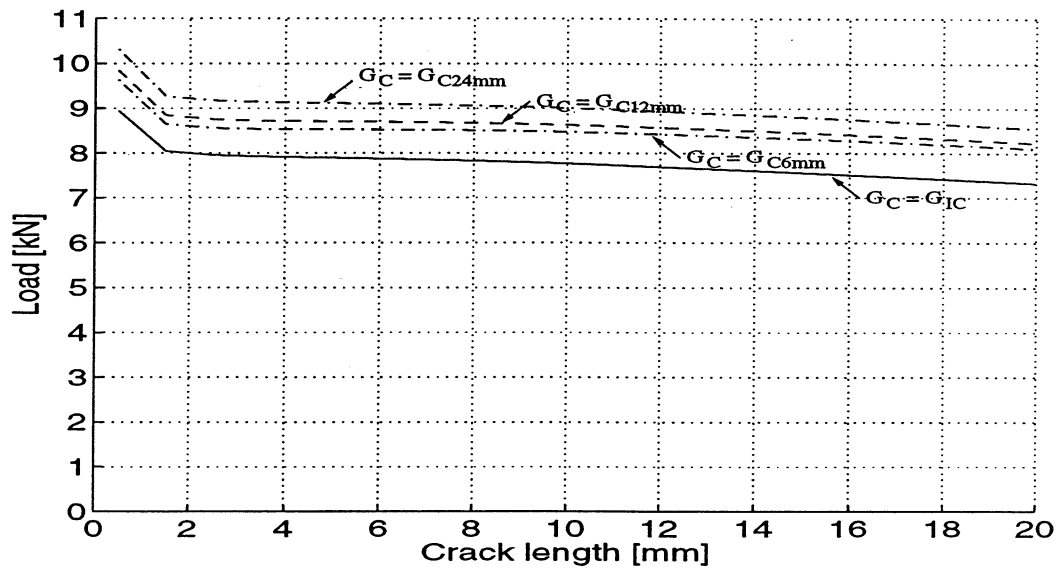
Results are presented in Figures 14 to 19. In each figure the finite element mesh used is shown at the top. Then the relation between the crack load V_f at support and the initial crack length are given for the beam depth $h = 0.095\text{m}$ and $h = 0.6\text{m}$.

The much higher values of V_f obtained for very small initial crack lengths is here of minor interest to study as also longer initial crack lengths must be considered in practice. Further, the assumptions applied in linear elastic fracture mechanics will probably lead to very crude approximations in the studied examples when the initial crack lengths are very small.

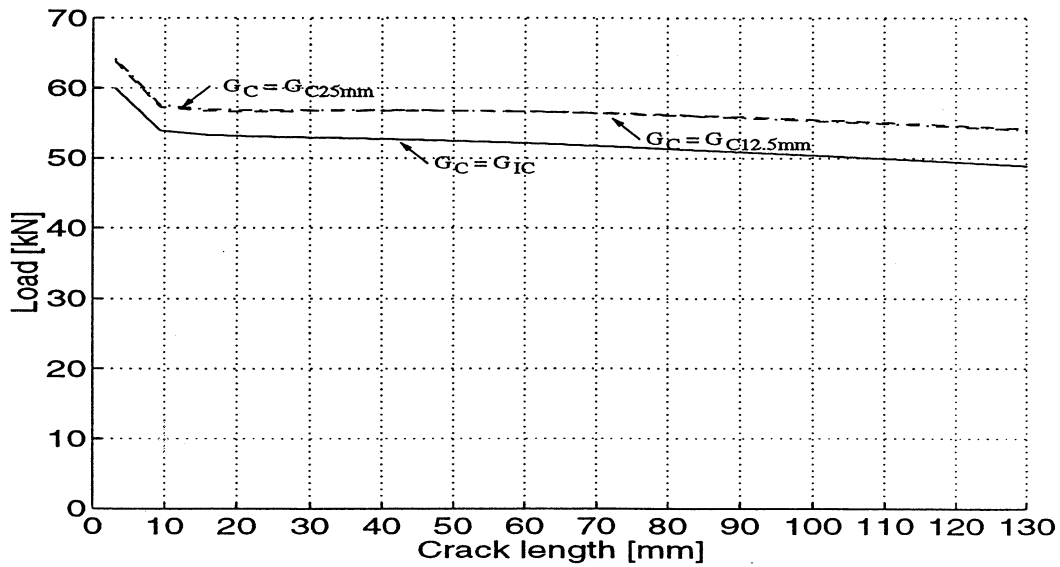
The influence of mixed mode seems to be modest in almost all of the cases studied, at least for reasonable design values of the initial crack length (say between 6mm and 50mm for the examples).



Deformed finite element mesh

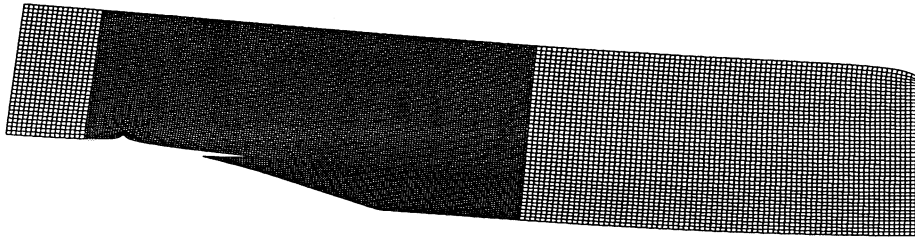


Notched beam with $h=95$ mm

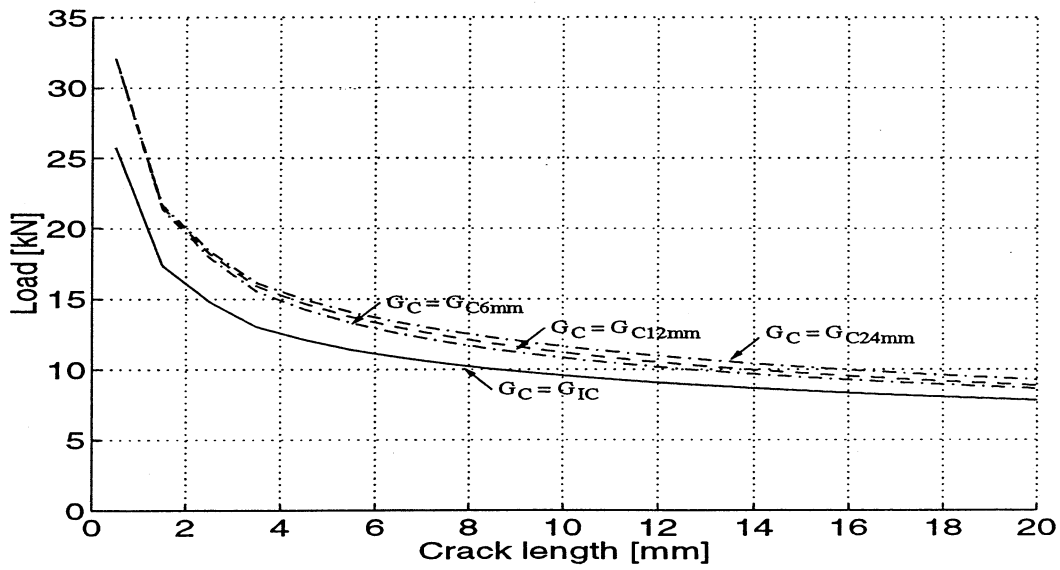


Notched beam with $h=600$ mm

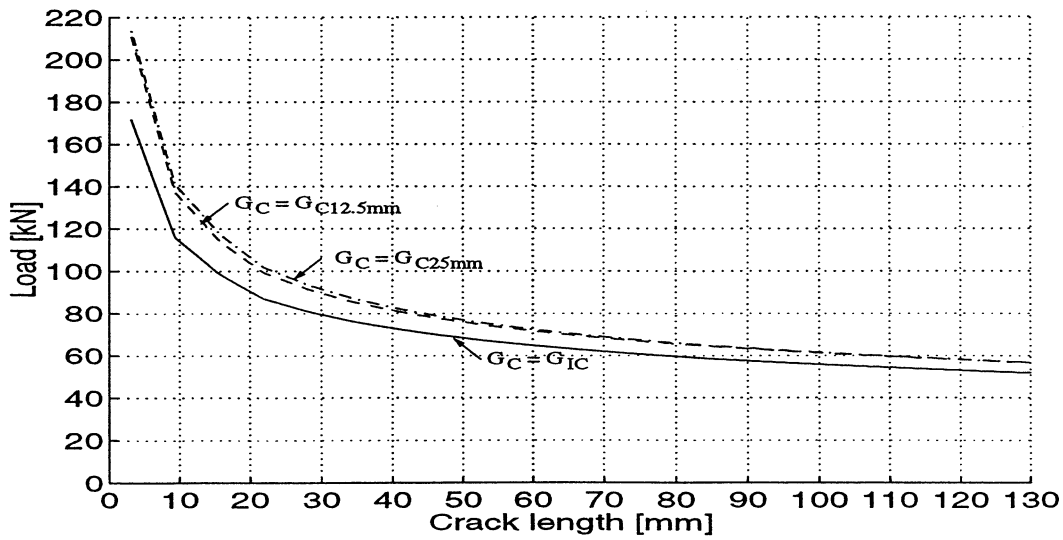
Figure 14 Relation between crack load and initial crack length for case a.



Deformed finite element mesh

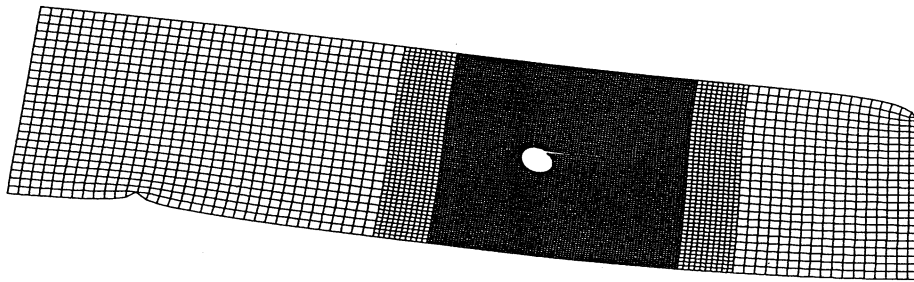


Notched beam with $h=95$ mm

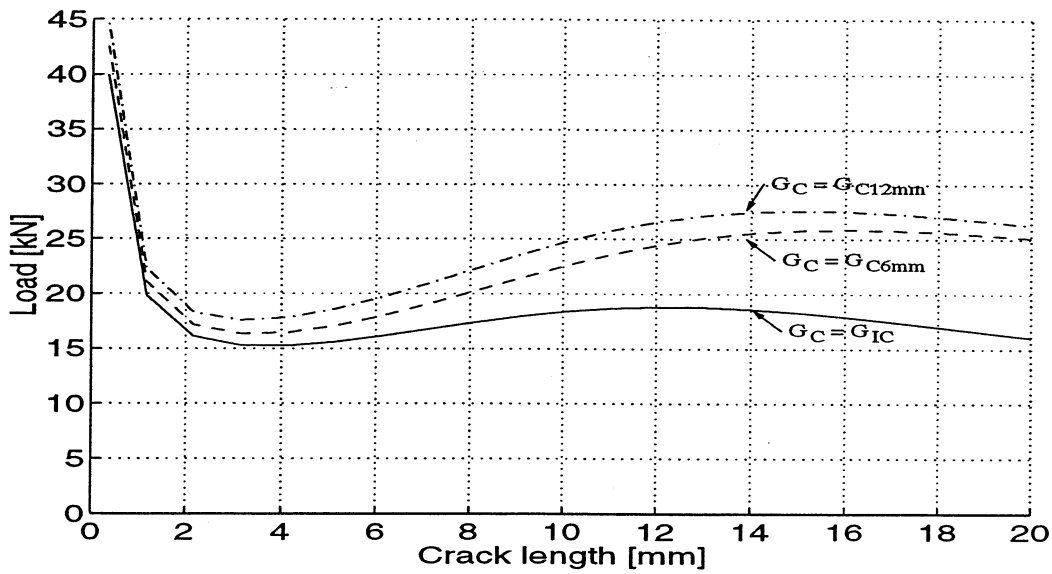


Notched beam with $h=600$ mm

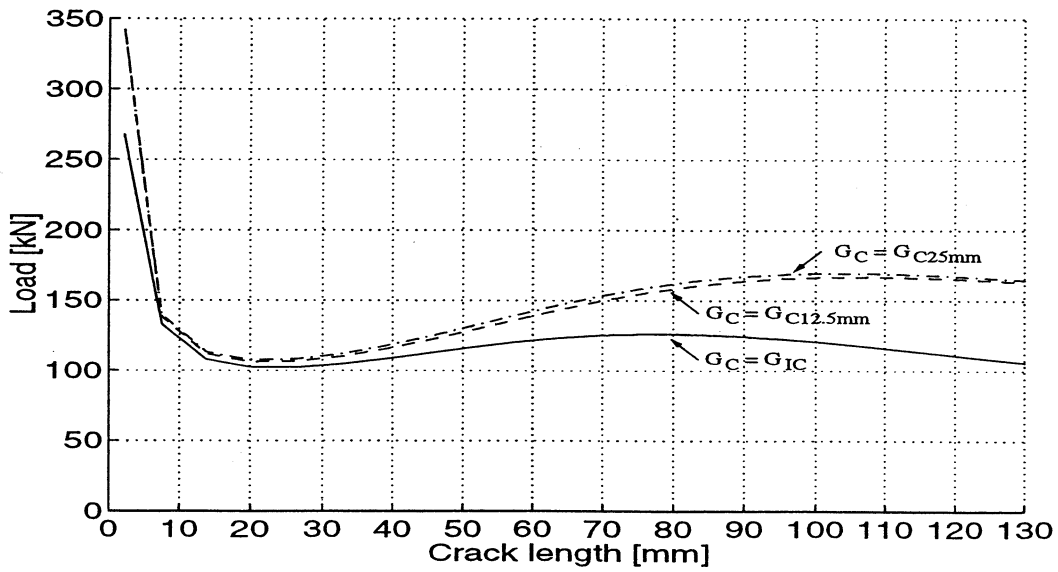
Figure 15 Relation between crack load and initial crack length for case b.



Deformed finite element mesh

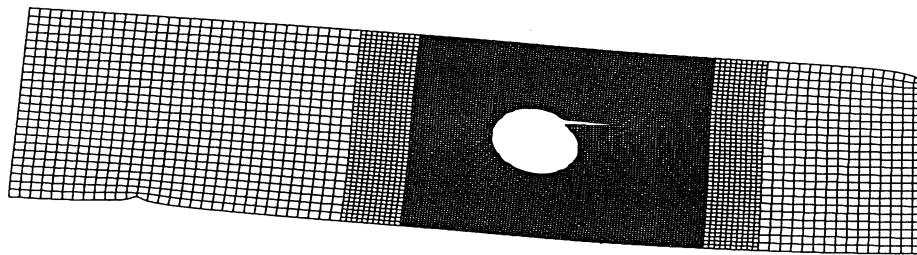


Beam with circular hole, $h=95$ mm, $\text{Ø}=h/8$

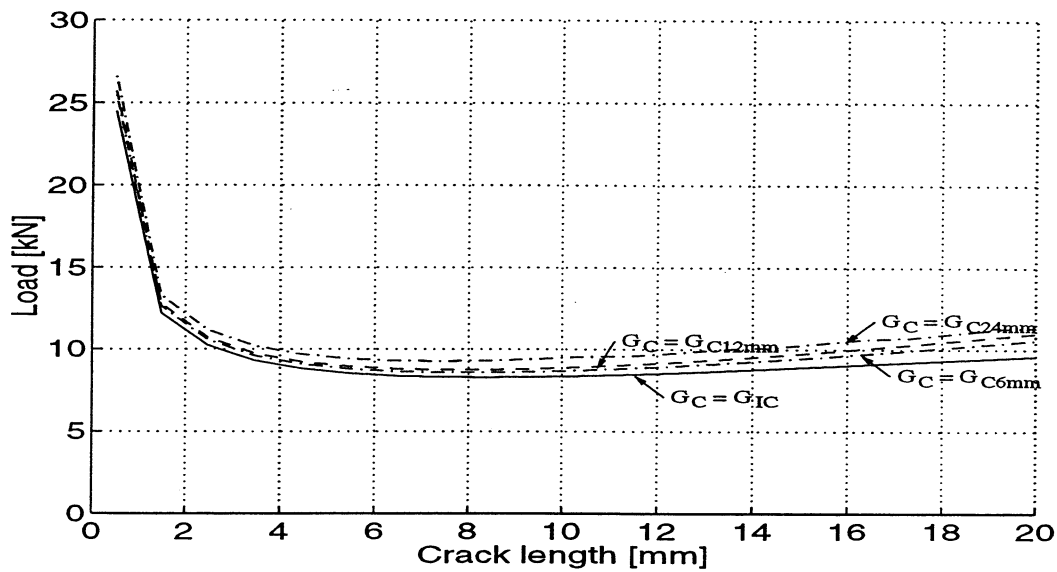


Beam with circular hole, $h=600$ mm, $\text{Ø}=h/8$

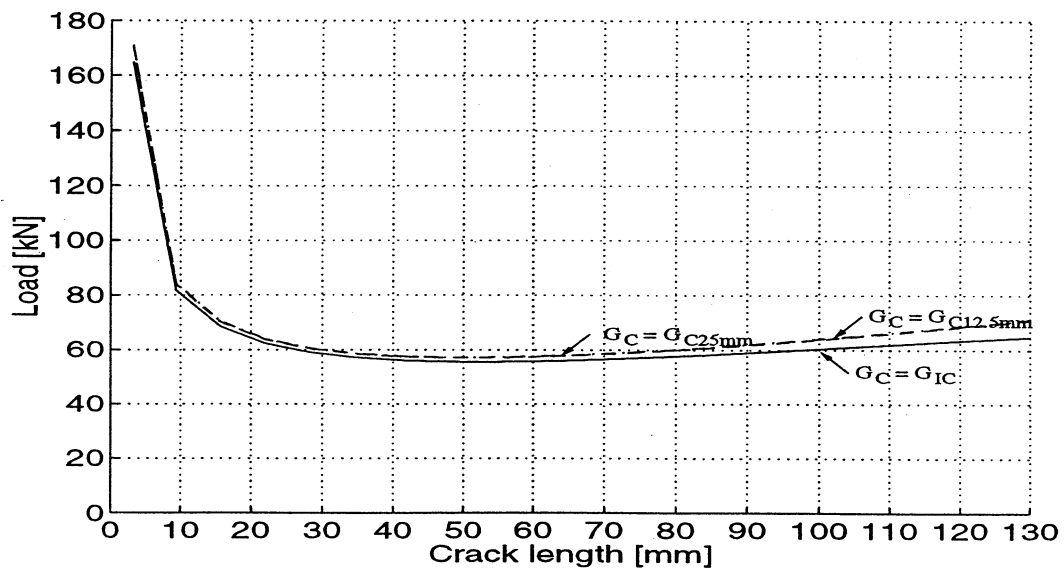
Figure 16 Relation between crack load and initial crack length for case d.



Deformed finite element mesh

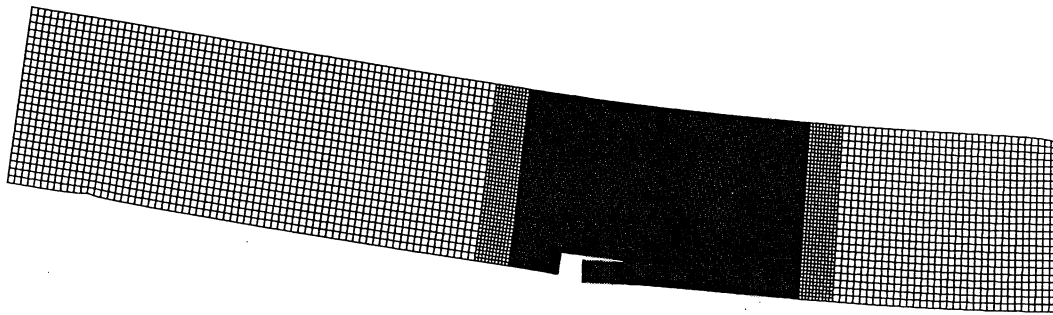


Beam with circular hole, $h=95 \text{ mm}$, $\text{Ø}=h/3$

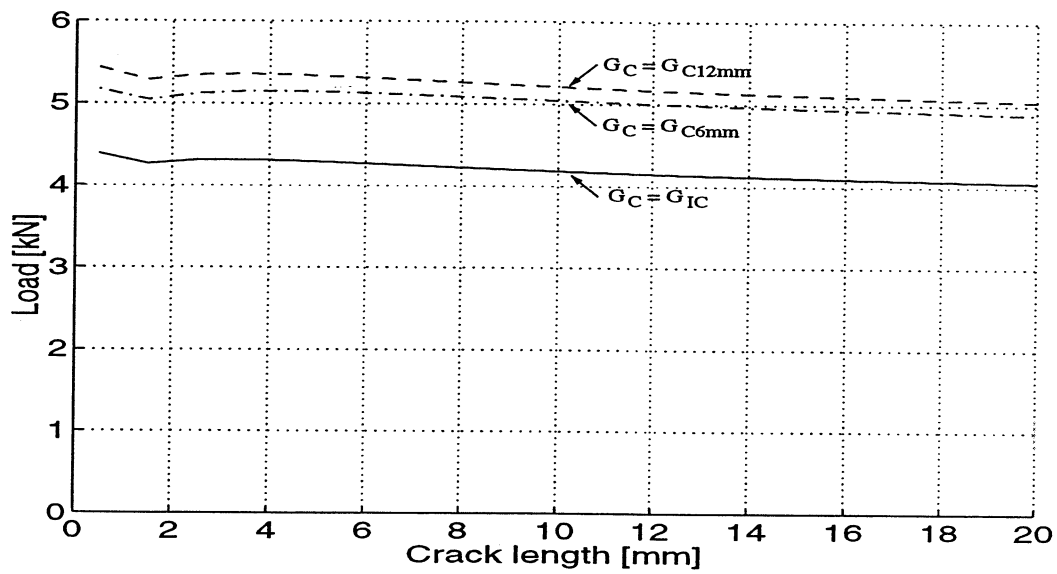


Beam with circular hole, $h=600 \text{ mm}$, $\text{Ø}=h/3$

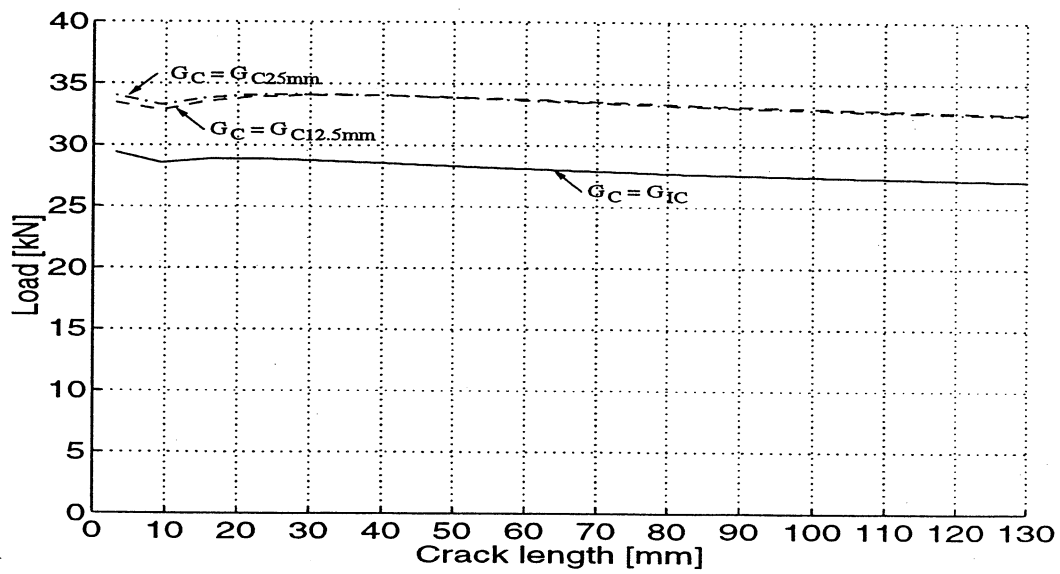
Figure 17 Relation between crack load and initial crack length for case e.



Deformed finite element mesh

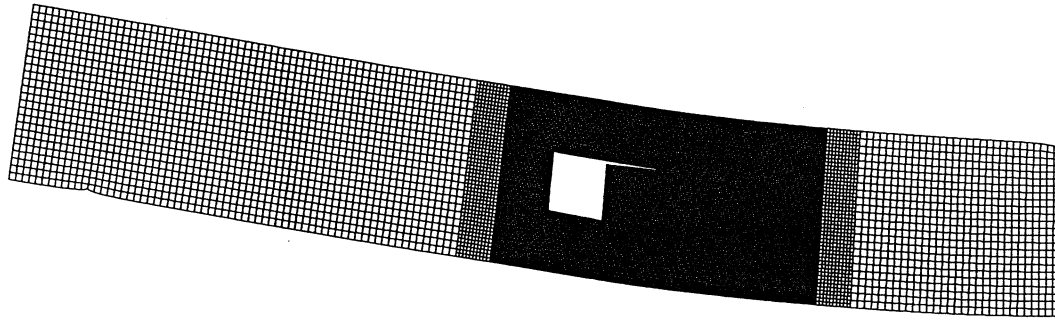


Notched beam with $h=95$ mm

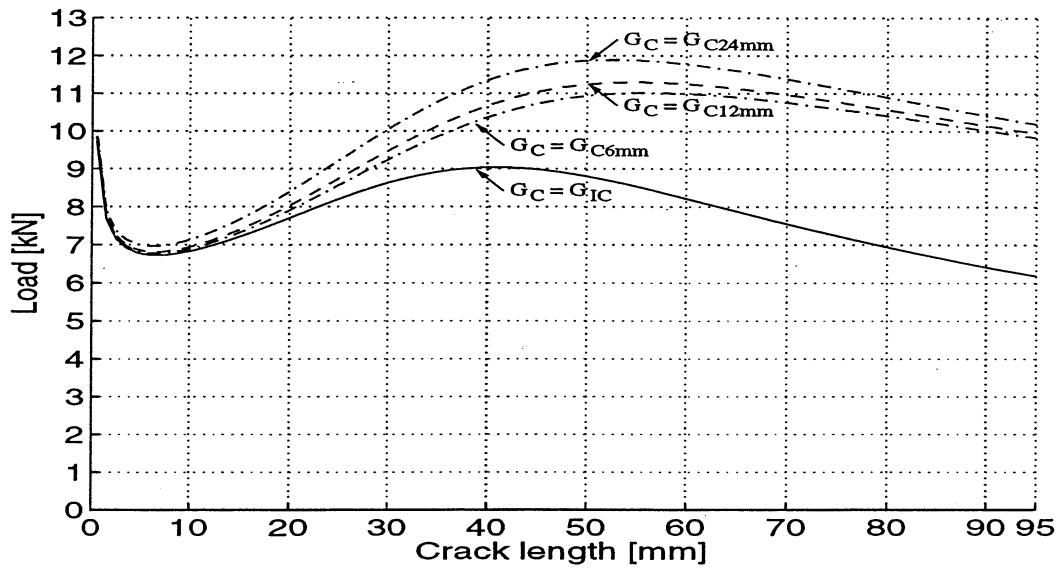


Notched beam with $h=600$ mm

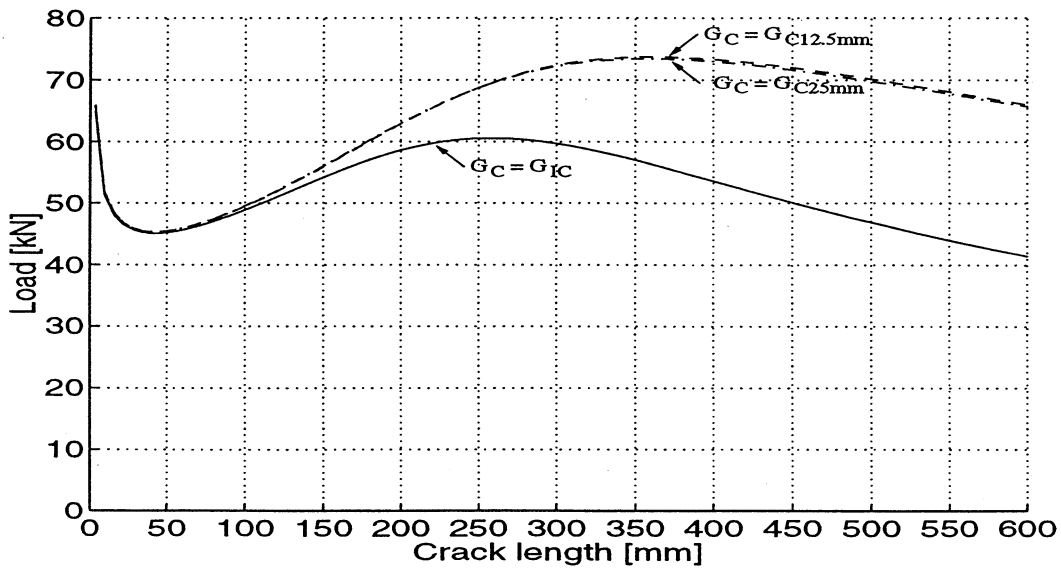
Figure 18 Relation between crack load and initial crack length for case *f*.



Deformed finite element mesh



Beam with quadratic hole, $h=95$ mm



Beam with quadratic hole, $h=600$ mm

Figure 19 Relation between crack load and initial crack length for case g.

6 Concluding remarks

It is obvious that the choice of a proper initial crack length at a notch or a hole is of importance in practical design. Such cracks must be considered unless some kind of reinforcement is provided. It seems reasonable to choose the design value for the initial crack length from the calculated relation between the crack load and the crack length, see Figures 14 to 19.

In Table 2 an attempt is made to estimate a reasonable value of the initial crack length a_0 to be used for determining the support load V_f in the studied examples. It is interesting to observe that the differences of V_f based on $G_c = G_{Ic}$ and $G_c = G_{c12mm}$ are small, which clearly indicate that G_{Ic} is the prime fracture material parameter to be used in design.

From a computation point of view it is of interest to compare the results in Table 1 for a relative coarse mesh with those in Table 2 for a fine mesh. The results are obviously in good agreement. Thus, by use of an energy release rate approach reasonable good results will normally be obtained even with a relatively coarse mesh in the finite element analysis.

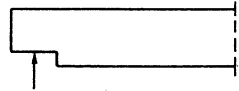
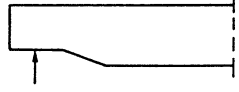
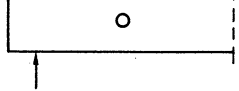
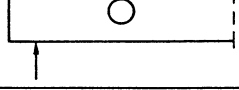
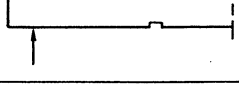
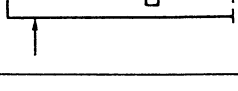
Geometry	h (mm)	a_0 (mm) FEM	V_f (kN) $G_c = G_{Ic}$	V_f (kN) $G_c = G_{c12mm}$	$(\bar{\sigma}/\bar{\tau})$
a) 	95	6	7.9	8.7	1.9
	600	10	53.9	57.2	1.4
b) 	95	6	11.1	13.4	2.9
	600	30	79.5	89.6	2.1
d) 	95	4	15.3	17.8	2.5
	600	20	102.5	106.3	1.0
e) 	95	6	8.4	8.9	1.2
	600	40	56.2	57.6	0.8
f) 	95	6	4.3	5.3	3.5
	600	10	28.6	32.9	2.4
g) 	95	6	6.7	6.8	0.6
	600	40	45.1	45.3	0.3

Table 2. Estimated values for design of initial crack length and crack load based on Figures 14 to 19

6.1 References

- [1] Ottosen, N.S. and Petersson, H: Introduction to the Finite Element Method, Prentice Hall, New York 1992.
- [2] Sih, G.C., Paris, P.C. and Irwin, G.R.: On cracks in reatilinearly anisotropic bodies. International Journal of Fracture mechanics, Vol 1 (1965), pp. 189-200.
- [3] Valentin, G.H. .et al.: Application of fracture mechanics to timber structures. RILEM state-of-the-art report, Technical Research Centre of Finland, Research Notes No. 1262, Espoo Finland 1991.

Acknowledgements

The assistance from Johan Gullander in carrying out a substantial part of the numerical calculations is acknowledged.

FRACTURE MECHANICS MODELS FOR STRENGTH ANALYSIS OF
TIMBER BEAMS WITH A HOLE OR A NOTCH

Paper 4:

Energy Approach Used in a Draft Eurocode ¹⁾

by

Per Johan Gustafsson

Division of Structural Mechanics, Lund University,
Box 118, SE-221 00 Lund, Sweden

¹⁾1993, 6 pages

Energy Approach Used in a Draft Eurocode

by

Per Johan Gustafsson

1. Introduction

The equation for calculating the load carrying capacity of a beam with a rectangular or tapered end-notch, see Figure 1 a) and b), included in the current draft version of Eurocode 5 emanates from fracture mechanics analysis. The actual code equation has been modified a number of times in draft-codes that has been published in the last few years. Here, the basic strength equation and its derivation and limitations will be discussed. Also some feasible modifications and extensions shall be mentioned. The actual strength equation shows that rational fracture mechanics can make possible simple engineering derivations of simple and useful equations for load carrying capacity.

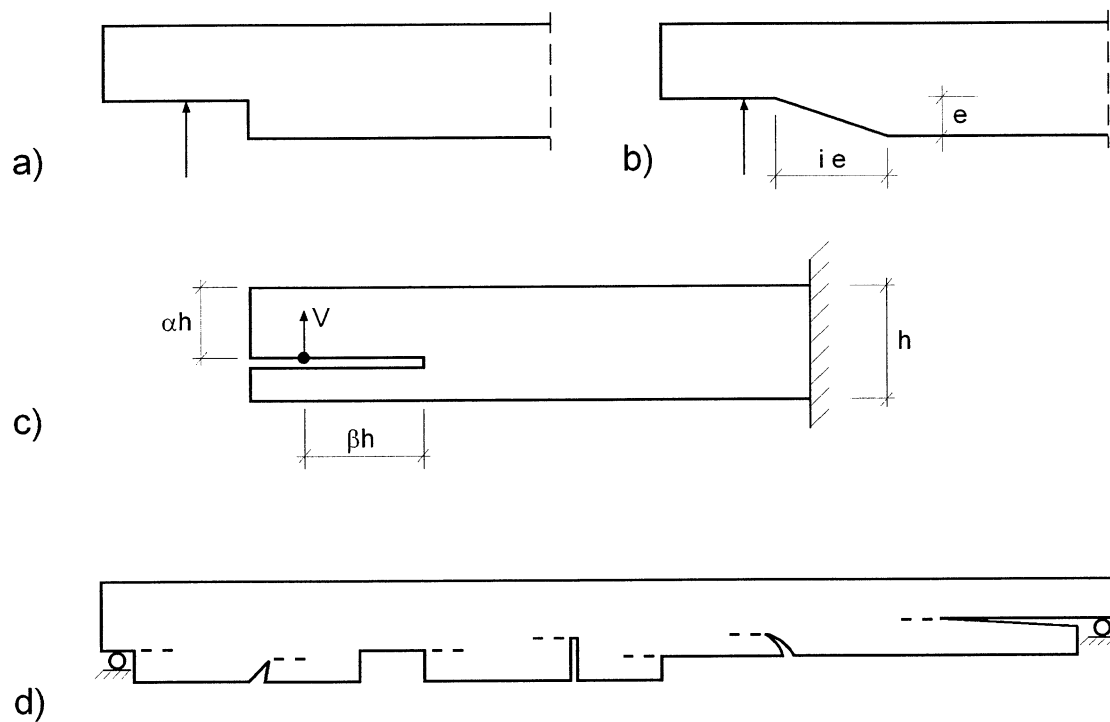


Figure 1. Beams with various types of notches.

2. Derivation of basic equation

The derivation is within the framework of conventional linear elastic fracture mechanics and carried out by calculating the total energy release rate during crack extension. This rate is obtained from beam compliance calculated essentially by conventional engineering beam theory. A beam shaped and loaded according to Figure 1c) is studied. The total energy release rate during crack extension is

$$G = \frac{-\partial U}{b\partial a} = \frac{\partial(V\delta/2)}{b\partial(\beta h)} = \frac{V^2}{2bh} \frac{\partial C}{\partial \beta} \quad (1)$$

where $U = -V\delta/2$ is the potential energy, $a = \beta h$ the crack length, b the beam width and $C = \delta V$ the compliance. The fracture criterion used is

$$G = G_c \quad (2)$$

where the critical value of the total energy release rate, G_c , in general depends on the mixed mode ratio. For mixed mode ratios it may be regarded as a fair approximation and for $\tau/\sigma > 2$ as a simplifying estimation on the safe side to take G_c as the fracture energy value of pure mode 1, i.e.

$$G_c = G_{Ic} \quad (3)$$

Equations (1)-(3) give the magnitude of V , V_f , corresponding to fracture:

$$V_f = \sqrt{\frac{2bhG_{Ic}}{\partial C / \partial \beta}} \quad (4)$$

Now the compliance $C = \delta V$ needs to be calculated. Inspired by the accuracy in compliance obtained for isotropic beams and striving for simplicity, δV is written the form

$$C = A(B + \beta h)^3 + constant \quad (5)$$

where the constant is constant with respect to variation of the normalized crack length, β , and where A and B are coefficients. The value of the constant is of no matter since it disappears at the derivation with respect to β . Equation (5) is of the same form as the compliance of a cantilever beam for which $C = L^3/(3EI)$ or a three point bending beam for which $C = L^3/(48EI)$. In equation (5) the third degree term with respect to beam length corresponds to bending moment and curvature of the beam, and the first degree term corresponds to shear force and shear deformation of the beam. The coefficients A and B are determined by calculating third and first degree

terms corresponding to the beam curvature and the shear deformation by conventional beam theory. This gives

$$A = \frac{4(1/\alpha^3 - 1)}{E_x b} \quad (6)$$

$$B = \sqrt{\frac{E_x (1/\alpha - 1)}{10G_{xy} (1/\alpha^3 - 1)}} \quad (7)$$

where E_x is the modulus of elasticity in the grain direction and G_{xy} the modulus of shear rigidity. With C from equation (5), equation (4) gives a simple explicit formula for V_f :

$$\frac{V_f}{b\alpha h} = \frac{\sqrt{G_{Ic}/h}}{\sqrt{0.6(\alpha - \alpha^2)/G_{xy} + \beta\sqrt{6(1/\alpha - \alpha^2)/E_x}}} \quad (8)$$

Further details about the derivation of this equation are given in the paper “A study of strength notched beams” by P.J. Gustafsson, published as paper CIB-W18A/21-10-1 in the proceedings of Meeting 21 of CIB-W18A, Vancouver Island, Canada, 1988.

3. Applicability and numerical results

Equation (8) was derived for the geometry shown in Figure 1c). However, according to beam theory the unloaded part of the beam below the crack is not active. Therefore the equation is valid also for the beam shown in Figure 1a) and also for the kinds of notches shown in Figure 1d), provided that the signs of the bending moment and shear force are such that the direction of the crack propagation becomes as indicated in the figure.

The equation is not strictly valid for a notch as shown in Figure 1b). For this geometry there is no square root singularity of the stress at the notch. Conventional linear elastic fracture mechanics is accordingly not applicable and the energy release rate during the first small crack propagation is found to be zero, both according to beam theory and plane stress theory. Looking at the beams in the Appendix, the present strength equation is according to theory not applicable to beams b)-e) and h). For beam g) a non-zero energy release rate will be obtained if using beam theory analysis. The equation for the compliance of a beam with a hole will, however, be different from the equation obtained for a beam with a notch.

A general limitation for the present theory as well as for linear elastic fracture mechanics in general is that the size of the fracture process region must be small

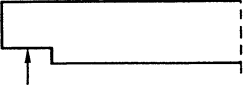
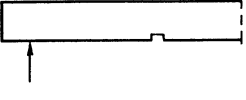
Geometry	h (mm)	$\frac{h}{G_{Ic} \sqrt{E_x G_{xy}} / f_t^2}$	V_f (kN)	$\frac{V_f}{b\alpha h (2/3) f_v}$
a) 	95	0.95	9.6	0.50
	600	6.00	64.3	0.20
f) 	95	0.95	4.1	0.183
	600	6.00	27.5	0.073

Table 1. Beam strength predictions according to equation (8). Material parameters and beam geometries are given in Appendix. Beam width $b=120\text{mm}$.

compared to the size of the structural member. In the present case this general requirement can be quantified by demanding that the ratio between length $G_{Ic} \sqrt{E_x G_{xy}} / f_t^2$ and the length βh must be sufficiently small. If the ratio is too large, then equation (8) will overestimate the strength of the beam.

The material parameter values needed for applied calculations are E_x , G_{xy} and G_{Ic} . With numerical values of these parameters according to Appendix, the load carrying predictions of equation (8) for the beams defined in Appendix becomes as indicated in Table 1. The value of the normalized beam strength is valid for any beam size as long as the brittleness ratio given in the table, the stiffness and strength ratios of the material and the shape of the beam are kept constant.

4. Modifications and extensions

Various modifications and extensions have been proposed in order to improve the accuracy or widen the applicability of equation (8). To improve the accuracy in the analysis of small beams for which the length of the fracture zone is not small compared to the length βh , it can in the calculations be assumed that the tip of the crack, i.e. a centre of the fracture zone, is located a small distance ahead of the of the notch. This virtual displacement of the tip of the crack may be taken as a fraction, γ , of the intrinsic material length $G_{Ic} \sqrt{E_x G_{xy}} / f_t^2$. Values of γ in the order of 0.1 or 0.2 has been discussed, for common properties of softwood corresponding to a virtual increase of βh by about 10 or 20 mm.

An extended and modified version of equation (8) is included in the current draft of Eurocode 5 (August, 1992). Based partly on theoretical estimations and partly on experimental results, the influence of taper of the notch, Figure 1b), is considered by including the slope ratio i in the calculation. Furthermore, by assuming for the qualities of wood used in design that that E_x is proportional to G_{xy} and that $\sqrt{E_x G_{IC}}$ is proportional to the shear strength of the wood, f_v , the material parameters in equation (8) can all be replaced by f_v . Finally, by reasons of safety and by means of comparison to test results, the predicted values of V_f have been decreased, altogether giving the current draft code equation as:

$$\tau_d \leq k_v f_{v,d} \quad (9)$$

where for solid timber

$$k_v = \frac{(5/\sqrt{h})(1+1.1i^{1.5}/\sqrt{h})}{\sqrt{\alpha - \alpha^2} + 0.8\beta\sqrt{1/\alpha - \alpha^2}} \quad (10)$$

and where τ_d is the formal design shear stress in the net cross section of the beam and where $f_{v,d}$ is the design shear strength material parameter. k_v may for gluelam be taken 30 per cent higher than as given by equation (10).

5. Concluding remarks

Beam theory compliance analysis is fairly simple and leads to explicit equations for beam strength. Relating in particular to equation (8), a number of comparisons to test results have indicated that fracture mechanics almost surprisingly well can predict the effect of changes in beam geometry, i.e. the shape parameters α and β and the size parameter h . The predicted absolute values of beam strength are in general fairly good or good, much dependent on how the material parameters of the wood are tested. The beam strength seems in general to be somewhat overestimated by the theory.

A drawback of the beam theory compliance analysis is the limited applicability. The method has basically the same limitations as other linear elastic fracture mechanics methods: the geometry must by principle produce a square root singularity in stress and size of fracture zone must be small compared with the length of the crack or notch. Another drawback is the lack of information about the fracture mode, i.e. the normal stress to shear stress ratio in the fracture region. Using the pure mode I value of the fracture energy of the wood throughout, safe side approximations of the beam strength are obtained. Using this material property value in the case of pure mode II fracture, an approximation on the safe side by a factor of $\sqrt{3.5} = 1.87$ is obtained for a material with properties according to Appendix.

In conclusion, the method of calculation discussed in this section may be well suited for the development of special purpose strength equations. If in design it by safety reasons or any other reason is assumed that timber always have cracks, the beam theory compliance method would have the potential to become a tool of more general applicability.

--

FRACTURE MECHANICS MODELS FOR STRENGTH ANALYSIS OF
TIMBER BEAMS WITH A HOLE OR A NOTCH

Paper 5:

Mean Stress Approach and Initial Crack Approach ¹⁾

by

Per Johan Gustafsson

Division of Structural Mechanics, Lund University,
Box 118, SE-221 00 Lund, Sweden

¹⁾1993, 15 pages

Mean Stress Approach and Initial Crack Approach

by

Per Johan Gustafsson

1. Introduction

A severe limitation of conventional stress criteria is that such criteria can not be used in the case of a stress singularity. On the other hand, a severe limitation of the classical linear elastic fracture mechanics is that it can be used only in the case of a square root singularity. In this section two linear elastic failure criterion methods of more general applicability shall be discussed. The two methods here called the mean stress approach and the initial crack approach, are partly analogous but still different.

The idea of the mean stress approach is to adopt in the actual stress criterion the mean stress acting across an area or within a volume instead of the stress in a point. The size of the area is governed by the properties of the material.

The idea of the initial crack approach is to assume the existence of a sharp crack of a certain length in the highly stresses region. Some linear elastic fracture mechanics criterion is then applied. The length of the assumed crack is governed by the properties of the material.

For both approaches are several alternative variants imaginable, both with respect to basic formulation and with respect to method of calculation. Here, only one variant of each approach shall be studied. Plane stress is assumed throughout the present study. Fracture is in the present applications assumed to develop along grain and as a result of tension perpendicular to grain and/or shear along grain. The stress analysis is throughout carried out at the assumption of a linear elastic orthotropic performance of the material.

A basic stress criterion and a basic linear elastic fracture mechanics crack propagation criterion have to be chosen, both for the mean stress approach and for the initial crack approach. Here the same basic criteria are used for both approaches: a stress criterion of Norris and a crack propagation criterion of Wu:

$$\left(\frac{\sigma}{f_t}\right)^2 + \left(\frac{\tau}{f_v}\right)^2 = 1.0 \quad (1)$$

$$\frac{K_I}{K_{IC}} + \left(\frac{K_{II}}{K_{IIC}} \right)^2 = 1.0 \quad (2)$$

where σ and f_t are the perpendicular to grain tensile stress and strength, respectively, and τ and f_v the longitudinal shear stress and strength, respectively. K_I and K_{II} are the mode I and II stress intensities, and K_{IC} and K_{IIC} the corresponding critical stress intensities.

2. Mean stress approach

2.1 Theory

In the fracture criterion of equation (1) are the stresses σ and τ replaced by mean stresses $\bar{\sigma}$ and $\bar{\tau}$, giving

$$\left(\frac{\bar{\sigma}}{f_t} \right)^2 + \left(\frac{\bar{\tau}}{f_v} \right)^2 = 1.0 \quad (3)$$

This criterion is shown in Figure 2. $\bar{\sigma}$ and $\bar{\tau}$ are the mean stresses acting across a possible fracture area b times x_0 , where b is the width of the plane stress body and x_0 a certain length along grain. In a more general case is x_0 a length along a possible crack path. The length is chosen in such a way that equation (3) will give the same strength prediction for a deep sharp crack in a large body as predicted by linear elastic fracture mechanics, equation (2).

By the definition of stress intensity, the stresses σ and τ a distance x in front of a sharp are

$$\begin{aligned} \sigma &= \frac{K_I}{\sqrt{2\pi x}} + \dots \\ \tau &= \frac{K_{II}}{\sqrt{2\pi x}} + \dots \end{aligned} \quad (4)$$

where the first term in each series is dominating for small x . Assuming that x_0 is small compared with other dimensions of the large body with a deep crack under consideration, the stresses in region $0 \leq x \leq x_0$ can be accurately calculated by use of only the first term in the series of equation (4). Thus the mean stresses in the high stress region $0 \leq x \leq x_0$ can be calculated, giving

$$\bar{\sigma} = \sqrt{\frac{2K_I^2}{\pi x_0}} \quad (5)$$

$$\bar{\tau} = \sqrt{\frac{2K_{II}^2}{\pi x_0}}$$

Substituting these mean stresses into the mean stress fracture criterion of equation (3), the length x_0 can be calculated, giving

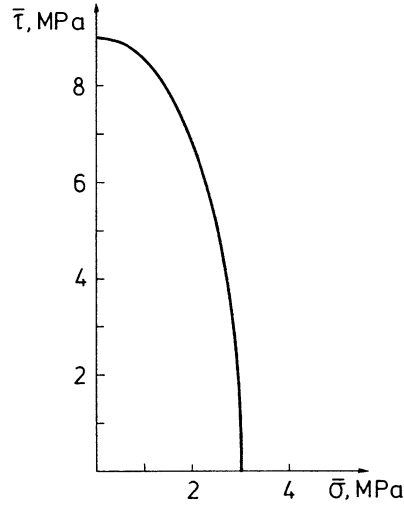


Figure 1. Mean stress fracture criterion.

$$x_0 = \frac{2 K_I^2}{\pi f_i^2} \left(1 + \frac{(K_{II} / K_I)^2}{(f_v / f_i)^2} \right) \quad (6)$$

where K_I is the magnitude of K_I at the instant of fracture at the actual mixed loading ratio. This magnitude of K_I is found by equation (2),

$$K_I = -\frac{K_{IIc}^2}{2K_{Ic}k^2} + \sqrt{\frac{K_{IIc}^4}{4K_{Ic}^2k^4} + \frac{K_{IIc}^2}{k^2}} \quad (7)$$

where k is the mixed mode ratio,

$$k = K_{II} / K_I = \bar{\tau} / \bar{\sigma} \quad (8)$$

Going from stress intensity analysis to energy release rate analysis by means of

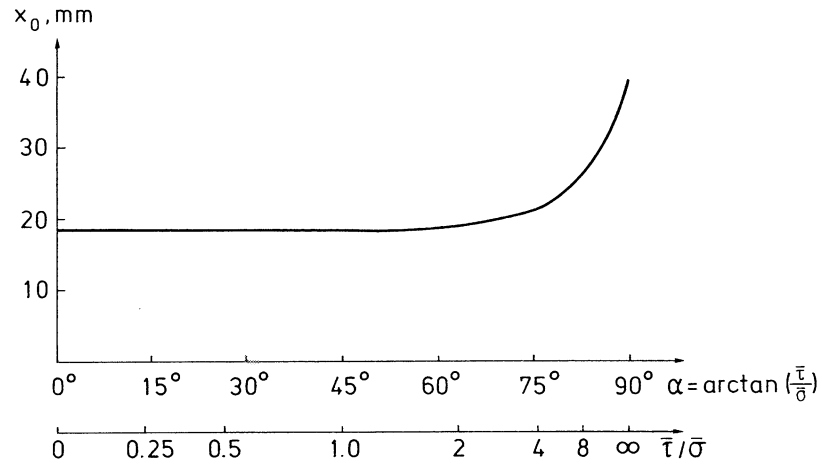


Figure 2. Mean stress length, x_0 , versus mixed mode ratio, $k = \bar{\tau} / \bar{\sigma}$.

$$\begin{aligned} K_I &= \sqrt{E_I G_I} \\ K_{II} &= \sqrt{E_{II} G_{II}} \end{aligned} \quad (9)^1$$

where

$$\frac{1}{E_I} = \frac{1}{E_x} \sqrt{\frac{E_x}{2E_y}} \sqrt{\sqrt{\frac{E_x}{E_y} + \frac{E_x}{2G_{xy}} - \nu_{yx} \frac{E_x}{E_y}}} \quad (10)^1$$

and

$$\frac{1}{E_{II}} = \frac{1}{E_x} \sqrt{\frac{1}{2}} \sqrt{\sqrt{\frac{E_x}{E_y} + \frac{E_x}{2G_{xy}} - \nu_{yx} \frac{E_x}{E_y}}} \quad (11)^1$$

with E_x , E_y , G_{xy} and ν_{yx} indicating modulus of elasticity in grain direction, perpendicular to grain, shear stiffness and Poisson's ratio, respectively, it is possible to obtain an expression for the length x_0 in terms of energy parameters. By use of equations (7), (9) and (10), equation (6) gives

$$x_0 = \frac{2}{\pi} \frac{E_I G_{IC}}{f_t^2} \frac{E_x}{E_y} \left(\frac{G_{IIC}}{G_{IC}} \right)^2 \frac{1}{4k^4} \left\{ \sqrt{1 + 4k^2 \sqrt{\frac{E_y}{E_x} \frac{G_{IC}}{G_{IIC}}}} - 1 \right\}^2 \left\{ 1 + \frac{k^2}{(f_v / f_t)^2} \right\} \quad (12)$$

¹⁾ After Paris, P.C. and Sih, G.C., 1965: *Stress Analysis of Cracks*, in *ASTM Special Technical Publication STP 381*, pp 30-80.

For the set of material parameters indicated in Table 1 in Appendix, x_0 versus the mixed mode ratio k is shown in Figure 2. Equation (12) shows that x_0 can be normalized with respect to the length $E_I G_{IC} / f_t^2$. For the material parameter values given in the appendix, this length is 28.6 mm.

For the special case of pure mode I, i.e. for $k=0$, equation (12) gives

$$x_0 = \frac{2}{\pi} \frac{E_I G_{IC}}{f_t^2} \quad (13)$$

and pure mode II, i.e. for $k \rightarrow \infty$, equation (12) gives

$$x_0 = \frac{2}{\pi} \frac{E_{II} G_{IIC}}{f_v^2}. \quad (14)$$

2.2 General characteristics

The mean stress approach can for a brittle body with a sharp crack be expected to give the same fracture load prediction as linear elastic fracture mechanics, equation (2). In the opposite case of a body in homogenous stress, the same fracture load prediction as predicted by a conventional stress criterion, equation (1), can be expected.

In the intermediate cases, going from a case with an extremely high stress gradient in the high stress region to a case with zero stress gradient, one may expect material parameters representing fracture energy and stiffness as well as the size of the body to become of gradually decreasing importance while instead the importance of material strength parameters f_t and f_v increases. As a mean stress always is less than the maximum stress, it is almost obvious that a conventional stress criterion always will give a fracture load prediction less or equal to the prediction given by the mean stress criterion. Use of a conventional stress criterion corresponds to zero fracture toughness of the material.

2.3 Method used in numerical calculations

Applied calculations were carried out by means of the FEM. The beams, see Figure 1 in Appendix, were modelled by linear elastic orthotropic plane stress elements with 4 nodes, quadratic shape and ordinary polynomial displacement shape functions. The element mesh was completed with a few constant strain triangular elements when needed due to beam geometry. The size of the elements in the region of interest was $h/96$ times $h/96$ for beams g) and h), and $h/48$ times $h/48$ for all other beams, where h is the depth of the beam.

The mean stress can be estimated in different ways by means of the results of the finite element analysis, giving the stresses in certain points and the element forces. In the

present study, the inter element nodal forces along possible fracture surfaces were utilized, Figure 3. From the nodal forces perpendicular to grain, P_{iy} , the mean normal stress, $\bar{\sigma}$, along the length x_0 is calculated from

$$\bar{\sigma} b x_0 = \sum_{i=1}^n P_{iy} + P_{(n+1)y} [(x_0 - (n-1/2)\Delta x) / \Delta x] \quad (15)$$

and the mean shear stress $\bar{\tau}$ was calculated from P_{ix} in the same manner.

By principle, the length x_0 has to be determined from Figure 2 by iteration. First some initial guess of k must be made, giving a first estimation of x_0 . For this x_0 is $\bar{\sigma}$ and $\bar{\tau}$ and a new value of $k = \bar{\tau} / \bar{\sigma}$ calculated, giving a new value of x_0 . In practice this iteration seems to converge rapidly and often the very first crude estimation of k can be sufficiently accurate.

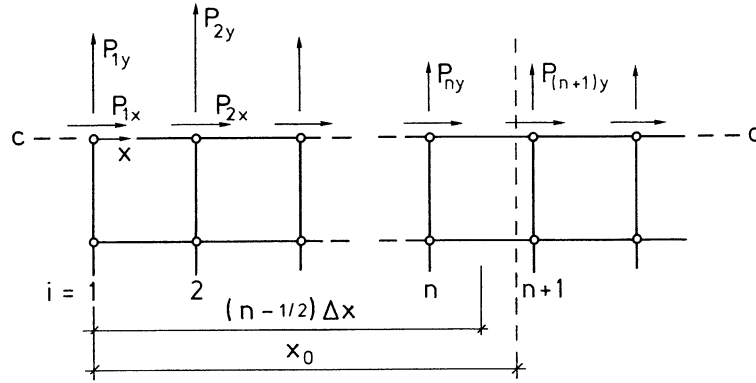


Figure 3. Nodal forces acting across a section C-C. Δx = length of an element.

2.4 Numerical results

The results of the present test calculations are shown in Table 1. It was possible to apply the mean stress method of calculations to all beams under consideration and the fracture load predictions are all of a reasonable magnitude. The predicted effects of changes of geometry seem reasonable. Thus for instance, the effect of the alteration from beam g) to beam h) is predicted to be more beneficial for the large beams than for the small beams. For all beams is an increase in beam size predicted to yield a decrease in the normalized load carrying capacity, $V_f / (bhf_t)$.

It is believed that the strength of small beams in general is somewhat overestimated by the present method. The length x_0 , which in the theory is independent of the size and shape of the beam, can from the physical point of view be regarded as a length measure that is proportional to the size of the fracture process region at the instant of beam failure. This length is indeed beam size independent for sufficiently large beams, but for smaller beams the fracture process region will occupy a significant part

of the beam and then the size of the fracture region at failure will be affected by the size of the beam.

The present failure load results obtained for large beams are probably somewhat low due to the use of coarse finite element meshes. Δx indicating the side length of an element, ratio $x_0/\Delta x$ is for the large beams with $h=600\text{mm}$ only 1.6 for beams a)-f) and 3.2 for beams g)-h). As a crude estimation, sufficient accuracy may in general be obtained with $x_0/\Delta x > 4$, i.e. for

$$\Delta x < 0.25x_0 \quad (16)$$

With the present set material data, this means that the length of an element should not be greater than about 5mm in the close vicinity of the fracture region.

The normalized predictions of load carrying capacity, $V_f/(bhf_t)$, are valid not only for the present absolute values of beam size and material parameters, but also for all values such that ratios $h/(E_I G_{IC}/f_t^2)$, $E_x:E_y:G_{xy}$, f_v/f_t , G_{IC}/G_{IIC} and ν_{xy} are kept constant.

3. Initial crack approach

3.1 Theory

An assumed crack is introduced in the high stress region. The length of this crack is denoted a_0 if located at an edge of a plate. If the crack is in the interior of a plate and accordingly having two tips, the length of the crack is made equal to $2a_0$. Having introduced this new crack or this addition to the length of an existing crack, the failure load of the structure is calculated according to some conventional linear elastic fracture mechanics crack growth criterion such as equation (2) or a corresponding energy release criterion.

An expression for the length a_0 is derived in such a way that for infinite plate in a homogenous state of stress, Figure 4a), the initial crack approach gives exactly the same strength prediction as the actual choice of a conventional stress criterion, e.g. equation (1), would give. The stress intensities at the tips of the crack in Figure 4b) are

$$\begin{aligned} K_I &= \sigma \sqrt{\pi a_0} \\ K_{II} &= \tau \sqrt{\pi a_0} \end{aligned} \quad (17)$$

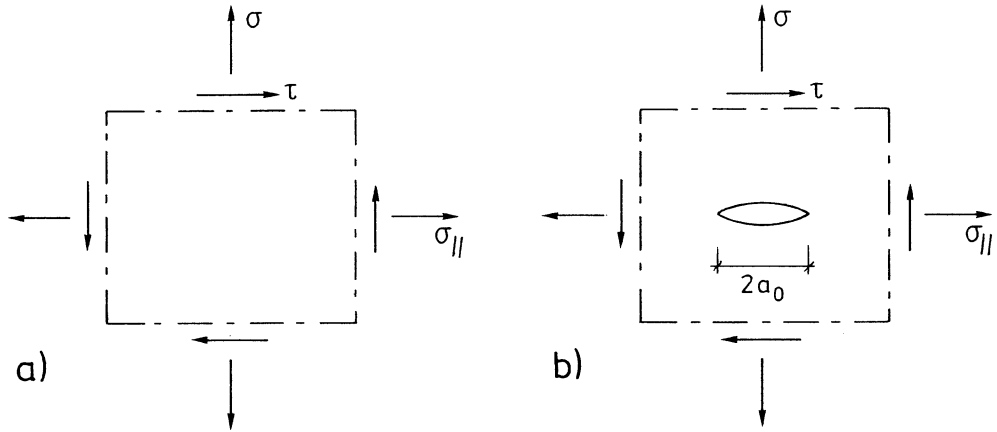


Figure 4. a) Infinite plate in a homogeneous state of stress.
 b) Infinite plate with a crack and loaded remotely.

This equation is analogous to Equation (5) in the derivation of the length x_0 in the mean stress criterion. Substituting in Equation (5) $2/\pi$ with π and the mean stresses $\bar{\sigma}$ and $\bar{\tau}$ with the remote stresses σ and τ , the derivation of a_0 becomes similar to the derivation of x_0 . This gives

$$a_0 = x_0 / 2 \tag{18}$$

where x_0 is given by Equation (12). Numerical values of a_0 versus k are shown in Figure 5 for the set of material data indicated in Table 1 in Appendix.

In applied calculations by the FEM it is often more convenient to calculate the total energy release rate G than the stress intensities K_I and K_{II} . G together with the mixed mode ratio k gives the same information as K_I and K_{II} . The value of G at the instant of fracture, i.e. the critical total energy release rate at the mixed mode condition under consideration, is

$$G = G_I + G_{II} = \frac{K_I^2}{E_I} + \frac{K_{II}^2}{E_{II}} = K_I^2 \left(\frac{1}{E_I} + \frac{k^2}{E_{II}} \right) = \left[-\frac{K_{IIc}^2}{2K_{Ic}k^2} + \sqrt{\frac{K_{IIc}^4}{4K_{Ic}^2k^4} + \frac{K_{IIc}^2}{k^2}} \right]^2 \left(\frac{1}{E_I} + \frac{k^2}{E_{II}} \right) \tag{19}$$

where the last part of the equation is according to Equation (7). K_{Ic} and K_{IIc} can be replaced by $\sqrt{E_I G_{Ic}}$ and $\sqrt{E_{II} G_{IIc}}$, respectively. Numerical values of G at the instant of fracture versus k are shown in Figure 6 for the set of material data indicated in Table 1 in Appendix.

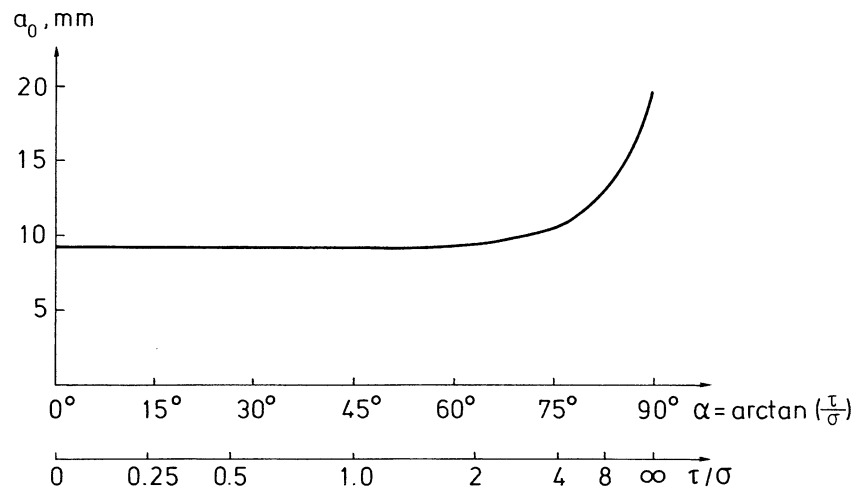


Figure 5. Crack length a_0 versus mixed mode ratio τ/σ .

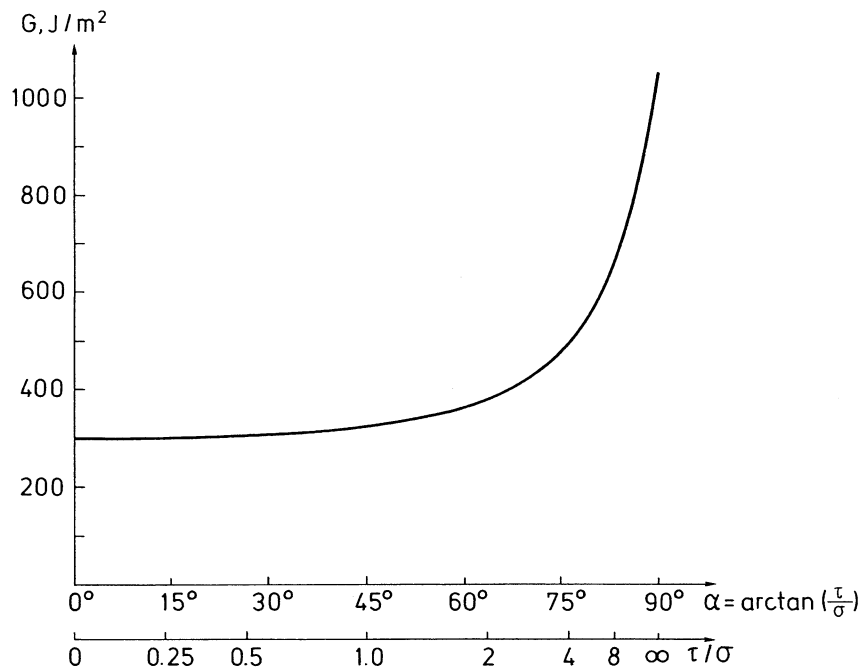


Figure 6. Critical value of the total energy release rate versus mixed mode ratio τ/σ .

3.2 Method used in numerical calculations

The FE-models described in section 2.3 were used also in the calculations by the initial crack method. The total energy release rate G was calculated from the change of compliance during crack extension simulated by opening of nodes along the crack path. The mixed mode ratio k was calculated as the ratio between the inter-element nodal forces P_x and P_y in the node at the tip of the crack.

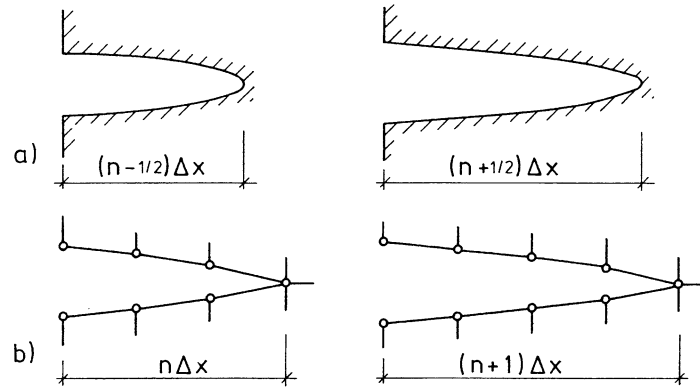


Figure 7. a) A crack in an elastic medium before and after crack extension.
b) FE-representation of the crack by 4-node elements with length Δx .

When a beam is loaded by a single load P the energy release rate during crack extension is

$$G = \frac{-\partial U}{\partial a} = \frac{\partial(P\delta/2)}{b\partial a} = \frac{P^2}{2b} \frac{\partial C}{\partial a} \quad (20)$$

where U is the potential energy, a the crack length $C = \delta/P$ the compliance. Equations (19) and (20) give the critical magnitude of the load P , P_f :

$$P_f = \sqrt{\frac{2b}{\partial C / \partial a}} K_I \sqrt{\frac{1}{E_I} + \frac{k^2}{E_{II}}} \quad (21)$$

where K_I , the magnitude of the mode I stress intensity at failure, is given by Equation (7).

Numerically, $\partial C / \partial a$ at crack length $a = n\Delta x$ is obtained from the FE-analysis as illustrated in Figure 7. Δx is the side length of the finite elements along the crack and $n=3$ for the case illustrated in Figure 7. The crack length is denoted a and the distance from the root of the crack to the first node is denoted x . Modelling the vicinity of a crack tip by 4 node elements, by experience a reasonable assumption for good modelling of stiffness and displacements is

$$x = a + \Delta x / 2 \quad (22)$$

It is moreover reasonable to calculate $\partial C / \partial a$ for crack length $a = n\Delta x$ from the difference between C at $a = (n-1/2)\Delta x$ and at $a = (n+1/2)\Delta x$, giving

$$\left. \frac{\partial C}{\partial a} \right|_{a=n\Delta x} = \frac{-C|_{x=n\Delta x} + C|_{x=(n+1)\Delta x}}{\Delta x} \quad (23)$$

Having calculated $\partial C/\partial a$ for certain values of a , $\partial C/\partial a$ at $a=a_0$ was estimated by linear interpolation or extrapolation.

3.3 Numerical results

The results are shown in Table 2. They are from a general point of view much the same as those of the mean stress method: it was possible to obtain failure load predictions for all beam geometries, the predicted influences of alterations of beam shape and size seem reasonable and none of the predicted failure loads are in some obvious way of a wrong magnitude.

The initial crack method can in general be expected to underestimate load carrying capacity, in particular for small beams. Beam d) is an example of an exception to this general rule. For this beam, just as for all the beams studied, the length of the initial crack is made equal to a_0 , not $2a_0$, since the crack starts from an edge, not from the interior of the beam. For beam d), the crack starts at a small hole, a_0 being of the same order of magnitude as the diameter of the hole, it is not self-evident that the crack should be regarded as an edge-crack and thus assigned the length a_0 , and not as interior crack and thus assigned the length $2a_0$.

For beams such as a), b), c) and f) where the crack starts from an edge, a slight underestimation can be expected even for large beams since the present derivation of assumed crack lengths was carried out for an inner crack. If the derivation had been carried out for an edge crack, its length had been somewhat less, $0.8a_0$ instead of a_0 , giving a somewhat higher predicted load carrying capacity.

The finite element meshes used in the calculations were probably on the coarse side for the large beams. With $h=600\text{mm}$ the element length Δx is 12.5mm for beams a)-f) and 6.25mm for beams g)-h). The length a_0 is with the present material data in the order of 10mm, Table 2. Although $a_0=x_0/2$ it is not believed that the initial crack method in general requires a finer mesh than the mean stress method. Using the present method of the numerical calculations one may suggest

$$\Delta x < 0.5a_0 \quad (24)$$

as an estimation of required element mesh fineness in the vicinity of the crack. If using ordinary elements with compatible shape functions a coarse mesh is known to produce an underestimation of the potential energy, i.e. a value of the compliance C on the low side. If C is underestimated, in general also $\partial C/\partial a$ will be underestimated, giving an overestimation of the load carrying capacity as a result of using a coarse element mesh.

4. Comparison and concluding remarks

In Table 3 the results of the present test calculations are compared. Also the strength predictions obtained by a beam compliance theory energy release based analysis are shown where possible. That theory is in greater detail discussed in another paper in this report. The calculated values of V_f are in Table 3 normalised with respect to the formal shear force capacity of a beam without any notch or hole, $bh(2/3)f_v$. The normalised value greater than 1.00 found by the initial crack method for the small beam with a small hole is probably a result of regarding the fracture as starting from an edge rather than from the interior of the beam, corresponding to a crack length of a_0 rather than $2a_0$. The mixed mode ratios, k , are shown in Tables 1 and 2. In the beam theory compliance method it is tacitly assumed that $k=0$.

Disregarding effects of numerical approximations and leaving out the discussion of edge cracks versus interior cracks, some general features of the two methods can be identified: in the case of a deep sharp in a brittle material both methods are expected to give the same failure load prediction, coinciding with LEFM. In the case of a large specimen without any stress singularity made of a brittle material, both methods are expected to give the same result as a conventional stress criterion. Going from the first extreme of a square root singularity to zero stress gradient, one may expect a gradual shift in character from of the strength predictions from the one theory to the other.

An advantage of the methods is that they seem to have a general applicability. The initial crack method produces in general strength predictions that are on the safe side as compared to the predictions of the mean stress method. The mean stress method is from a computational point of view commonly the more convenient method: only a single linear elastic stress is required; no incremental crack propagation analysis neither possible testing of alternative crack locations are required.

It can be concluded that the two methods discussed seem to have several attractive features and should deserve further attention. At the present stage of development and knowledge it is not possible state whether or not both methods, one or none are suitable for use in future codes of strength design practise.

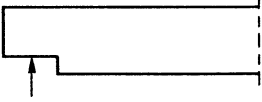

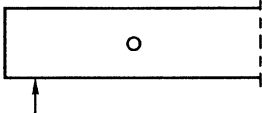
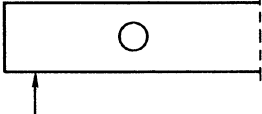
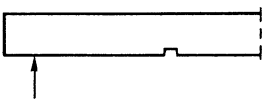
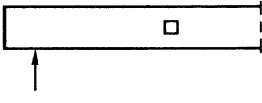
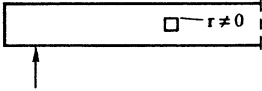
Geometry	h (mm)	k = = $\bar{\tau} / \bar{\sigma}$	x_0 (mm)	V_f (kN)	$\frac{V_f}{bh f_t}$
a) 	95	2.3	19	10.3	0.81
	600	1.7	19	55.2	0.26
b) 	95	3.5	21	13.9	1.08
	600	3.7	21	140.2	0.65
d) 	95	4.9	22	22.6	1.76
	600	1.3	19	152.3	0.71
e) 	95	1.3	19	10.3	0.80
	600	1.3	19	90.3	0.42
f) 	95	5.0	22	6.8	0.53
	600	2.7	20	30.5	0.14
g) 	95	0.7	18	7.2	0.56
	600	0.7	18	48.3	0.23
h) 	95	0.8	18	7.6	0.60
	600	1.0	18	61.8	0.29

Table 1. Mixed mode ratio, mean stress length and beam strength predictions obtained by mean stress criterion calculations. Material data and details about beam geometries are given in Appendix.

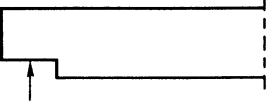
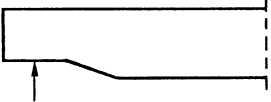
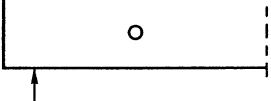
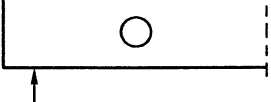
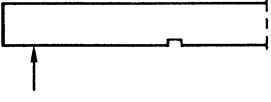
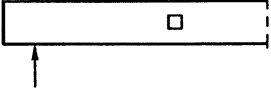
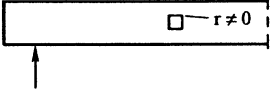
Geometry	h (mm)	k = = τ / σ	a_0 (mm)	V_f (kN)	$\frac{V_f}{bh f_t}$
a) 	95	1.9	9.5	8.6	0.67
	600	1.6	9.4	56.5	0.26
b) 	95	20	9.5	10.6	0.83
	600	2.5	9.7	114.3	0.53
d) 	95	8.3	12.9	27.7	2.16
	600	1.2	9.2	135.6	0.63
e) 	95	0.8	9.2	8.2	0.64
	600	1.1	9.2	75.6	0.35
f) 	95	3.4	10.3	5.1	0.40
	600	2.8	9.9	34.0	0.16
g) 	95	0.4	9.1	6.0	0.47
	600	0.6	9.1	45.5	0.21
h) 	95	0.5	9.1	6.2	0.48
	600	0.5	9.1	52.6	0.24

Table 2. Mixed mode ratio, initial crack length and beam strength predictions obtained by initial crack criterion calculations. Material data and details about beam geometries are given in Appendix.

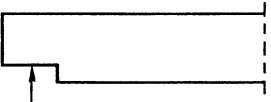
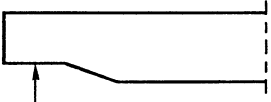
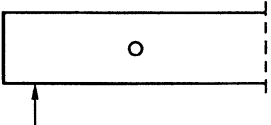
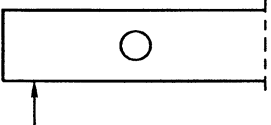
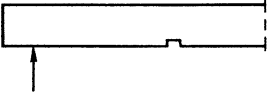
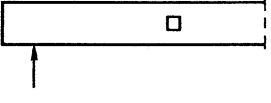
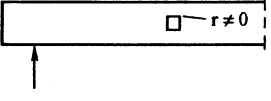
Geometry	$h/(E_I G_{Ic}/f_t^2)$	$V_f/(bh (2/3) f_v)$		
		"Mean stress"	"Init. crack"	"Beam compl."
a) 	3.32	0.40	0.34	0.37
	20.97	0.13	0.13	0.15
b) 	3.32	0.54	0.42	-
	20.97	0.33	0.27	-
d) 	3.32	0.88	1.08	-
	20.97	0.36	0.32	-
e) 	3.32	0.40	0.32	-
	20.97	0.21	0.18	-
f) 	3.32	0.27	0.20	0.16
	20.97	0.071	0.079	0.064
g) 	3.32	0.28	0.24	-
	20.97	0.12	0.11	-
h) 	3.32	0.30	0.24	-
	20.97	0.15	0.12	-

Table 3. Brittleness number and normalised beam strength according to three methods of calculation. Material data and details about beam geometries are given in Appendix.

--

FRACTURE MECHANICS MODELS FOR STRENGTH ANALYSIS OF
TIMBER BEAMS WITH A HOLE OR A NOTCH

Appendix:

Geometry of Beams and Material Parameter Data ¹⁾

by

Per Johan Gustafsson

Division of Structural Mechanics, Lund University,
Box 118, SE-221 00 Lund, Sweden

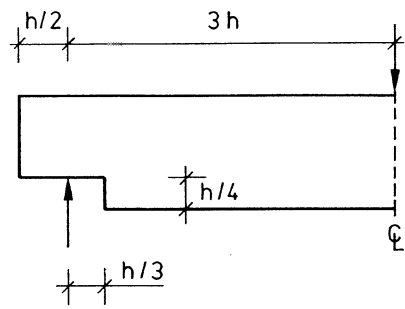
¹⁾1993, 2 pages

A

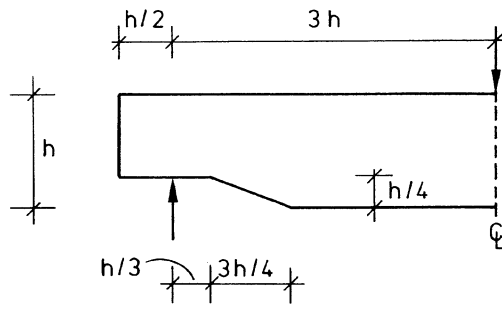
Contents:

Figure 1. Geometry of beams used in beam strength test calculations.

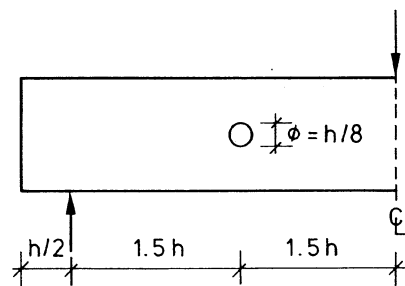
Table 1. Material property parameters for wood and gluelam assumed
in beam strength test calculations.



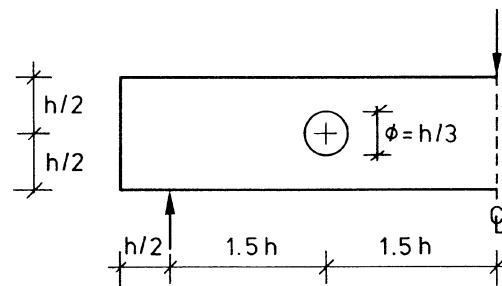
a) $h = 95$ mm, $b = 45$



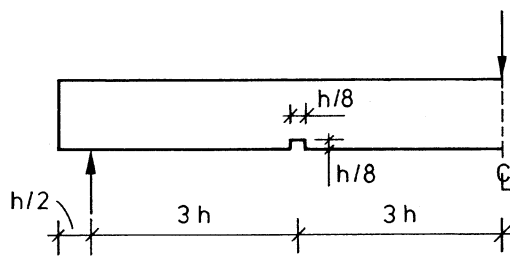
b) $h = 95$, $b = 45$
 c) $h = 600$, $b = 120$



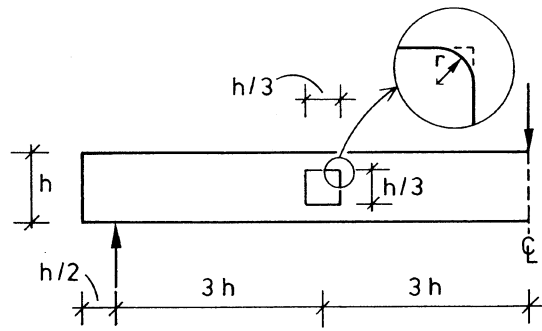
d) $h = 95$, $b = 45$



e) $h = 600$, $b = 120$



f) $h = 95$, $b = 45$



g) $h = 600$, $b = 120$, $r = 0$
 h) $h = 600$, $b = 120$, $r = 30$

Figure 1. Geometry of beams used in beam strength test calculations.
 Beam width is indicated by b .

Table 1. Material property parameters for wood and gluelam assumed in beam strength test calculations.

<u>Strength</u>	
$f_v = 3 f_{t,\perp}$	
$f_{t,\parallel} = 30 f_{t,\perp}$	$f_{t,\perp} = 3.0 \text{ MPa}$
<u>Stiffness</u>	
$E_{\perp} = E_{\parallel} / 30$	
$G_{\parallel} = E_{\parallel} / 16$	$E_{\parallel} = 12000 \text{ MPa}$
<u>Fracture energy</u>	
$G_{IIc} = 3.5 G_{IC}$	$G_{IC} = 300 \text{ J/m}^2$
<u>Corresponding plane stress critical stress intensity</u>	
$K_{IIc} = 4.37839 K_{IC}$	$K_{IC} = 0.507476 \text{ MPa m}^{1/2}$